TU Delft

Delft University of Technology

Stimuli Sensitive Polymer Materials For Signal Transduction

Breve, T.

DOI
10.4233/uuid:da8543c4-e407-473c-80e1-6d0c0add180f

Publication date
2022

Document Version
Final published version

Citation (APA)
Breve, T. (2022). *Stimuli Sensitive Polymer Materials For Signal Transduction*. [Dissertation (TU Delft), Delft University of Technology]. https://doi.org/10.4233/uuid:da8543c4-e407-473c-80e1-6d0c0add180f

Important note
To cite this publication, please use the final published version (if applicable).
Please check the document version above.

Copyright
Other than for strictly personal use, it is not permitted to download, forward or distribute the text or part of it, without the consent of the author(s) and/or copyright holder(s), unless the work is under an open content license such as Creative Commons.

Takedown policy
Please contact us and provide details if you believe this document breaches copyrights.
We will remove access to the work immediately and investigate your claim.

This work is downloaded from Delft University of Technology.
For technical reasons the number of authors shown on this cover page is limited to a maximum of 10.

Stimuli Sensitive Polymer Materials For Signal Transduction

PhD Thesis

Tobias Gerard BREVE

Copyright © Tobias Brevé, 2022
All rights reserved. The author encourages the communication of scientific contents and explicitly allows reproduction for scientific purposes with proper citation of the source. Some chapters of this thesis have been published in scientific journals and copyright is subject to different terms and conditions.

An electronic version of this thesis is freely available at http://repository.tudelft.nl

Stimuli Sensitive Polymer Materials For Signal Transduction

Proefschrift

ter verkrijging van de graad van doctor
aan de Technische Universiteit Delft,
op gezag van Rector Magnificus, prof. dr. ir. T.H.J.J. van der Hagen
voorzitter van het College voor Promoties,
in het openbaar te verdedigen op

dinsdag 22 maart 2022 om 15:00 uur

door

Tobias Gerard BREVE

Master of Science in Chemistry
Universiteit Leiden, Nederland
geboren te Delft, Nederland

Dit proefschrift is goedgekeurd door de promotoren.

Samenstelling promotiecommissie:

Rector magnificus	voorzitter
Prof. dr. J.H. van Esch	Technische Universiteit Delft, promotor
Dr. R. Eelkema	Technische Universiteit Delft, promotor

Onafhankelijke leden:

Prof. dr. F. Hollmann	Technische Universiteit Delft
Prof. dr. S. A. Bonnet	Universiteit Leiden
Prof. dr. J. N. H. Reek	Universiteit Amsterdam
Dr. D. P. W. M. Löwik	Radboud Universiteit
Prof. dr. U. Hanefeld	Technische Universiteit Delft, reserve lid

Andere leden:

Dr. Ir. A. G. Denkova	Technische Universiteit Delft

The research described in this thesis was performed in the Advanced Soft Matter (ASM) group at Delft University of Technology, Department of Chemical Engineering, Faculty of Applied Sciences. The research has been funded by a consolidator grant (726381) from the European Research Council (ERC).

Cover by:	Tobias Brevé In Blender software
Printed by:	Ipskamp Drukkers, Enschede
ISBN:	978-94-6421-690-5

TABLE OF CONTENTS

CHAPTER

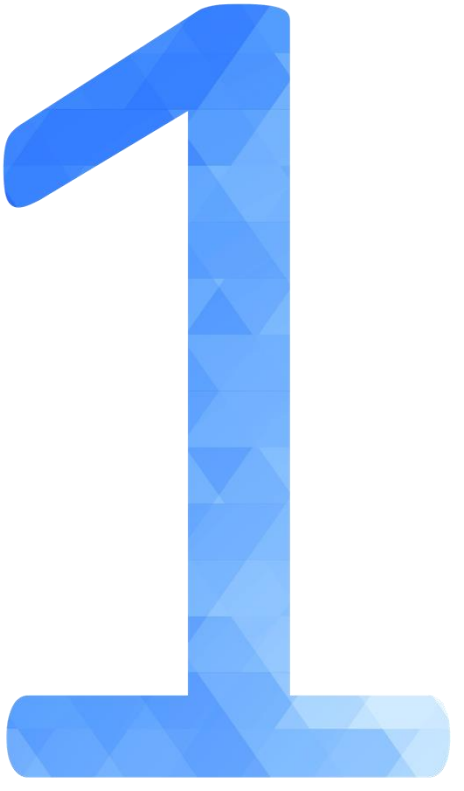

GENERAL INTRODUCTION

Smart materials are materials that are capable of responding in a programmable and predictive manner. Such materials respond to a broad variety of internal and external triggers and modulate one or more material properties accordingly. Common material responses are controlled release, color changes, morphological changes or changing the mechanical properties of the bulk material. Well known examples of smart materials in our life are chromoactive materials in sunglasses or windows that change color or transparency when subjected to (sun)light, self-healing concrete and plastics or shape memory materials being responsive to heat.[1, 2] Smart materials often reside in a stationary phase, where built-in molecular functionality can respond autonomously to a changing environment. A material's response can be triggered by many different stimuli having a chemical nature (e.g. pH, salts and metals), biochemical nature (e.g. peptides, nucleic acids, metabolites and polysaccharides) or a physical nature (e.g. temperature, light, magnetic field and pressure). Materials constructed from polymers, particles or gels can be used for applications such as self-healing, sensing, tissue engineering and drug delivery. Smart materials described in this thesis are designed to respond to signaling molecules, UV light, γ-radiation or mechanical force. In the following subsections these triggers will be discussed in detail.

1

1.1 CHEMICAL SIGNALLING ENABLES CONTROL OVER CATALYTIC ACTIVITY

Living systems are regulated by the capability of responding to external stimuli that induce a signaling cascade which changes specific physicochemical properties. Cellular signaling networks are complex and rely on ligands binding non-covalently to a specific receptor, resulting in a programmed response. Therefore, ligand receptor binding is an important component in natural signal transduction relying on non-covalent interactions.[3] An interesting approach to translate natural signal transduction into synthetic signal transduction, is the use of host guest chemistry. In host-guest chemistry the host can be seen as the ligands' binding site and the guest as the ligand, binding non-covalently to the host. Binding of the guest to the host can be used to control the chemical properties of encapsulated guests, such as their fluorescence, solubility or catalytic activity. Upon competitive binding of a signal molecule, the first encapsulated guest is released, restoring the initial chemical properties of the guest. A widely applied host for encapsulation is the

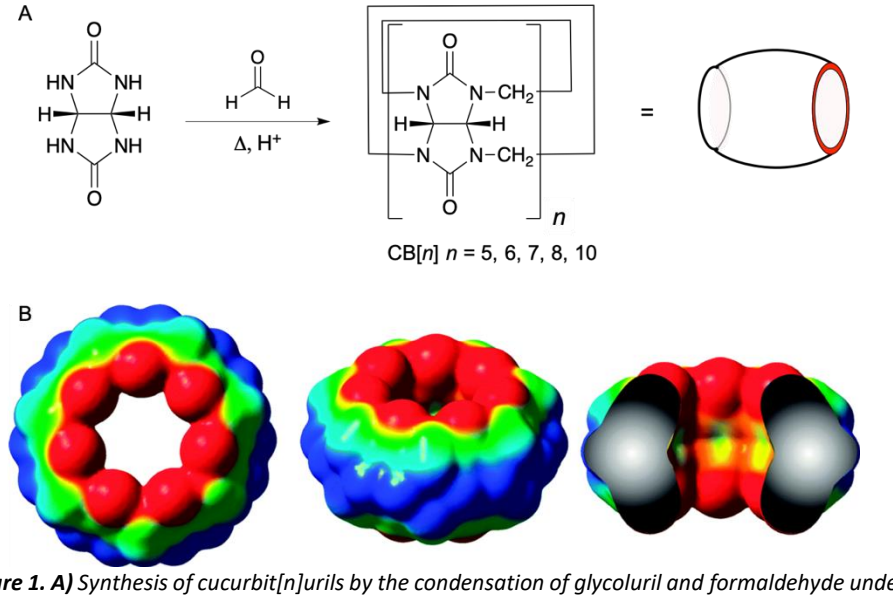

Figure 1. A) *Synthesis of cucurbit[n]urils by the condensation of glycoluril and formaldehyde under acidic conditions.* ***B)*** *Electrostatic map showing the charge distribution of CB[7]. Negatively charged carbonyl portal area is shown in red and hydrophobic cavity in yellow and green. Figure* ***1B*** *is taken from ref. [4].*

cucurbituril family, having a macrocyclic structure containing 5, 6, 7, 8 or 10 glycoluril units (Figure **1A**). The structure of cucurbiturils is characterized by their apolar interior and polar electronegative portal regions (Figure **1B**). Cucurbiturils' electrostatic dipole can play a crucial role in molecular recognition and enables (strong) binding to neutral and positively charged guest molecules. [4] [5] An example of a synthetic chemical signaling cascade relying on cucurbiturils host-guest chemistry is given in figure **2**. This research demonstrates how the cucurbit[n]uril family (CB[6], CB[7] and CB[8]) non-covalently binds two competing guest molecules with different binding affinities, resulting in the regulation of the folding behavior of pseudo-rotaxane foldamers.[6]

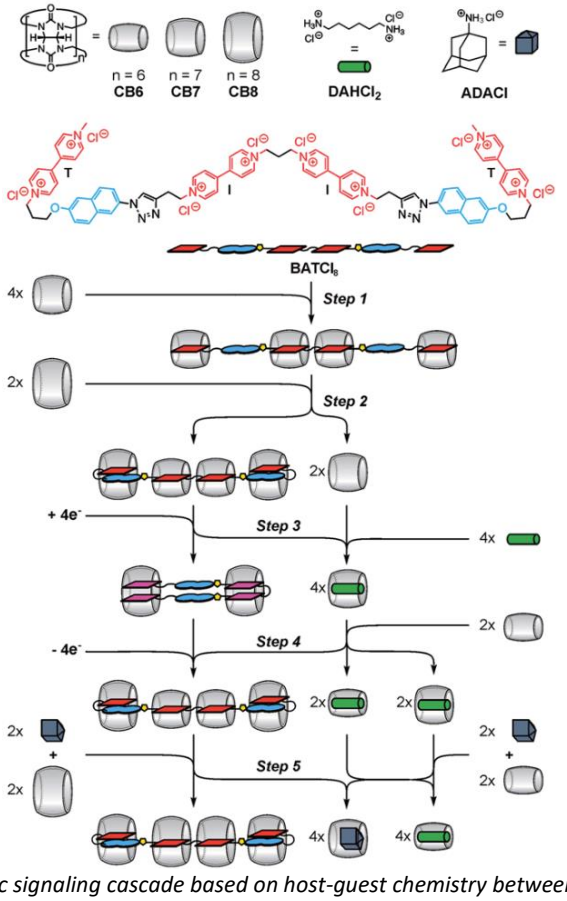

Figure 2. *Synthetic signaling cascade based on host-guest chemistry between cucurbit[n]urils (n = 6, 7 or 8) and signaling molecules (DAHCl$_2$ green rod) and (ADACl blue cube), resulting in control over the folding behavior of a pseudo-rotaxane foldamer. Figure is taken from ref. [6].*

A prime example of synthetic chemical signaling in cells is demonstrated by Rotello et al., here gold nanozymes are decorated with polyethylene glycol chains that are capped with a positively charged quaternary amine having strong affinity for CB[7], resulting in a sterically blocking corona in which the catalyst is separated from its substrate (Figure **3**). Adding a chemical signal with a very high affinity for CB[7] results in the displacement of CB[7] and liberates the ruthenium catalyst that subsequently converts a non-fluorescent substrate to a fluorescent molecule.[7] A similar approach was employed to sterically retain fluorescent molecules inside the nanopores of mesoporous silica nanoparticles that are responsive to light irradiation and pH changes.[8, 9] In previous examples, control of the catalytic activity is achieved by steric seclusion of the catalysts.

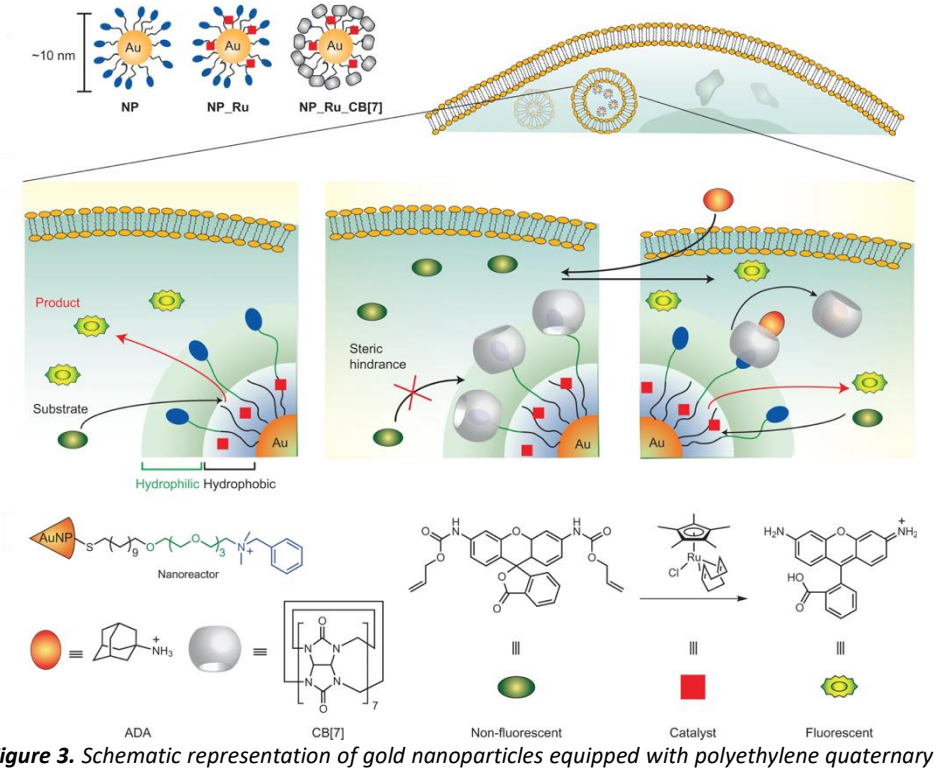

Figure 3. *Schematic representation of gold nanoparticles equipped with polyethylene quaternary amine moieties (blue ellipse) that bind strongly to CB[7], forming a sterically blocking corona that shields the catalyst (red square) from its substrate (green ellipse). When a stronger binding guest (orange ellipse) is added and binds to CB[7], the blocking corona is removed and the catalyst free to diffuse resulting in the onset of catalysis. Figure taken from ref. [7].*

Alternatively, by encapsulating a catalyst inside the cucurbituril cavity, catalyst activity can be upregulated, downregulated or completely inhibited. By applying this host-guest complexation approach, CB[7] is employed for upregulating the catalytic activity of radical initiator TEMPO, accelerating the Fenton reaction and upregulation of H_2 generation.[10-13] In contrast, downregulating catalytic activity is achieved by encapsulating viologen dimers with CB[8] that prevents the electron transfer from viologen dimers to the platinum catalyst and thereby downregulates H_2 generation.[14]

Recently, our lab has developed a generic method to control the catalytic activity of several organocatalysts such as: aniline, benzimidazole, prolinol, DABCO and nornicotine.[15] Here, we encapsulate various catalysts resulting in the downregulation of the catalytic activity except for benzimidazole of which the catalytic activity is upregulated upon CB[7] complexation. Restoring catalytic activity to its initial catalytic rate was achieved by replacing the catalyst from CB[7] by the

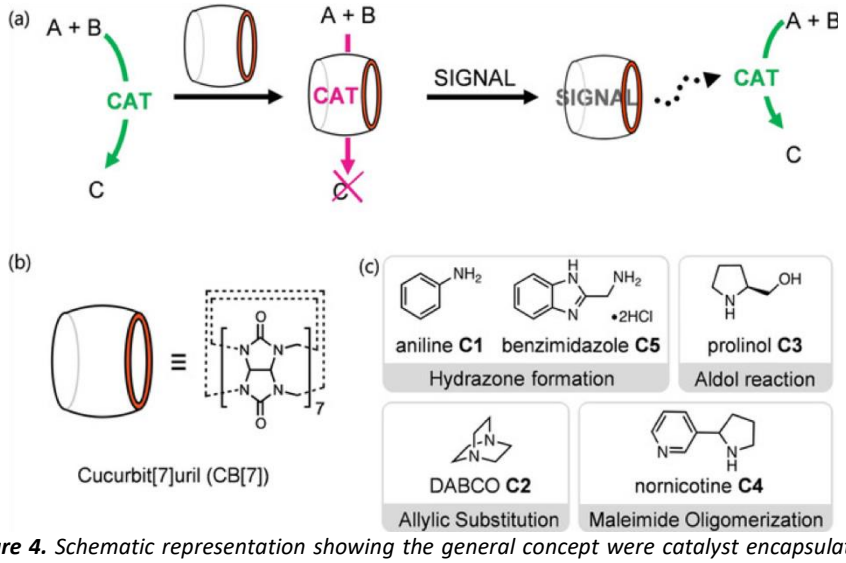

Figure 4. *Schematic representation showing the general concept were catalyst encapsulation is employed to control the catalytic activity of several organocatalysts.* ***A)*** *catalyst encapsulation by CB[7] hinders the catalytic activity. After the addition of a stronger binding signal molecule the catalyst is liberated and the catalytic activity is restored.* ***B)*** *schematic representation of CB[7].* ***C)*** *The catalytic activity of organocatalysts* ***C1*** *–* ***C5*** *is modulated upon binding with CB[7]. Figure is taken from ref. [15].*

addition of chemical signaling molecules having a higher affinity for CB[7] compared to the corresponding catalyst (Figure **4A**). Catalyst encapsulation by cucurbiturils is thus a powerful strategy to modulate catalytic activity and can be controlled using chemical signal molecules. Moreover, cucurbiturils are employed to modulate fluorescence intensity,[16-20] control drug delivery,[21-24] interact with proteins[25-27] or to act as catalyst itself.[28, 29]

In chapter 2 of this thesis, we present a molecular inclusion complex of a copper carbene catalyst and CB[7]. The copper carbene catalyst is an efficient catalyst for the copper catalyzed azide-alkyne cycloaddition (CuAAC). By encapsulating the catalyst, using CB[7], we demonstrate direct control over CuAAC.

1.2 LIGHT SENSITIVE PHENACYL CROSSLINKED HYDROGELS FOR CONTROLLED RELEASE

Hydrogels are three-dimensional structures having a hydrophilic polymeric network that can absorb large amounts of water or biological fluid and are thereby capable of storing (bio) molecules. Hydrogels are being used in many different (commercial) applications, for example in contact lenses, wound dressings, drug delivery devices, tissue engineering and hygiene products.[30, 31] Hydrogels having built-in functionality responding to external stimuli are of particular interest, as the pre-programmed functions can be triggered on demand. A broad variety of external triggers is applied in academic and clinical settings including, heat, magnetism, (UV) light, ultrasound, radiation and chemical signals.[32] Light is an interesting trigger as it can be applied spatio-temporally and its intensity and wavelength can be precisely controlled. Light as external stimulus is enabled to control the chemical structure of the hydrogels' polymer backbone or its side groups. By altering the chemical integrity of the hydrogels chemical structure using for example light, controlled cargo release can be achieved. A limitation of using light as an external trigger is the short penetration depth through skin and tissue. UV light has a penetration depth of just 1-2 mm and

visible light penetrates tissue a maximal 10 mm, depending on the wavelength. Therefore, it is important when designing light triggered applications that the spectral window to which the application is responsive, matches with the applicability of the light source. Using external light sources, clinical application can be modulated in near-surface tissues such as the skin, the ear, transdermal delivery or the back of the eye. An internal light source, such as optical fibers can partly overcome issues arising from limiting light penetration in tissue. Optical fibers are being used to transmit (external) light deep into diseased tissue and initiate photo dynamic therapy (PDT) or photoactivated chemotherapy (PACT).[33, 34] Alternatively, generating light *in vivo* could circumvent the limited penetration depth of external light sources and could be achieved using chemiluminescent compounds, bioluminescent compounds or the process known as Cerenkov luminescence.[35, 36] Cerenkov luminescence is generated when a charged particle travels faster than the speed of light through a medium such as water, resulting in the polarization of water molecules, which emit light when relaxing back to the ground state (Figure **5**).[37] In chapter 3 of this thesis we describe a light sensitive hydrogel that is designed to be responsive to Cerenkov light.

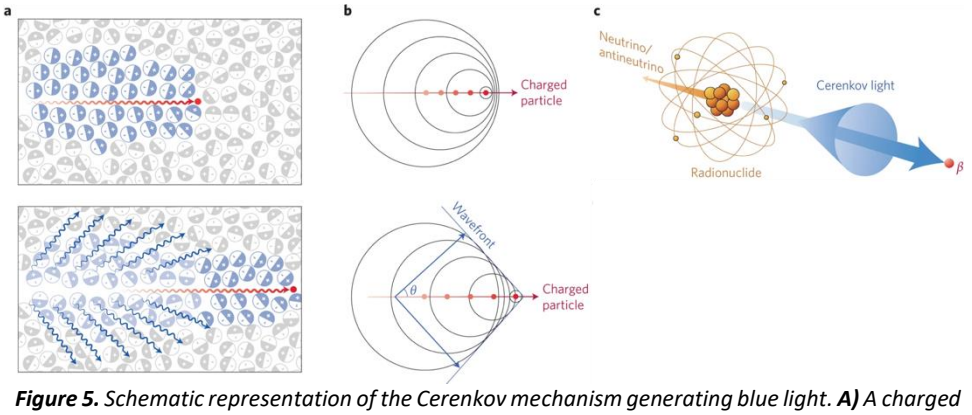

Figure 5. *Schematic representation of the Cerenkov mechanism generating blue light.* ***A)*** *A charged particle (red dot) travels faster than light in a particular medium, polarizing the medium. Blue light (blue arrows) is emitted when the polarized medium returns to its ground state.* ***B)*** *charged particle produces coherent waves, leading to a photonic wave front (top). When the charged particle is moving forward the photonic wave front propagates forward at angle* θ *(bottom).* ***C)*** *A radionuclide emits a beta-particle with an energy greater than the Cerenkov threshold (261 KeV in water), resulting in the emission of blue Cerenkov light. Figure is taken from ref. [37].*

There are many examples known of micellar carriers, (micro/nano) hydrogel carriers and liposomal structures that retain the loaded cargo inside the polymer matrix and either burst release or slowly release upon (UV) light irradiation. Photochemical control is achieved using mechanisms including photoisomerization leading to leaky membranes,[38] photosensitization-induced reactive oxygen species (ROS) damaging lipid bilayers,[39] photothermal induced carrier rupture,[40, 41] photochemical hydrophobicity switch to disintegrate micellar structures[42] and light induced polymer backbone cleavage or light induced de-crosslinking.[43, 44]

In this thesis we focus on photosensitive hydrogels, that through light irradiation de-crosslink and release their cargo. The ultimate goal in such applications is having a high photo-responsiveness of the photocleavable group that ideally absorbs light in a non-invasive photo spectral window and leaves no toxic or strongly absorbing photoproducts. By controlling the intensity of the light source, the release rate can be controlled based on the specific requirements of the application. The most commonly used photolabile moiety incorporated in the backbone or in crosslinks of photosensitive hydrogels is the ortho-nitrobenzyl (*o*NB) group.[45, 46] Hydrogels having *o*NB photo reactivity are employed in various ways, for example to provide for an artificial 3D matrix to culture cells in, to create 3D micropatterns in macroscopic hydrogel patches[47] and for controlled release of proteins or drugs.[48, 49] Anseth et al. prepared an *o*NB crosslinked hydrogel matrix hosting human mesenchymal stem cells (hMSCs). By irradiating the macroscopic hydrogel with light, the crosslink density decreases resulting in a reduced hydrogel stiffness. The light sensitivity is used to alter the morphology of the embedded hMSCs and study cell behaviour.[46] Moreover, Kloxin et al. prepared polyethylene glycol (PEG) based hydrogels that are crosslinked with either non photosensitive crosslinkers (Figure **6B**), light sensitive *o*NB moieties (Figure **6C**) or with light sensitive coumarin moieties (Figure **6D**) and demonstrated that the hydrogels can retain antibodies in the hydrogel matrix. Upon light irradiation both light sensitive crosslinkers break

leading to disintegration of the hydrogel matrix and release of the antibody (Figure **6A**).[49]

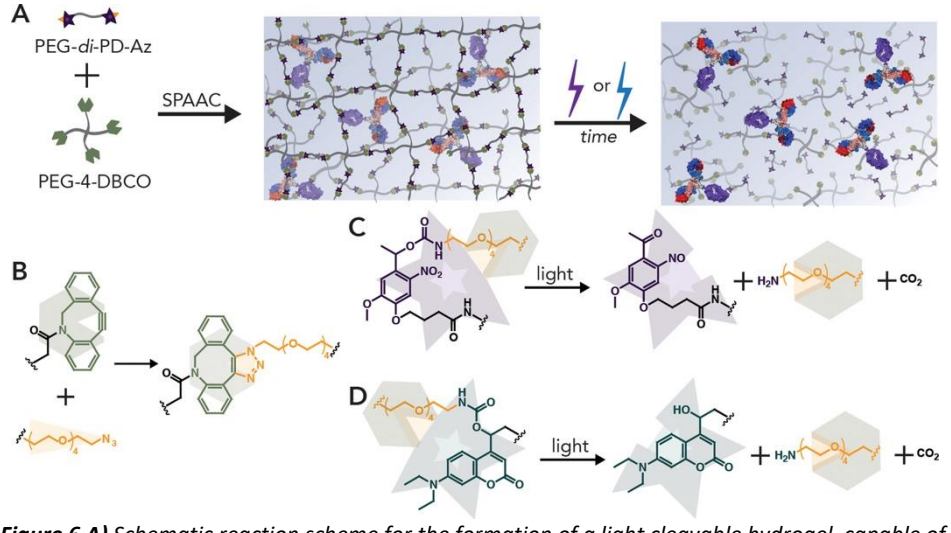

Figure 6 A) *Schematic reaction scheme for the formation of a light cleavable hydrogel, capable of retaining antibodies in its polymer network. Irradiation with UV-light (365 nm) triggers cleavage of oNB based crosslinker and irradiation with blue (400-500 nm) light triggers cleavage of coumarin based crosslinkers.* ***B)*** *light insensitive crosslinks.* ***C)*** *oNB based light sensitive crosslinks.* ***D)*** *coumarin based light sensitive crosslinks. Figure taken from ref. [49]*

In chapter 3 of this thesis we describe a light cleavable crosslinker strategy where we use the phenacyl scaffold as photosensitive moiety. Para-hydroxyphenacyl (*p*Hp) is commonly used as a photo protective group (PPG) for a variety of functional groups and is mostly cleaved using UV-C light (254 nm). We selected the *p*Hp photosensitive moiety as it is absorbing in the Cerenkov emission window and has higher quantum yields compared to *o*NB moieties. Until now, no light sensitive hydrogels crosslinked by phenacyl functionality are reported. In chapter 3, dextran-based hydrogels crosslinked by two different phenacyl groups absorbing in the UV-C and UV-A region are presented. The synthesis, photochemical properties and light triggered protein release studies are discussed.

1.3 γ-RADIATION SENSITIVE HYDROGELS

An interesting physical stimulus to control the behavior of smart materials is γ-radiation. γ-radiation can be emitted by radionuclides following radioactive decay, having enough energy to penetrate many materials including human tissue. In general, there are two classes of radiation; non-ionizing radiation and ionizing radiation. γ-radiation belongs to the ionizing class of radiation, which makes it capable of generating free negatively charged electrons, positively charged ionized atoms and radicals.[50] γ-irradiation can lead to the generation of solvent radicals, which subsequently can react with molecular functionalities, such as hydroxyls, unsaturated C-C bonds and carboxyl's forming new chemical bonds.[51-53] Therefore, using γ-radiation as radical initiator is an attractive method for the preparation of hydrogels, rubbers, plastics and nanocomposites. γ-radiation synthesized materials are sterile directly after preparation of the materials, making them very suitable for clinical applications such as wound dressings and drug delivery devices.[54]

The penetration depth of γ-radiation through tissue is, compared for example with visible light, very high. However, when employing γ-rays as stimulus for smart materials in a clinical setting the applied dose has to be minimized. Severe health issues arise even from low doses of radiation,[55] although in some cases patients are exposed to an accumulated dose of 40-60 Gy given in daily fractionated doses of 1.8 Gy.[56] An example of γ-radiation triggered drug release is shown in figure **7**. In this research an ABA block copolymer is synthesized from hydrophilic PEG (block A) and a diselenide hydrophobic core (block B), forming micelles in water that are capable of retaining the drug doxorubicin. The Se-Se bonds in the hydrophobic core are prone to cleavage upon reacting with radicals generated by radiolysis of H_2O, due to their reductive nature, resulting in the release of doxorubicin.[57]

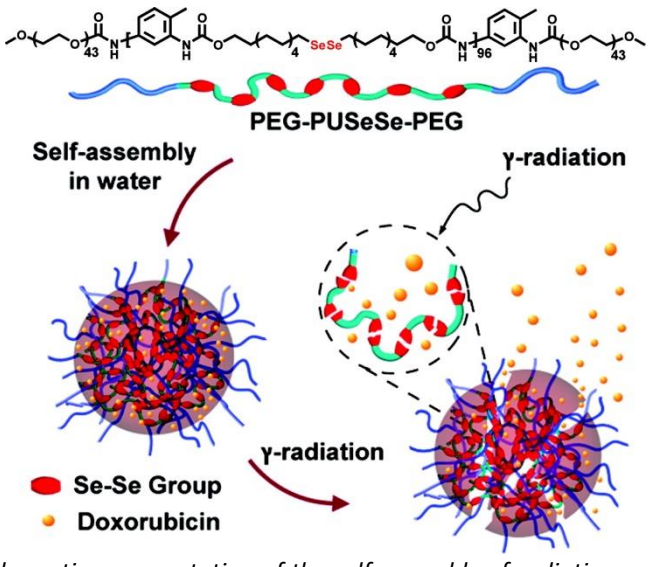

Figure 7. *Schematic representation of the self-assembly of radiation sensitive micelles, loaded with doxorubicin. Upon γ-radiation the Se-Se bonds in PEG-PUSeSe-PEG block copolymers are cleaved, resulting in the disassembly of micelles and the release of doxorubicin. Figure is taken from ref. [57].*

Moreover, also X-rays are employed to trigger the cleavage of Se-Se bond, resulting in the subsequent release of doxorubicin from micelles.[58] The release efficiency of doxorubicin in aforementioned applications after a radiation dose of 5 Gy is 40% and 30%, respectively, indicating the high reactivity of the diselenides towards radicals generated by the radiolysis of water. Alternatively, X-rays were employed indirectly to trigger pulsatile behavior of self-assembled nanocapsules, resulting in the controlled release of doxorubicin (Figure **8**). The X-rays are converted *in vivo* to UV-light as a result of the scintillation of zinc sulfide nanoparticles that are embedded in the membrane of the nanocapsules. The locally emitted UV-light initiates the isomerization of azo-benzene moieties in the nanocapsules membrane altering the diameter of the nanocapsules allowing controlled diffusion of doxorubicin. The reversible isomerization of the azo-benzene moieties enables reversibility of the nanocapsules size and the stepwise release of doxorubicin.[59] The

benefit of virtually unlimited penetration depth of radiation in tissue is clearly demonstrated here as X-rays reach deep tissue and generate locally UV light to control drug release, that would not be possible with externally applied UV light. Moreover, a similar drug release strategy was employed for a liposomal drug delivery system bearing gold nanoparticles in the bilayer that produce reactive oxygen species (ROS) upon X-ray radiation. The ROS generated destabilizes the membrane resulting in the release of anticancer drugs and overcoming the issues of penetration depth limitation.[60]

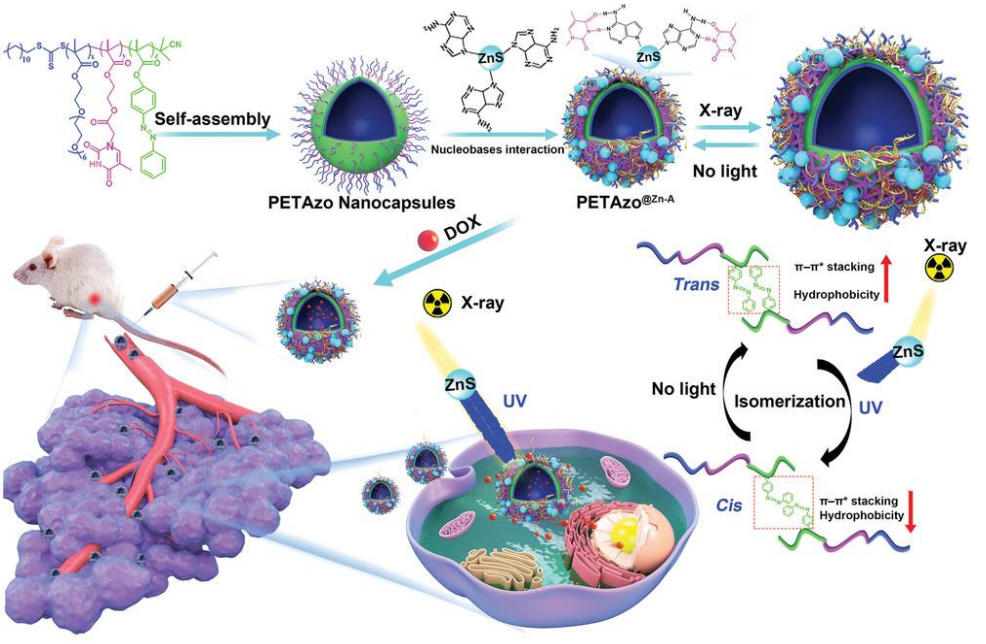

Figure 8. *Schematic overview of X-ray triggered doxorubicin release through reversible nanocapsule size increments. Nanocapsules are obtained after self-assembly of a poly(ethylene glycol)-b-polythymine-b-polyazobenzene ABC block copolymer (top left), which are then decorated with zinc sulfide nanoparticles via hydrogen bonding with the B-block. Scintillation by X-ray irradiation of the zinc sulfide nanoparticles, results in the emission of UV-light and the subsequent isomerization of the azo-benzene moieties in the C-block. The UV-light triggered isomerization to the cis-azo-benzene species lowers π-π stacking between azo-benzene groups, increasing the nanocapsules diameter and enables diffusion of doxorubicin out of the nanocapsules. Figure is taken from ref. [59].*

Gamma- and x-ray triggers typically lead to material disintegration, which is ideal for release applications such as drug delivery devices. In contrast bond formation induced by gamma radiation can be desirable in for example a self-healing process or when morphological changes of a material are desired. In chapter 4 of this thesis we present a secondary alkyne-alkyne crosslink strategy for dextran-based hydrogels, which allows for controlled contraction of the macroscopic 3D hydrogel structure.

1.4 MECHANICAL FORCE INDUCED MOLECULAR SIGNALLING

Mechanochemical activation is the result of mechanical forces such as shearing, scratching, impact, compression or ultrasound, causing chemical bonds to break or to rearrange. When applying mechanical force as physical trigger in smart materials it can be valuable in for example personal protection gear, sensing and indicating damage or initiate self-healing. Alternatively, mechanical force can trigger biological processes and initiate a signaling cascade. An early example of a force triggered biological process established in the laboratory is enzyme activation controlled by macroscopic stretching of fibers to which the enzymes are covalently attached (Figure **9**). By covalently binding the enzyme to the fiber, the enzyme and its active

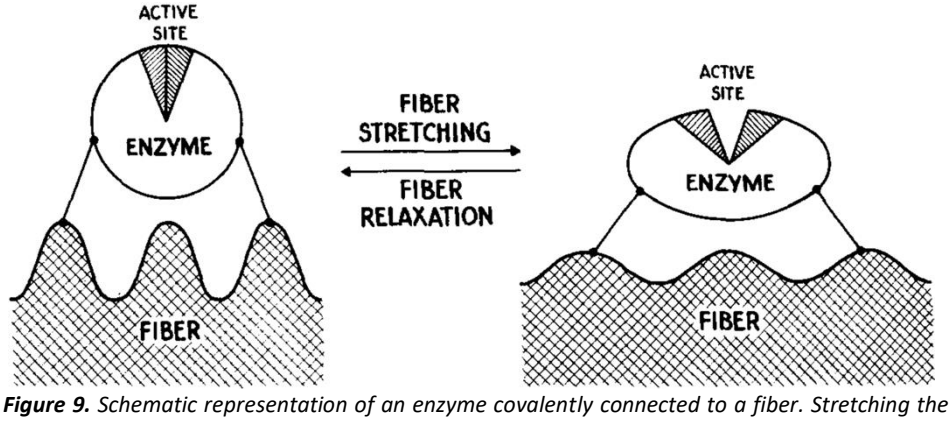

Figure 9. *Schematic representation of an enzyme covalently connected to a fiber. Stretching the fiber causes enzyme deformation resulting in an inactive enzyme. After relaxation of the fiber the enzyme returns to the original active conformation. Figure is taken from ref. [61].*

side is deformed when mechanical force is applied to the fiber resulting in an inactive enzyme, the enzymatic activity is restored when the fiber relaxes and the enzyme returns to the active conformational state.[61] Mechanical force is often used as physical trigger to break one specific bond in mechanophores. One such mechanophore is the spiropyran scaffold which has a yellow appearance, and when force is applied the C-O spiro bond ruptures and yields the purple merocyanine. This process is reversible as the C-O spiro bond can be restored by irradiating 6 hours with light.[62] Using this strategy polymeric materials are prepared that change their color when experiencing mechanical force. Such materials are employed as force sensor providing for visual detection and mapping of mechanical stresses in bulk

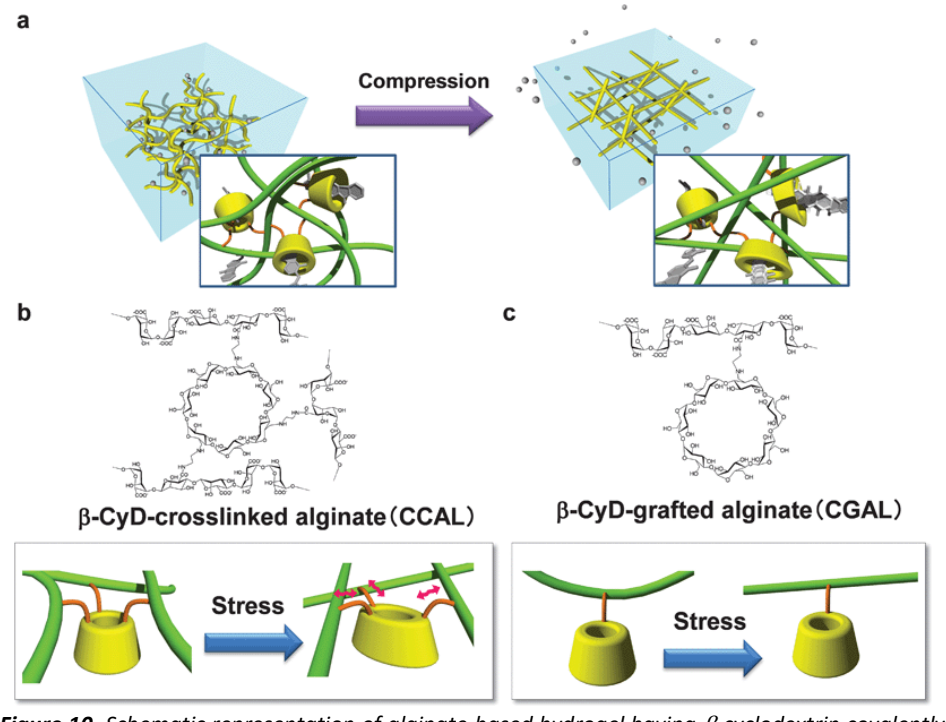

Figure 10. *Schematic representation of alginate-based hydrogel having β-cyclodextrin covalently crosslinked in its polymer network.* ***A)*** *In the initial state the β-cyclodextrin macrocycles efficiently bind a guest molecule. When the hydrogel is compressed the polymer chains are stretched, resulting in the deformation of β-cyclodextrin in which substrate binding is unfavorable leading to the release of the substrate.* ***B)*** *multi-crosslinked β-cyclodextrin, deforming after mechanical stress is applied.* ***C)*** *Single-crosslinked β-cyclodextrin, showing no deformation after mechanical stress is applied. Figure is taken from ref. [65].*

materials.[62-64] Alternatively, mechanical force is employed to liberate molecules that are covalently bound to the parent molecular structure, without breaking the materials polymer backbone. The liberation of such molecules could be the start signal for further 'smart' material behavior, such as the onset of catalyst activity catalyzing a specific reaction. Several methods are known and can be applied to translate mechanical force into the liberation of a chemical signal molecule or drug. One strategy relies on host-guest chemistry where β-cyclodextrin is covalently crosslinked to polysaccharide alginate and complexes in the uncompressed state ondansetron, an anti-emetic drug. Applying mechanical force to the hydrogel results in the deformation of the β-cyclodextrin, much alike enzyme deformation (Figure **9**), that lowers the binding affinity to ondansetron and results in the liberation of ondansetron (Figure **10**).[65] In this example, stretching the polymer backbone leads to molecular deformation. Alternatively, polymer stretching is employed to transmit force to relatively weak bonds that undergo cleavage to yield an expulsed molecule and a more stable polymer backbone. Using this strategy, dichlorocyclopropanes interconnected between long polymer chains, are stressed and release HCl that triggers a color change or induces fluorescence.[66, 67] A similar force transmitting strategy is used to break ferrocene and release Fe ions that might be employed as catalyst.[68, 69] Moreover, five mechanophores are shown in figure **11**, that upon force release potentially interesting molecules for the initiation of a signaling cascade. Example A, B and C all rely on a force induced retro-Diels Alder reaction, resulting in the expulsion of a (signaling) molecule. The mechanophore in example A is triggered by ultrasound after which an unstable furfuryl carbonate intermediate (end-group) is generated, that further decomposes in polar protic media to CO_2 and a leaving group of interest.[70] Example B and C show mechanophores that are triggered by applying macroscopic force (compression or strain), leading to the retro-Diels Alder reaction generating a small molecule while retaining an intact backbone structure.[71-74] The mechanophore in example D (Figure **11**) is also triggered by applying macroscopic force and releases a stable N-heterocyclic carbene (NHC), that

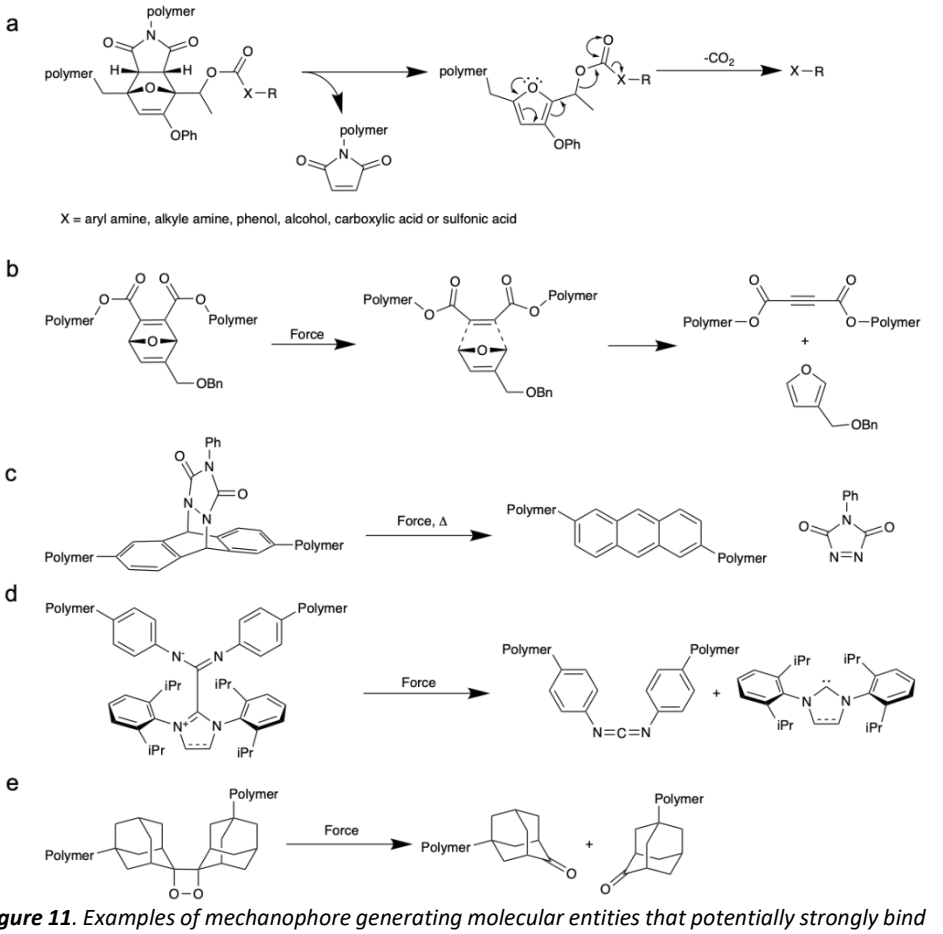

***Figure 11**. Examples of mechanophore generating molecular entities that potentially strongly bind to CB[7]. **A)** A genal approach for the release of small molecules triggered by sonication. **B)** A Retro Diels-Alder reaction triggered by mechanical compression, releasing a substituted furan. **C)** An anthracene based mechanophore releasing a small molecule after mechanical compression and heating. **D)** The N-heterocyclic carbene-carbodiimide (NHC-CDI) mechanophore releases the NHC after mechanical compression. **E)** A bis(adamantyl)-1,2-dioxetane unit incorporated between polymer chains, being cleaved by sonication leaving adamantyl end-groups.*

is particularly interesting considering the potentially strong binding to CB[7].[75] Alternatively, some polymer end groups might strongly bind to CB[7] and could act as a signal molecule (Figure **11E**). Potentially interesting mechanophores are polymeric bis(adamantly)dioxetanes, that are triggered upon sonication and after cleavage leave an adamantyl end-group.[76]

In chapter 2 we describe a catalyst inhibited when bound to CB[7] and the triggered onset of catalysis when a competitive guest is added. All molecules being expelled by the force activated mechanophores shown in figure **11** can have a strong interaction with CB[7], making them interesting to investigate. In chapter 5 of this thesis we present the synthesis of a mechanophore, having a signal molecule incorporated that is proven to instantly activate a copper carbene click chemistry catalyst.[77]

1.5 RESEARCH AIM AND THESIS OUTLINE

The aim of the work described in this thesis is to design smart polymer materials that through signal transduction triggered by external stimuli, such as small molecules, (UV) light, γ-radiation or mechanical force, enact a specific pre-programmed function. Signal generation and detection in several applications is presented and discussed in chapter 2, 3 ,4 and 5.

In chapter 1 we provide an overview of the state of the art of the four specific stimuli being employed in this thesis to control materials' behavior. In chapter 2 we focus on the design and synthesis of a copper carbene catalyst that we designed to strongly interact with CB[7]. Utilizing host-guest chemistry between catalyst and CB[7], we report catalyst inhibition and we demonstrate signal transduction using a small signaling molecule designed to competitively bind to CB[7] for the controlled activation of our catalyst. In chapter 3 we introduce the phenacyl scaffold as photocleavable moiety in hydrogel crosslinks enabling controlled release of cargo from dextran-based hydrogels. Also, we discuss Cerenkov light generated *in vivo* as stimulus for controlled release. In Chapter 4 we describe the phenomenon of γ-radiation controlled macroscopic hydrogel contraction and discuss possible future applications of the prepared hydrogels. Finally, in chapter 5 we present a strategy for the generation of chemical signals, that could be employed to control the copper

click catalysis presented in chapter 2. Furthermore, synthetic procedures for the synthesis of an oxanorbornadiene mechanophore are presented and discussed.

1.6 REFERENCES

1. Fernandez, C. A.; Correa, M.; Nguyen, M.-T.; Rod, K. A.; Dai, G. L.; Cosimbescu, L.; Rousseau, R.; Glezakou, V.-A., Progress and challenges in self-healing cementitious materials. *J. Mat. Sci.* **2021,** *56* (1), 201-230.
2. Zhang, H.; Ba, S.; Lee, J. Y.; Xie, J.; Loh, T.-P.; Li, T., Cancer Biomarker-Triggered Disintegrable DNA Nanogels for Intelligent Drug Delivery. *Nano Lett.* **2020,** *20* (11), 8399-8407.
3. Shi, Y.; Massagué, J., Mechanisms of TGF-β Signaling from Cell Membrane to the Nucleus. *Cell* **2003,** *113* (6), 685-700.
4. Assaf, K. I.; Nau, W. M., Cucurbiturils: from synthesis to high-affinity binding and catalysis. *Chem. Soc. Rev.* **2015,** *44* (2), 394-418.
5. Lee, J. W.; Samal, S.; Selvapalam, N.; Kim, H.-J.; Kim, K., Cucurbituril Homologues and Derivatives: New Opportunities in Supramolecular Chemistry. *Acc. Chem. Res.* **2003,** *36* (8), 621-630.
6. Cera, L.; Schalley, C. A., Stimuli-induced folding cascade of a linear oligomeric guest chain programmed through cucurbit[n]uril self-sorting (n = 6, 7, 8). *Chem. Sci.* **2014,** *5* (6), 2560-2567.
7. Tonga, G. Y.; Jeong, Y.; Duncan, B.; Mizuhara, T.; Mout, R.; Das, R.; Kim, S. T.; Yeh, Y.-C.; Yan, B.; Hou, S.; Rotello, V. M., Supramolecular regulation of bioorthogonal catalysis in cells using nanoparticle-embedded transition metal catalysts. *Nat. Chem.* **2015,** *7* (7), 597-603.
8. Angelos, S.; Yang, Y.-W.; Khashab, N. M.; Stoddart, J. F.; Zink, J. I., Dual-Controlled Nanoparticles Exhibiting AND Logic. *J. Am. Chem. Soc.* **2009,** *131* (32), 11344-11346.
9. Khashab, N. M.; Belowich, M. E.; Trabolsi, A.; Friedman, D. C. Valente, C.; Lau, Y.; Khatib, H. A.; Zink, J. I.; Stoddart, J. F., pH-Responsive mechanised nanoparticles gated by semirotaxanes. *Chem. Comm.* **2009,** (36), 5371-5373.
10. Jiao, Y.; Tang, B.; Zhang, Y.; Xu, J.-F.; Wang, Z.; Zhang, X., Highly Efficient Supramolecular Catalysis by Endowing the Reaction Intermediate with Adaptive Reactivity. *Angew. Chem. Int. Ed.* **2018,** *57* (21), 6077-6081.
11. Jiao, Y.; Li, W.-L.; Xu, J.-F.; Wang, G.; Li, J.; Wang, Z.; Zhang, X., A Supramolecularly Activated Radical Cation for Accelerated Catalytic Oxidation. *Angew. Chem. Int. Ed.* **2016,** *55* (31), 8933-8937.
12. Tang, B.; Zhao, J.; Jiao, Y.; Xu, J.-F.; Zhang, X., Cucurbit[7]uril promoted Fenton oxidation by modulating the redox property of catalysts. *Chem. Comm.* **2019,** *55* (94), 14127-14130.
13. Song, D.; Li, B.; Li, X.; Sun, X.; Li, J.; Li, C.; Xu, T. Zhu, Y.; Li, F.; Wang, N., Orthogonal Supramolecular Assembly Triggered by Inclusion and Exclusion

Interactions with Cucurbit[7]uril for Photocatalytic H2 Evolution. *ChemSusChem* **2020,** *13* (2), 394-399.

14. Lu, H.; Hu, R.; Bai, H.; Chen, H.; Lv, F.; Liu, L.; Wang, S.; Tian, H., Efficient Conjugated Polymer–Methyl Viologen Electron Transfer System for Controlled Photo-Driven Hydrogen Evolution. *ACS Appl. Mater. & Interfaces* **2017,** *9* (12), 10355-10359.
15. Li, G.; Trausel, F.; van der Helm, M. P.; Klemm, B.; Brevé, T. G.; van Rossum, S. A. P.; Hartono, M.; Gerlings, H. H. P. J.; Lovrak, M.; van Esch, J. H.; Eelkema, R., Tuneable Control of Organocatalytic Activity through Host–Guest Chemistry. *Angew. Chem. Int. Ed.* **2021,** *60* (25), 14022-14029.
16. Shaikh, M.; Mohanty, J.; Bhasikuttan, A. C.; Uzunova, V. D.; Nau, W. M.; Pal, H., Salt-induced guest relocation from a macrocyclic cavity into a biomolecular pocket: interplay between cucurbit[7]uril and albumin. *Chem. Comm.* **2008,** (31), 3681-3683.
17. Ghale, G.; Lanctôt, A. G.; Kreissl, H. T.; Jacob, M. H.; Weingart, H.; Winterhalter, M.; Nau, W. M., Chemosensing Ensembles for Monitoring Biomembrane Transport in Real Time. *Angew. Chem. Int. Ed.* **2014,** *53* (10), 2762-2765.
18. Remón, P.; González, D.; Romero, M. A.; Basílio, N.; Pischel, U., Chemical signal cascading in a supramolecular network. *Chem. Comm.* **2020,** *56* (26), 3737-3740.
19. Mohanty, J.; Thakur, N.; Dutta Choudhury, S.; Barooah, N.; Pal, H.; Bhasikuttan, A. C., Recognition-Mediated Light-Up of Thiazole Orange with Cucurbit[8]uril: Exchange and Release by Chemical Stimuli. *J. Phys. Chem. B* **2012,** *116* (1), 130-135.
20. Florea, M.; Nau, W. M., Strong Binding of Hydrocarbons to Cucurbituril Probed by Fluorescent Dye Displacement: A Supramolecular Gas-Sensing Ensemble. *Angew. Chem. Int. Ed.* **2011,** *50* (40), 9338-9342.
21. Carvalho, C. P.; Uzunova, V. D.; Da Silva, J. P.; Nau, W. M.; Pischel, U., A photoinduced pH jump applied to drug release from cucurbit[7]uril. *Chem. Comm.* **2011,** *47* (31), 8793-8795.
22. Oun, R.; Floriano, R. S.; Isaacs, L.; Rowan, E. G.; Wheate, N. J., The ex vivo neurotoxic, myotoxic and cardiotoxic activity of cucurbituril-based macrocyclic drug delivery vehicles. *Toxicol. Res.* **2014,** *3* (6), 447-455.
23. Walker, S.; Oun, R.; McInnes, F. J.;Wheate, N. J., The Potential of Cucurbit[n]urils in Drug Delivery. *Isr. J. Chem.* **2011,** *51* (5-6), 616-624.
24. Chen, Y.; Huang, Z.; Zhao, H.; Xu, J.-F.; Sun, Z.; Zhang, X., Supramolecular Chemotherapy: Cooperative Enhancement of Antitumor Activity by Combining Controlled Release of Oxaliplatin and Consuming of Spermine by Cucurbit[7]uril. *ACS Appl. Mater. & Interfaces* **2017,** *9* (10), 8602-8608.

25. Dang, D. T.; Nguyen, H. D.; Merkx, M.; Brunsveld, L., Supramolecular Control of Enzyme Activity through Cucurbit[8]uril-Mediated Dimerization. *Angew. Chem. Int. Ed.* **2013,** *52* (10), 2915-2919.
26. Chinai, J. M.; Taylor, A. B.; Ryno, L. M.; Hargreaves, N. D.; Morris, C. A.; Hart, P. J.; Urbach, A. R., Molecular Recognition of Insulin by a Synthetic Receptor. *J. Am. Chem. Soc.* **2011,** *133* (23), 8810-8813.
27. Urbach, A. R.; Ramalingam, V., Molecular Recognition of Amino Acids, Peptides, and Proteins by Cucurbit[n]uril Receptors. *Isr. J. Chem.* **2011,** *51* (5-6), 664-678.
28. Palma, A.; Artelsmair, M.; Wu, G.; Lu, X.; Barrow, S. J.; Uddin, N.; Rosta, E.; Masson, E.; Scherman, O. A., Cucurbit[7]uril as a Supramolecular Artificial Enzyme for Diels–Alder Reactions. *Angew. Chem. Int. Ed.* **2017,** *56* (49), 15688-15692.
29. Krasia, T. C.; Steinke, J. H. G., Formation of oligotriazoles catalysed by cucurbituril. *Chem. Comm.* **2002,** (1), 22-23.
30. Peppas, N. A.; Bures, P.; Leobandung, W.; Ichikawa, H., Hydrogels in pharmaceutical formulations. *Eur. J. Pharm. Biopharm.* **2000,** *50* (1), 27-46.
31. Caló, E.; Khutoryanskiy, V. V., Biomedical applications of hydrogels: A review of patents and commercial products. *Eur. Polym. J.* **2015,** *65*, 252-267.
32. Wang, Y.; Kohane, D. S., External triggering and triggered targeting strategies for drug delivery. *Nat. Rev. Mater.* **2017,** *2* (6), 17020.
33. Sunar, U.; Rohrbach, D.; Rigual, N.; Tracy, E.; Keymel, K.; Cooper, M. T.; Baumann, H.; Henderson, B. H., Monitoring photobleaching and hemodynamic responses to HPPH-mediated photodynamic therapy of head and neck cancer: a case report. *Opt. Express* **2010,** *18* (14), 14969-78.
34. Janis, S.; Daumants, P. In *Clinical potential of the side-glowing optical fibers*, Proc. SPIE, 1997.
35. Yang, M.; Huang, J.; Fan, J.; Du, J.; Pu, K.; Peng, X., Chemiluminescence for bioimaging and therapeutics: recent advances and challenges. *Chem. Soc. Rev.* **2020,** *49* (19), 6800-6815.
36. Chen, F.; Warnock, R. L.; Van der Meer, J. R.; Wegner, S. V., Bioluminescence-Triggered Photoswitchable Bacterial Adhesions Enable Higher Sensitivity and Dual-Readout Bacterial Biosensors for Mercury. *ACS Sensors* **2020,** *5* (7), 2205-2210.
37. Shaffer, T. M.; Pratt, E. C.; Grimm, J., Utilizing the power of Cerenkov light with nanotechnology. *Nat. Nanotechnol.* **2017,** *12* (2), 106-117.
38. Kano, K.; Tanaka, Y.; Ogawa, T.; Shimomura, M.; Okahata, Y.; Kunitake, T., photoresponsive membranes. regulation of membrane properties by photoreversible cis–trans isomerization of azobenzenes. *Chem. Lett.* **1980,** *9* (4), 421-424.

39. Girotti, A. W., photodynamic lipid peroxidation in biological systems. *Photochemistry and Photobiology* **1990,** *51* (4), 497-509.
40. Wu, G.; Mikhailovsky, A.; Khant, H. A.; Fu, C.; Chiu, W.; Zasadzinski, J. A., Remotely Triggered Liposome Release by Near-Infrared Light Absorption via Hollow Gold Nanoshells. *J. Am. Chem. Soc.* **2008,** *130* (26), 8175-8177.
41. Wu, W.; Shen, J.; Banerjee, P.; Zhou, S., Core–shell hybrid nanogels for integration of optical temperature-sensing, targeted tumor cell imaging, and combined chemo-photothermal treatment. *Biomaterials* **2010,** *31* (29), 7555-7566.
42. Goodwin, A. P.; Mynar, J. L.; Ma, Y.; Fleming, G. R.; Fréchet, J. M. J., Synthetic Micelle Sensitive to IR Light via a Two-Photon Process. *J. Am. Chem. Soc.* **2005,** *127* (28), 9952-9953.
43. Fomina, N.; Sankaranarayanan, J.; Almutairi, A., Photochemical mechanisms of light-triggered release from nanocarriers. *Adv. Drug Del. Rev.* **2012,** *64* (11), 1005-1020.
44. Men, Y.; Brevé, T.G.; Liu, H.; Denkova, A. G.; Eelkema, R., Photo cleavable thioacetal block copolymers for controlled release. *Polym. Chem.* **2021**.
45. LeValley, P. J.; Neelarapu, R.; Sutherland, B. P.; Dasgupta, S.; Kloxin, C. J.; Kloxin, A. M., Photolabile Linkers: Exploiting Labile Bond Chemistry to Control Mode and Rate of Hydrogel Degradation and Protein Release. *J. Am. Chem. Soc.* **2020,** *142* (10), 4671-4679.
46. Kloxin, A. M.; Kasko, A. M.; Salinas, C. N.; Anseth, K. S., Photodegradable hydrogels for dynamic tuning of physical and chemical properties. *Science (New York, N.Y.)* **2009,** *324* (5923), 59-63.
47. Bryant, S. J.; Cuy, J. L.; Hauch, K. D.; Ratner, B. D., Photo-patterning of porous hydrogels for tissue engineering. *Biomaterials* **2007,** *28* (19), 2978-2986.
48. Kharkar, P. M.; Kiick, K. L.; Kloxin, A. M., Design of thiol- and light-sensitive degradable hydrogels using Michael-type addition reactions. *Polym. Chem.* **2015,** *6* (31), 5565-5574.
49. LeValley, P. J.; Sutherland, B. P.; Jaje, J.; Gibbs, S.; Jones, R. M.; Gala, R. P.; Kloxin, C. J.; Kiick, K. L.; Kloxin, A. M., On-Demand and Tunable Dual Wavelength Release of Antibodies Using Light-Responsive Hydrogels. *ACS Appl. Bio Mater.* **2020,** *3* (10), 6944-6958.
50. More, C. V.; Alsayed, Z.; Badawi, M. S.; Thabet, A. A.; Pawar, P. P., Polymeric composite materials for radiation shielding: a review. *Environ. Chem. Lett.* **2021,** *19* (3), 2057-2090.
51. Ghobashy, M. M.; El-Sattar, N. E. A. A., Radiation Synthesis of Rapidly Self-Healing Hydrogel Derived from Poly(acrylic acid) with Good Mechanical Strength. *Macromol. Chem. Phys.* **2020,** *221* (19), 2000218.

52. Peppas, N. A.; Keys, K. B.; Torres-Lugo, M.; Lowman, A. M., Poly(ethylene glycol)-containing hydrogels in drug delivery. *J. Contr. Rel.* **1999,** *62* (1), 81-87.
53. Kim, J.; Oh, I.; Park, S.; Nguyen, N. Q.; Ryu, J.; Sohn, D., Characteristics of self-healable laponite-poly(N-isopropylacrylamide) hydrogels prepared by γ-ray irradiation. *Polymer* **2021,** *214*, 123365.
54. Wang, M.; Xu, L.; Hu, H.; Zhai, M.; Peng, J.; Nho, Y.; Li, J.; Wei, G., Radiation synthesis of PVP/CMC hydrogels as wound dressing. *Nucl. Instrum. Methods Phys. Res. B: Beam Interactions with Materials and Atoms* **2007,** *265* (1), 385-389.
55. Berrington de González, A.; Mahesh, M.; Kim, K.-P.; Bhargavan, M.; Lewis, R.; Mettler, F.; Land, C., Projected Cancer Risks From Computed Tomographic Scans Performed in the United States in 2007. *Arch. Intern. Med.* **2009,** *169* (22), 2071-2077.
56. Hodge, J. W.; Guha, C.; Neefjes, J.; Gulley, J. L., Synergizing radiation therapy and immunotherapy for curing incurable cancers. Opportunities and challenges. *Oncology (Williston Park)* **2008,** *22* (9), 1064-70; discussion 1075, 1080-1, 1084.
57. Ma, N.; Xu, H.; An, L.; Li, J.; Sun, Z.; Zhang, X., Radiation-Sensitive Diselenide Block Co-polymer Micellar Aggregates: Toward the Combination of Radiotherapy and Chemotherapy. *Langmuir* **2011,** *27* (10), 5874-5878.
58. Wang, J.; Xu, W.; Zhang, N.; Yang, C.; Xu, H.; Wang, Z.; Li, B.; Ding, J.; Chen, X., X-ray-responsive polypeptide nanogel for concurrent chemoradiotherapy. *J. Contr. Rel.* **2021,** *332*, 1-9.
59. Deng, H.; Lin, L.; Wang, S.; Yu, G.; Zhou, Z.; Liu, Y.; Niu, G.; Song, J.; Chen, X., X-ray-Controlled Bilayer Permeability of Bionic Nanocapsules Stabilized by Nucleobase Pairing Interactions for Pulsatile Drug Delivery. *Adv. Mater.* **2019,** *31* (37), 1903443.
60. Deng, W.; Chen, W.; Clement, S.; Guller, A.; Zhao, Z.; Engel, A.; Goldys, E. M., Controlled gene and drug release from a liposomal delivery platform triggered by X-ray radiation. *Nat. Comm.* **2018,** *9* (1), 2713.
61. Klibanov, A. M.; Samokhin, G. P.; Martinek, K.; Berezin, I. V., Enzymatic mechanochemistry: A new approach to studying the mechanism of enzyme action. *Biochim. Biophys. Acta (BBA) - Enzymology* **1976,** *438* (1), 1-12.
62. Davis, D. A.; Hamilton, A.; Yang, J.; Cremar, L. D.; Van Gough, D.; Potisek, S. L.; Ong, M. T.; Braun, P. V.; Martínez, T. J.; White, S. R.; Moore, J. S.; Sottos, N. R., Force-induced activation of covalent bonds in mechanoresponsive polymeric materials. *Nature* **2009,** *459*, 68.
63. Li, M.; Liu, W.; Zhang, Q.; Zhu, S., Mechanical Force Sensitive Acrylic Latex Coating. *ACS Appl. Mater. & Interfaces* **2017,** *9* (17), 15156-15163.

64. Chen, H.; Yang, F.; Chen, Q.; Zheng, J., A Novel Design of Multi-Mechanoresponsive and Mechanically Strong Hydrogels. *Adv. Mater.* **2017,** *29* (21), 1606900.
65. Izawa, H.; Kawakami, K.; Sumita, M.; Tateyama, Y.; Hill, J. P.; Ariga, K., β-Cyclodextrin-crosslinked alginate gel for patient-controlled drug delivery systems: regulation of host–guest interactions with mechanical stimuli. *J. Mater. Chem.* **2013,** *1* (16), 2155-2161.
66. Lin, Y.; Kouznetsova, T. B.; Craig, S. L., A Latent Mechanoacid for Time-Stamped Mechanochromism and Chemical Signaling in Polymeric Materials. *J. Am. Chem. Soc.* **2020,** *142* (1), 99-103.
67. Diesendruck, C. E.; Steinberg, B. D.; Sugai, N.; Silberstein, M. N.; Sottos, N. R.; White, S. R.; Braun, P. V.; Moore, J. S., Proton-Coupled Mechanochemical Transduction: A Mechanogenerated Acid. *J. Am. Chem. Soc.* **2012,** *134* (30), 12446-12449.
68. Sha, Y.; Zhang, Y.; Xu, E.; Wang, Z.; Zhu, T.; Craig, S. L.; Tang, C., Quantitative and Mechanistic Mechanochemistry in Ferrocene Dissociation. *ACS Macro Lett.* **2018,** *7* (10), 1174-1179.
69. Di Giannantonio, M.; Ayer, M. A.; Verde-Sesto, E.; Lattuada, M.; Weder, C.; Fromm, K. M., Triggered Metal Ion Release and Oxidation: Ferrocene as a Mechanophore in Polymers. *Angew. Chem. Int. Ed.* **2018,** *57* (35), 11445-11450.
70. Hu, X.; Zeng, T.; Husic, C. C.; Robb, M. J., Mechanically Triggered Small Molecule Release from a Masked Furfuryl Carbonate. *J. Am. Chem. Soc.* **2019,** *141* (38), 15018-15023.
71. Ghanem, M. A.; Basu, A.; Behrou, R.; Boechler, N.; Boydston, A. J.; Craig, S. L.; Lin, Y.; Lynde, B. E.; Nelson, A.; Shen, H.; Storti, D. W., The role of polymer mechanochemistry in responsive materials and additive manufacturing. *Nat. Rev. Mater.* **2021,** *6* (1), 84-98.
72. Gossweiler, G. R.; Hewage, G. B.; Soriano, G.; Wang, Q.; Welshofer, G. W.; Zhao, X.; Craig, S. L., Mechanochemical Activation of Covalent Bonds in Polymers with Full and Repeatable Macroscopic Shape Recovery. *ACS Macro Lett.* **2014,** *3* (3), 216-219.
73. Larsen, M. B.; Boydston, A. J., "Flex-Activated" Mechanophores: Using Polymer Mechanochemistry To Direct Bond Bending Activation. *J. Am. Chem. Soc.* **2013,** *135* (22), 8189-8192.
74. Larsen, M. B.; Boydston, A. J., Successive Mechanochemical Activation and Small Molecule Release in an Elastomeric Material. *J. Am. Chem. Soc.* **2014,** *136* (4), 1276-1279.

75. Shen, H.; Larsen, M. B.; Roessler, A. G.; Zimmerman, P. M.; Boydston, A. J., Mechanochemical Release of N-Heterocyclic Carbenes from Flex-Activated Mechanophores. *Angew. Chem. Int. Ed.* **2021,** *60* (24), 13559-13563.

76. Chen, Y.; Sijbesma, R. P., Dioxetanes as Mechanoluminescent Probes in Thermoplastic Elastomers. *Macromol.* **2014,** *47* (12), 3797-3805.

77. Brevé, T. G.; Filius, M.; Araman, C.; van der Helm, M. P.; Hagedoorn, P.-L.; Joo, C.; van Kasteren, S. I.; Eelkema, R., Conditional Copper-Catalyzed Azide–Alkyne Cycloaddition by Catalyst Encapsulation. *Angew. Chem. Int. Ed.* **2020,** *59* (24), 9340-9344.

CHAPTER

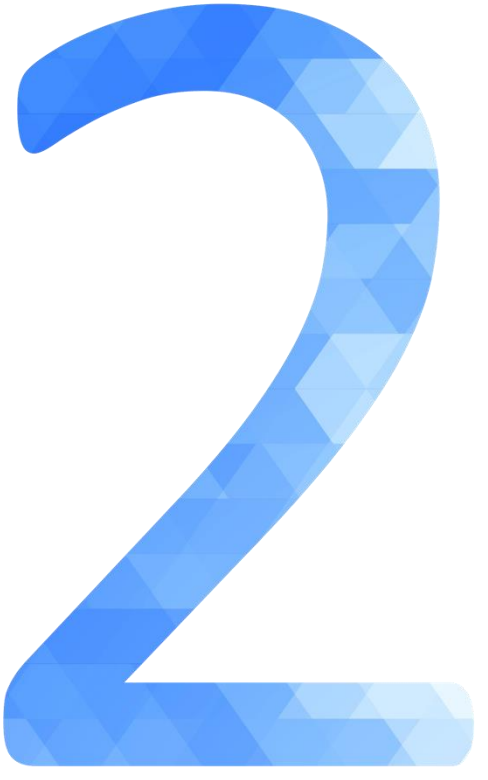

CONDITIONAL COPPER-CATALYZED AZIDE-ALKYNE CYCLOADDITION BY CATALYST ENCAPSULATION

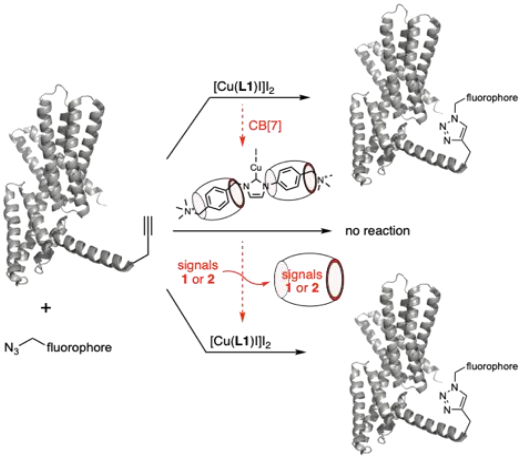

Supramolecular encapsulation is known to alter chemical properties of guest molecules. Here we apply this strategy of molecular encapsulation to temporally control the catalytic activity of a stable Cu(I)-carbene catalyst. Encapsulation of the Cu(I)-carbene catalyst by supramolecular host cucurbit[7]uril (CB[7]) resulted in the complete inactivation of a copper catalyzed alkyne-azide cycloaddition (CuAAC) reaction. The addition of a chemical signal achieved the near instantaneous activation of the catalyst, by releasing the catalyst from the inhibited CB[7] catalyst complex. To broaden the scope of our on demand CuAAC reaction, we demonstrated the protein labelling of Vinculin using the Cu(I)-carbene catalyst, to inhibit its activity by encapsulation with CB[7], and to initiate labelling at any moment by adding a specific signal molecule. Ultimately, this strategy allows for temporal control over copper-catalyzed click chemistry, on small molecules as well as protein targets.

This chapter is published as:
Brevé, T. G.; Filius, M.; Araman, C.; van der Helm, M. P.; Hagedoorn, P.-L.; Joo, C.; van Kasteren, S. I.; Eelkema, R., conditional copper catalyzed azide-alkyne cycloaddition by catalyst encapsulation, Angew. Chem. Int. Ed. ***2020****, 59 (24), 9340-9344.*

2.1 INTRODUCTION

2

In this chapter we use an external chemical signal to control the rate of copper catalyzed alkyne-azide cycloaddition (CuAAC) reactions. CuAAC, commonly viewed as one of the primary click reactions[1], is a robust way of 'clicking'[2] a large range of azide and terminal alkyne functionalized molecules together in biological and material-based environments and has been used in many different settings.[3-6] There is, however, also an increased need for the spatiotemporal control of these click reactions,[7, 8] usually instilled by light activated click chemistry, with potential phototoxicity and side-reactions offering problems in this approach. In expanding the CuAAC toolbox there is therefore a desire to also have a general method to spatiotemporally control the catalytic activity of the CuAAC. Using this tool would allow spatiotemporal control over gel formation[9], polymer conjugation, material properties, fluorescent properties and biomolecule labelling. Host-guest chemistry is an approach that could serve to control the chemical properties of encapsulated guests.[10-14] Here, we use host-guest chemistry to switch from an inactive catalytic state of the Cu-catalyst to an active one. A promising class of hosts for encapsulating small molecule guests in aqueous environments is the cucurbituril family. Cucurbituril is a versatile molecular container (Figure **1A**) that is biocompatible, has a relatively low toxicity[15] and has been used in many different systems to encapsulate drugs[16-20], fluorescent dyes[21-25] and biologically active molecules[26-28]. In some specific cases, cucurbiturils can also act as catalysts themselves, for example in the cycloaddition[29, 30] of alkynes and alkyl azides or in promoting acid hydrolysis.[31] Furthermore, compartmentalized structures with a cucurbituril barrier can be used to shield substrate from catalyst, leading to reduced turnover. There, addition of a competitive guest removes the cucurbiturils and restores catalytic activity.[32] In that respect, Leigh and co-workers showed using rotaxane based switchable organocatalysts, that shielding the catalytic center with a macrocycle is an effective approach to regulate catalytic activity.[33-35] In our work we want to use cucurbiturils

to encapsulate a copper catalyst to directly modulate its catalytic activity in the CuAAC.

There are reports of triggered CuAAC, which rely on mechanochemical processes converting an inactive copper(I) biscarbene catalyst to an active copper(I) monocarbene catalyst.[36, 37] Besides mechano-based triggers, on demand CuAAC can also be achieved by electro-[38] and light-based[39-41] triggers. Another interesting strategy for control over catalytic activity in the CuAAC is reported by Schmittel and co-workers, where they prepared a molecular switch that can release a Cu(I) catalyst.[42]

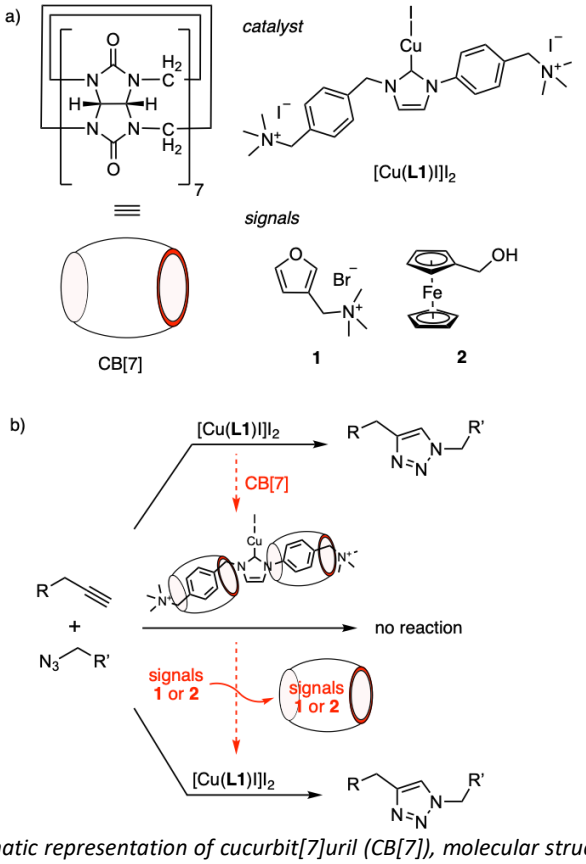

Figure 1. A) *Schematic representation of cucurbit[7]uril (CB[7]), molecular structure of Cu(I)-NHC [Cu(**L1**)I]I2, signal molecule **1** (3-((furylmethyl)trimethyl ammonium) bromide) and signal molecule **2** (hydroxymethyl ferrocene).* ***B)*** *when [Cu(**L1**)I]I2 is encapsulated by CB[7] the catalytic activity in the CuAAC is 'switched off'. After the addition of the signal molecule **1** or **2**, [Cu(**L1**)I]I2 is released which 'switches on' the catalytic activity.*

In this chapter, the basic switching from an 'off' state to an 'on' state relies on the host guest chemistry between the catalyst and cucurbit[7]uril (CB[7]). The catalyst is designed in such a way that CB[7] binds with high affinity to the *N*-heterocyclic carbene (NHC) ligand coordinating to the Cu(I) center. When CB[7] is bound to the Cu(I)-NHC, the Cu(I) center is not catalytically active, most likely because it is not accessible for substrates or unable to form a catalytically active species. However, when a stronger binding guest (a chemical signal) is added to the system, the catalyst will be released from CB[7], after which the liberated catalyst can catalyze the click reaction (Figure **1B**). We selected copper carbene catalysts because of their high stability in aqueous environments, high activity in bioconjugation settings[43] and the possibility to modify the NHC ligand in such a way that it binds to CB[7]. The ligand can bind to CB[7] through favorable interactions between its positively charged ammonium groups and the polar portal area of CB[7], as well as interactions between the apolar benzene rings and the apolar cavity of CB[7]. Using this catalyst, we demonstrate temporal control over catalytic activity in copper catalyzed azide alkyne cycloaddition in a controlled model reaction and on a biomacromolecule, where protein labelling is initiated on demand.

2.2 RESULTS AND DISCUSSION

The catalyst was synthesized in five steps to yield stable Cu(I)-NHC [Cu(**L1**)I]I_2 (elaborate synthesis details in SI). The complex is soluble in a DMSO/MES buffer (100 mM, pH 6.4, 25% v/v DMSO) solution. We used the model reaction shown in Figure **2A** to explore the activity of [Cu(**L1**)I]I_2. Azide **3** and propargyl alcohol (**4**) were selected based on their water solubility and low binding affinity to CB[7] (Figure **S15**). In a typical reaction, azide **3** and propargyl alcohol (**4**) were dissolved in MES buffer after which the catalyst (2 mol% relative to **3**) dissolved in DMSO was added. Under these conditions at 25 °C, full conversion to triazole **5** was reached after approximately 180 min (Figure **2B**, magenta line). An estimate of the reaction rate

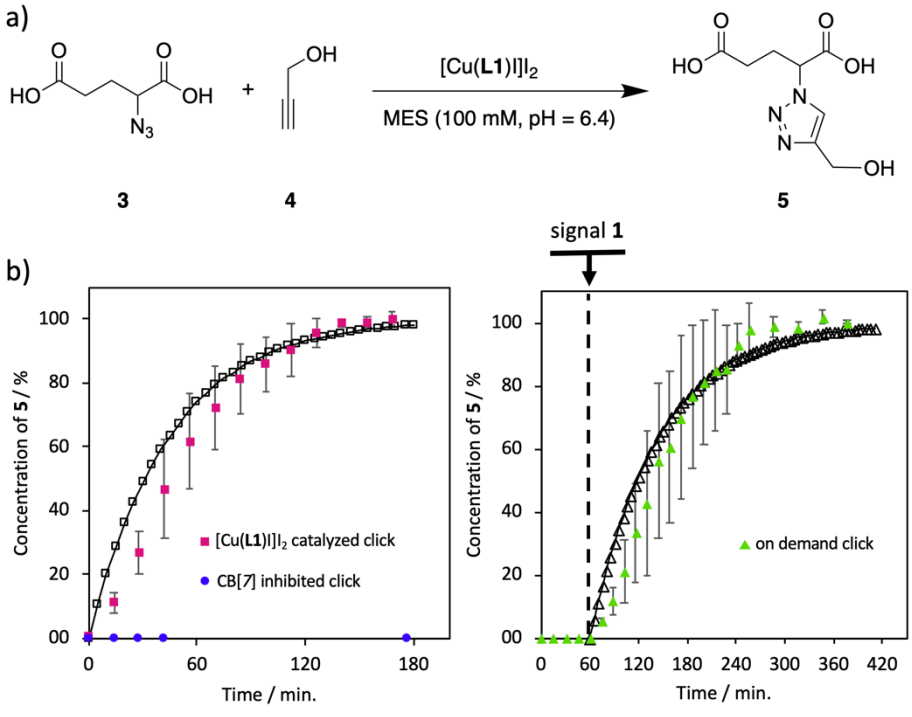

Figure 2. A) *Model click reaction used to investigate the catalytic activity of [Cu(**L1**)I]I$_2$.* ***B left)*** *formation of triazole **5** in MES buffer (100 mM, pH = 6.4, 25% (v/v) DMSO) catalyzed by [Cu(**L1**)I]I$_2$ (0.4 mM) ([**3**] = 15 mM, [**4**] = 57 mM). Full conversion is reached after 180 min (magenta). Error bars are standard deviations after n = 3 experiments. Open squares represent a pseudo-first order model fit to experimental data. Encapsulating [Cu(**L1**)I]I$_2$ with CB[7] results in a catalyst CB[7] complex that does not show any catalytic activity (blue).* ***B right)*** *To restore catalytic activity, signal molecule **1** is added at t = 60 min. (dashed line) to the inhibited catalyst CB[7] complex. This results in the immediate activation of Cu(I) catalyzed click reaction (green). Error bars are standard deviations after n = 2 experiments. Open triangles represent a pseudo-first order model based on signal activation of CB[7] inhibited [Cu(**L1**)I]I$_2$ (Figure **S9**).*

constant gave the same order of magnitude value ((6 $\pm$ 2) x 10^4 M^{-1} s^{-1} (per M Cu), n = 3) as with reported systems using typical Cu(I) with activating triazole ligands in similar reaction conditions (see SI for detailed description).[44] When determining the rate constant under pseudo first order conditions (Figure **S16**), a rate constant of 2 x 10^4 M^{-1} s^{-1} (per M Cu) was found, confirming the model in Figure **2A**.

The binding between CB[7] and [Cu(**L1**)I]I$_2$ was examined using ^{1}H-NMR and isothermal titration calorimetry (ITC) (Figure **S12**-**14**). Using the method of

continuous variation (Figure **S12** and **S13**) we determined that the binding stoichiometry between CB[7] and [Cu(**L1**)I]I_2 is 2:1, and binding constants K_{a1} and K_{a2} are (1.21 ± 0.08) x 10^9 M^{-1} and (3.5 ± 0.3) x 10^6 M^{-1}, respectively (Figure **S14**). When using catalyst [Cu(**L1**)I]I_2 that was pre-mixed with 4.6 equivalents of CB[7] (2:1 CB[7]⊂[Cu(**L1**)I]I_2 complex formation is ≥99.97% in these conditions), no formation of triazole **5** was detected over the course of 7.5 h (Figure **2B**, blue, data shown up to 180 min). This result demonstrates that the 2:1 binding of CB[7] to [Cu(**L1**)I]I_2 effectively switches off the catalytic activity of [Cu(**L1**)I]I_2. The catalytic activity of the 1:1 CB[7]:[Cu(**L1**)I]I_2 complex was also examined and shows conversion of azide **3** to triazole **5** (Figure **S10**, reaction rate constant is in the same order of magnitude compared to the uninhibited experiment). In order to demonstrate the temporal control in CuAAC, an experiment was conducted in which signal molecule **1** 3-(furylmethyl)trimethyl ammonium bromide (Figure **1A**, compound **1**) was added (8.8 equivalents relative to CB[7], compound **1**⊂CB[7] complex formation is ≥99.99% in these conditions) to the CB[7] inhibited catalyst CB[7] complex.

Positively charged signal molecule **1** has a strong interaction (K_a = (1.8 ± 0.2) x 10^7 M^{-1}) to CB[7] in an aqueous environment. We therefore expect that the CB[7] bound catalyst (inactive) can be displaced from the CB[7] cavity by adding **1**, activating the catalyst. We added the 2:1 CB[7]⊂[Cu(**L1**)I]I_2 complex to a mixture of **3** and **4** in MES/DMSO, to confirm that no reaction took place over the course of 60 min. At t = 60 min we added signal molecule **1**, at which point the click reaction yielding triazole **5** immediately started (Figure **2B**, dashed line). The reaction reached complete conversion approximately 200 min after signal addition, showing a reaction rate after activation that is in the same order of magnitude as the free catalyst rate (Figure **2B**, green line). Combined, these results show that it is possible to deactivate a click catalyst by supramolecular encapsulation, and that it can be reactivated using a chemical signal. With this in hand, we were interested to find

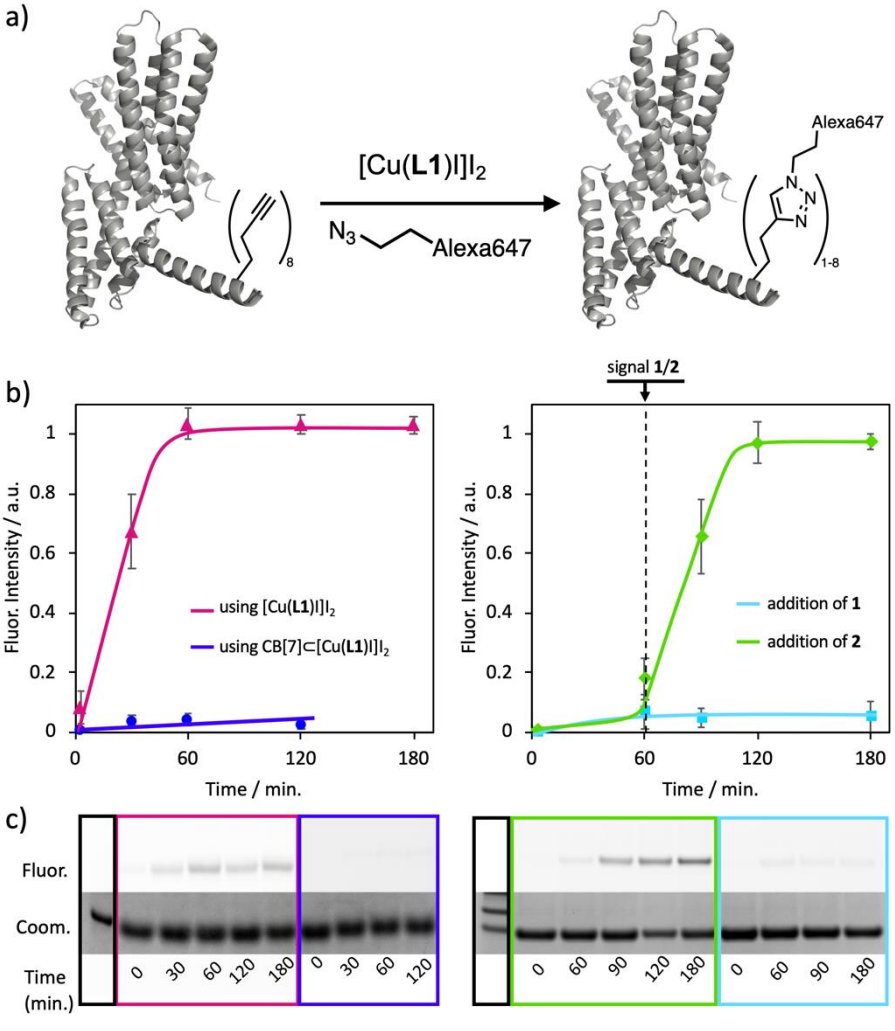

***Figure 3**. **A)** schematic illustration of alkyne handle modified Vinculin protein, which can be fluorescently labelled with azide-Alexa 647, catalyzed by [Cu(**L1**)I]I$_2$. The recombinant Vinculin protein has 8 alkyne groups at various positions in its structure. **B)** left panel: relative fluorescence labeling conversion over time, showing uninhibited fluorescence labeling reaching its maximum value after approximately 60 min (magenta); CB[7] inhibited fluorescence labeling, over the course of 120 min no significant labeling is observed (blue). Right panel: activation of fluorescence labeling using signal molecules. After 60 min (dashed line) of reaction using CB[7]-inhibited catalyst, signal molecule **1** was added, showing no catalyst activation (cyan). In a similarly inhibited sample, signal molecule **2** was added after 60 min (dashed line), leading to immediate fluorescent labeling (green). Lines are drawn to guide the eye. **C)** Scans of stained gels with Coomassie (Coom.), and analyzed for fluorescent intensity (Fluor.) over time (min.). Coomassie bands shown in the black frames indicate the 40 kDa protein marker (recombinant Vinculin MW (453-724 amino acid sequence of wild type Vinculin) is 35.6 kDa).*

out if our method would allow temporal control over protein labelling using a chemical trigger. To test this, we designed an assay of clicking fluorescent molecules to a protein. We obtained recombinant Vinculin[45] equipped with multiple alkyne click handles. Vinculin is a cytoskeletal protein with a molecular weight of 116 kDa and it has been shown to play a role in cell-matrix and cell-cell adhesions.[46] Moreover, it has been associated with anti-citrullinated protein antibody (ACPA) positive rheumatoid arthritis as an antigen.[47] Using alkyne-modified recombinant Vinculin (35.6 kDa), we sought to attach the azide version of the Alexa 647 fluorescent probe (Figure **3A**). We mixed Vinculin with Alexa 647 in MES buffer (100 mM, pH 6.4, 25% v/v DMSO) and observed that the reaction took place after addition of the catalyst (Figure **3B**, magenta line & **3C** magenta square).

Furthermore, we observed that the fluorescent labeling of Vinculin reaches its maximum relative value after 60 min, suggesting that the solvent available alkyne moieties have been labelled. Next we evaluated if we can inhibit the catalyst with CB[7]. Performing the labeling reaction with a mixture of CB[7] and [Cu(**L1**)I]I_2 (7.4:1 ratio) showed no conversion to the fluorescently labelled protein (Figure **3B** blue line & **3C**, blue square). This result agrees with our previous findings in the small molecule reaction forming triazole **5**. To switch on the catalytic activity and allow for a click reaction to occur, a stronger binding guest (signal molecule) for CB[7] was added as a signal molecule. In the first instance we used signal molecule **1** (Figure **1A**), as this triggered the model click reaction immediately after the addition (Figure **2B**). However, we found that signal molecule **1** was not able to trigger the protein labeling (Figure **3B** and **C**, cyan data). We tried various high affinity guests for CB[7], such as amantadine (K_a = 4.23 x 10^{12} M^{-1})[48], phenylalanine (K_a = 1.8 x 10^6 M^{-1})[28] and dimethylaminomethyl-ferrocene (K_a = 10^{12})[49, 50], but none of these guests triggered labeling of the protein. We hypothesized that these positively charged guests might have a strong non-specific interaction with the protein, due to a large negatively charged patch on the outside of the protein (Figure **S11**). This patch may bind the guests, thereby preventing the guests from interacting with the inactive CB[7]

catalyst complex. In order to test this hypothesis, we used non-charged hydroxymethyl ferrocene **2** (K_a = 3.0 x 10^9 M^{-1})[51] (Figure **1A**). The green line in figure **3B** shows that, directly after the addition of signal molecule **2** the protein labeling started. Absolute fluorescence reached its maximum value 60 min after the addition of the signal molecule, again showing a kinetic profile similar to the uninhibited catalyst. This result demonstrates that a competitive guest can act as a signal molecule to activate the Cu(I) catalyst for protein labeling using click chemistry.

2.3 CONCLUSION AND OUTLOOK

To conclude, we synthesized the [Cu(**L1**)I]I_2 catalyst and demonstrated that it effectively catalyzes the azide-alkyne click reaction. The catalyst binds to CB[7] in aqueous environments, leading to a complete loss in catalytic activity. A competitive guest for CB[7] can act as a chemical signal, leading to release and activation of the catalyst, as we have demonstrated in both a small molecule model reaction and in a protein labelling experiment. These results show that host guest chemistry is a powerful tool to exert temporal control over catalytic activity. For future applications it would be interesting to implement this chemically triggered CuAAC in biological processes that are regulated by alkaloids or other small organic cations such as choline, as these are potential signal molecules to activate the CB[7] inhibited catalyst.[52] On that note, cucurbituril complexes are known to facilitate delivery of a broad variety of cargos across the cell membrane.[53] We envision that the here presented chemistry could be used for 'on demand' labeling of biomolecules in the cell, which could have great implications for studying a variety of dynamic biological processes. We are currently looking into enhancing solvent and buffer tolerance to enable these applications in living systems. Lastly, the here presented work can be adopted to different biocompatible metal carbene catalysts such as NHC-Pd[54] and NHC-Ru[55, 56] in order to regulate their catalytic activity.[57]

2.4 REFERENCES

1. Meldal, M.; Tornøe, C. W., Cu-Catalyzed Azide−Alkyne Cycloaddition. *Chem. Rev.* **2008,** *108* (8), 2952-3015.
2. Rostovtsev, V. V.; Green, L. G.; Fokin, V. V.; Sharpless, K. B., A Stepwise Huisgen Cycloaddition Process: Copper(I)-Catalyzed Regioselective "Ligation" of Azides and Terminal Alkynes. *Angew. Chem. Int. Ed.* **2002,** *41* (14), 2596-2599.
3. Pickens, C. J.; Johnson, S. N.; Pressnall, M. M.; Leon, M. A.; Berkland, C. J., Practical Considerations, Challenges, and Limitations of Bioconjugation via Azide-Alkyne Cycloaddition. *Bioconj. Chem.* **2018,** *29* (3), 686-701.
4. Liang, L.; Astruc, D., The copper(I)-catalyzed alkyne-azide cycloaddition (CuAAC) "click" reaction and its applications. An overview. *Coord. Chem. Rev.* **2011,** *255* (23), 2933-2945.
5. Murakami, T.; Brown, H. R.; Hawker, C. J., One-pot fabrication of robust interpenetrating hydrogels via orthogonal click reactions. *J. Polym. Sci., Part A: Polym. Chem.* **2016,** *54* (11), 1459-1467.
6. Alzahrani, A. A.; Saed, M.; Yakacki, C. M.; Song, H. B.; Sowan, N.; Walston, J. J.; Shah, P. K.; McBride, M. K.; Stansbury, J. W.; Bowman, C. N., Fully recoverable rigid shape memory foam based on copper-catalyzed azide–alkyne cycloaddition (CuAAC) using a salt leaching technique. *Polym. Chem.* **2018,** *9* (1), 121-130.
7. Farahani, P. E.; Adelmund, S. M.; Shadish, J. A.; DeForest, C. A., Photo mediated oxime ligation as a bioorthogonal tool for spatiotemporally-controlled hydrogel formation and modification. *J. Mater. Chem.* **2017,** *5* (23), 4435-4442.
8. Ramil, C. P.; Lin, Q., Photo click chemistry: a fluorogenic light-triggered in vivo ligation reaction. *Curr. Opin. Chem. Biol.* **2014,** *21*, 89-95.
9. Trausel, F.; Maity, C.; Poolman, J. M.; Kouwenberg, D. S. J.; Versluis, F.; van Esch, J. H.; Eelkema, R., Chemical signal activation of an organocatalyst enables control over soft material formation. *Nat. Comm.* **2017,** *8* (1), 879.
10. Galán, A.; Gil-Ramírez, G.; Ballester, P., Kinetic Stabilization of N,N-Dimethyl-2-propyn-1-amine N-Oxide by Encapsulation. *Org. Lett.* **2013,** *15* (19), 4976-4979.
11. Horng, Y.-C.; Huang, P.-S.; Hsieh, C.-C.; Kuo, C.-H.; Kuo, T.-S., Selective encapsulation of volatile and reactive methyl iodide. *Chem. Comm.* **2012,** *48* (70), 8844-8846.
12. Nishimura, N.; Yoza, K.; Kobayashi, K., Guest-Encapsulation Properties of a Self-Assembled Capsule by Dynamic Boronic Ester Bonds. *J. Am. Chem. Soc.* **2010,** *132* (2), 777-790.

13. Quan, M. L. C.; Cram, D. J., Constrictive binding of large guests by a hemicarcerand containing four portals. *J. Am. Chem. Soc.* **1991,** *113* (7), 2754-2755.
14. Eelkema, R.; Maeda, K.; Odell, B.; Anderson, H. L., Radical Cation Stabilization in a Cucurbituril Oligoaniline Rotaxane. *J. Am. Chem. Soc.* **2007,** *129* (41), 12384-12385.
15. Jin Jeon, Y.; Kim, S.-Y.; Ho Ko, Y.; Sakamoto, S.; Yamaguchi, K.; Kim, K., Novel molecular drug carrier: encapsulation of oxaliplatin in cucurbit[7]uril and its effects on stability and reactivity of the drug. *Org. Biomol. Chem.* **2005,** *3* (11), 2122-2125.
16. Chen, Y.; Huang, Z.; Zhao, H.; Xu, J.-F.; Sun, Z.; Zhang, X., Supramolecular Chemotherapy: Cooperative Enhancement of Antitumor Activity by Combining Controlled Release of Oxaliplatin and Consuming of Spermine by Cucurbit[7]uril. *ACS Appl. Mater. & Interfaces* **2017,** *9* (10), 8602-8608.
17. Oun, R.; Floriano, R. S.; Isaacs, L.; Rowan, E. G.; Wheate, N. J., The ex vivo neurotoxic, myotoxic and cardiotoxic activity of cucurbituril-based macrocyclic drug delivery vehicles. *Toxicol. Res.* **2014,** *3* (6), 447-455.
18. Carvalho, C. P.; Uzunova, V. D.; Da Silva, J. P.; Nau, W. M.; Pischel, U., A photoinduced pH jump applied to drug release from cucurbit[7]uril. *Chem. Comm.* **2011,** *47* (31), 8793-8795.
19. Walker, S.; Oun, R.; McInnes, F. J.; Wheate, N. J., The Potential of Cucurbit[n]urils in Drug Delivery. *Isr. J. Chem.* **2011,** *51* (5-6), 616-624.
20. Zou, L.; Braegelman, A. S.; Webber, M. J., Spatially Defined Drug Targeting by in Situ Host–Guest Chemistry in a Living Animal. *ACS Cent. Sci.* **2019,** *5* (6), 1035-1043.
21. Lu, X.; Isaacs, L., Uptake of Hydrocarbons in Aqueous Solution by Encapsulation in Acyclic Cucurbit[n]uril-Type Molecular Containers. *Angew. Chem. Int. Ed.* **2016,** *55* (28), 8076-8080.
22. Mohanty, J.; Thakur, N.; Dutta Choudhury, S.; Barooah, N.; Pal, H.; Bhasikuttan, A. C., Recognition-Mediated Light-Up of Thiazole Orange with Cucurbit[8]uril: Exchange and Release by Chemical Stimuli. *J. Phys. Chem. B* **2012,** *116* (1), 130-135.
23. Shaikh, M.; Mohanty, J.; Bhasikuttan, A. C.; Uzunova, V. D.; Nau, W. M.; Pal, H., Salt-induced guest relocation from a macrocyclic cavity into a biomolecular pocket: interplay between cucurbit[7]uril and albumin. *Chem. Comm.* **2008,** (31), 3681-3683.
24. Biedermann, F.; Hathazi, D.; Nau, W. M., Associative chemosensing by fluorescent macrocycle–dye complexes – a versatile enzyme assay platform beyond indicator displacement. *Chem. Comm.* **2015,** *51* (24), 4977-4980.

25. Ghale, G.; Lanctôt, A. G.; Kreissl, H. T.; Jacob, M. H.; Weingart, H.; Winterhalter, M.; Nau, W. M., Chemosensing Ensembles for Monitoring Biomembrane Transport in Real Time. *Angew. Chem. Int. Ed.* **2014,** *53* (10), 2762-2765.
26. Brinkmann, J.; Wasserberg, D.; Jonkheijm, P., Redox-active host-guest supramolecular assemblies of peptides and proteins at surfaces. *Eur. Polym. J.* **2016,** *83*, 380-389.
27. Chinai, J. M.; Taylor, A. B.; Ryno, L. M.; Hargreaves, N. D.; Morris, C. A.; Hart, P. J.; Urbach, A. R., Molecular Recognition of Insulin by a Synthetic Receptor. *J. Am. Chem. Soc.* **2011,** *133* (23), 8810-8813.
28. Urbach, A. R.; Ramalingam, V., Molecular Recognition of Amino Acids, Peptides, and Proteins by Cucurbit[n]uril Receptors. *Isr. J. Chem.* **2011,** *51* (5-6), 664-678.
29. Mock, W. L.; Irra, T. A.; Wepsiec, J. P.; Manimaran, T. L., Cycloaddition induced by cucurbituril. A case of Pauling principle catalysis. *J. Org. Chem.* **1983,** *48* (20), 3619-3620.
30. Krasia, T. C.; Steinke, J. H. G., Formation of oligotriazoles catalyzed by cucurbituril. *Chem. Comm.* **2002,** (1), 22-23.
31. Klöck, C.; Dsouza, R. N.; Nau, W. M., Cucurbituril-Mediated Supramolecular Acid Catalysis. *Org. Lett.* **2009,** *11* (12), 2595-2598.
32. Tonga, G. Y.; Jeong, Y.; Duncan, B.; Mizuhara, T.; Mout, R.; Das, R.; Kim, S. T.; Yeh, Y.-C.; Yan, B.; Hou, S.; Rotello, V. M., Supramolecular regulation of bioorthogonal catalysis in cells using nanoparticle-embedded transition metal catalysts. *Nat. Chem.* **2015,** *7*, 597.
33. Blanco, V.; Carlone, A.; Hänni, K. D.; Leigh, D. A.; Lewandowski, B., A Rotaxane-Based Switchable Organocatalyst. *Angew. Chem. Int. Ed.* **2012,** *51* (21), 5166-5169.
34. Blanco, V.; Leigh, D. A.; Lewandowska, U.; Lewandowski, B.; Marcos, V., Exploring the Activation Modes of a Rotaxane-Based Switchable Organocatalyst. *J. Am. Chem. Soc.* **2014,** *136* (44), 15775-15780.
35. Blanco, V.; Leigh, D. A.; Marcos, V.; Morales-Serna, J. A.; Nussbaumer, A. L., A Switchable [2]Rotaxane Asymmetric Organocatalyst That Utilizes an Acyclic Chiral Secondary Amine. *J. Am. Chem. Soc.* **2014,** *136* (13), 4905-4908.
36. Michael, P.; Biewend, M.; Binder, W. H., Mechanochemical Activation of Fluorogenic CuAAC "Click" Reactions for Stress-Sensing Applications. *Macromol. Rapid Comm.* **2018,** *39* (22), 1800376.
37. Michael, P.; Binder, W. H., A Mechanochemically Triggered "Click" Catalyst. *Angew. Chem. Int. Ed.* **2015,** *54* (47), 13918-13922.
38. Hong, V.; Udit, A. K.; Evans, R. A.; Finn, M. G., Electrochemically protected copper(I)-catalyzed azide-alkyne cycloaddition. *Chembiochem: European J. Chem. Bio.* **2008,** *9* (9), 1481-1486.

39. Tasdelen, M. A.; Yagci, Y., Light-Induced Click Reactions. *Angew. Chem. Int. Ed.* **2013,** *52* (23), 5930-5938.
40. Stoll, R. S.; Hecht, S., Artificial Light-Gated Catalyst Systems. *Angew. Chem. Int. Ed.* **2010,** *49* (30), 5054-5075.
41. Maity, C.; Trausel, F.; Eelkema, R., Selective activation of organocatalysts by specific signals. *Chem. Sci.* **2018,** *9* (27), 5999-6005.
42. De, S.; Pramanik, S.; Schmittel, M., A Toggle Nanoswitch Alternately Controlling Two Catalytic Reactions. *Angew. Chem. Int. Ed.* **2014,** *53* (51), 14255-14259.
43. Gaulier, C.; Hospital, A.; Legeret, B.; Delmas, A. F.; Aucagne, V.; Cisnetti, F.; Gautier, A., A water soluble CuI-NHC for CuAAC ligation of unprotected peptides under open air conditions. *Chem. Comm.* **2012,** *48* (33), 4005-4007.
44. Presolski, S. I.; Hong, V.; Cho, S.-H.; Finn, M. G., Tailored Ligand Acceleration of the Cu-Catalyzed Azide−Alkyne Cycloaddition Reaction: Practical and Mechanistic Implications. *J. Am. Chem. Soc.* **2010,** *132* (41), 14570-14576.
45. Araman, C.; Pieper-Pournara, L.; van Leeuwen, T.; Kampstra, A. S. B.; Bakkum, T.; Marqvorsen, M. H. S.; Nascimento, C. R.; Groenewold, M.; G. J.; van der Wulp, W.; Camps, M. G. M.; Overkleeft, H. S.; Ossendorp, F. A.; Toes, R. E. M.; van Kasteren, S. I., Bioorthogonal antigens allow the unbiased study of antigen processing and presentation. *bioRxiv* **2019**, 439323.
46. Peng, X.; Nelson, E. S.; Maiers, J. L.; DeMali, K. A., Chapter five - New Insights into Vinculin Function and Regulation. In *Int. Rev. Cell Mol. Biol.*, Jeon, K. W., Ed. Academic Press: 2011; Vol. 287, pp 191-231.
47. van Heemst, J.; Jansen, D. T. S. L.; Polydorides, S.; Moustakas, A. K.; Bax, M.; Feitsma, A. L.; Bontrop-Elferink, D. G.; Baarse, M.; van der Woude, D.; Wolbink, G.-J.; Rispens, T.; Koning, F.; de Vries, R. R. P.; Papadopoulos, G. K.; Archontis, G.; Huizinga, T. W.; Toes, R. E., Cross reactivity to vinculin and microbes provides a molecular basis for HLA-based protection against rheumatoid arthritis. *Nat. Comm.* **2015,** *6* (1), 6681.
48. Yang, H.; Liu, Y.; Yang, L.; Liu, K.; Wang, Z.; Zhang, X., Cucurbit[7]uril as a “protective agent”: controlling photochemistry and detecting 1-adamantanamine. *Chem. Comm.* **2013,** *49* (37), 3905-3907.
49. Kaifer, A. E., Cucurbituril Hosts in Real-Life Action. *Chemphyschem* **2013,** *14* (6), 1107-1108.
50. Peng, L.; Feng, A.; Huo, M.; Yuan, J., Ferrocene-based supramolecular structures and their applications in electrochemical responsive systems. *Chem. Comm.* **2014,** *50* (86), 13005-13014.
51. Jeon, W. S.; Moon, K.; Park, S. H.; Chun, H.; Ko, Y. H.; Lee, J. Y.; Lee, E. S.; Samal, S.; Selvapalam, N.; Rekharsky, M. V.; Sindelar, V.; Sobransingh, D.; Inoue, Y.; Kaifer, A. E.; Kim, K., Complexation of Ferrocene Derivatives by the

Cucurbit[7]uril Host: A Comparative Study of the Cucurbituril and Cyclodextrin Host Families. *J. Am. Chem. Soc.* **2005,** *127* (37), 12984-12989.

52. Berdnikova, D. V.; Aliyeu, T. M.; Paululat, T.; Fedorov, Y. V.; Fedorova, O. A.; Ihmels, H., DNA–ligand interactions gained and lost: light-induced ligand redistribution in a supramolecular cascade. *Chem. Comm.* **2015,** *51* (23), 4906-4909.
53. Montes-Navajas, P.; González-Béjar, M.; Scaiano, J. C.; García, H., Cucurbituril complexes cross the cell membrane. *Photoch. Photobio. Sci.* **2009,** *8* (12), 1743-1747.
54. Cherukaraveedu, D.; Cowling, P. T.; Birch, G. P.; Bradley, M.; Lilienkampf, A., Solid-phase synthesis of biocompatible N-heterocyclic carbene–Pd catalysts using a sub-monomer approach. *Org. Biomol. Chem.* **2019,** *17* (22), 5533-5537.
55. Süßner, M.; Plenio, H., Redox-Switchable Phase Tags for Recycling of Homogeneous Catalysts. *Angew. Chem. Int. Ed.* **2005,** *44* (42), 6885-6888.
56. Tomasek, J.; Schatz, J., Olefin metathesis in aqueous media. *Green Chem.* **2013,** *15* (9), 2317-2338.
57. Peris, E., Smart N-Heterocyclic Carbene Ligands in Catalysis. *Chem. Rev.* **2018,** *118* (19), 9988-10031.

2.5 SUPPLEMENTARY INFORMATION

2.5.1 General considerations

All solvents and chemicals were purchased from Sigma Aldrich, TCI chemicals or Apollo scientific and used without any further purification. Silica (Sigma-Aldrich, 99.8%, 175-225 m^2/g) used for purification was used as received. ^{1}H-NMR and ^{13}C-NMR were recorded on an Agilent-400 MR DD2 (^{1}H-NMR: 399.67 MHz and ^{13}C-NMR: 100.5 MHz) at 298 K. ^{1}H-NMR studies to monitor CuAAC were performed using a H_2O pre-saturation sequence. The chemical shifts are given with respect to solvent residual signals as reported by Fulmer et al.[1] Mass spectra were recorded on a Shimadzu LCMS-2010 by electrospray ionization in positive or negative mode (ESI+ or ESI-). Isothermal titration calorimetry experiments were conducted at 25 °C on a Microcal VP-ITC titration microcalorimeter (stirring speed 459 rpm). All samples were degassed before use.

2.5.2 Catalyst synthesis

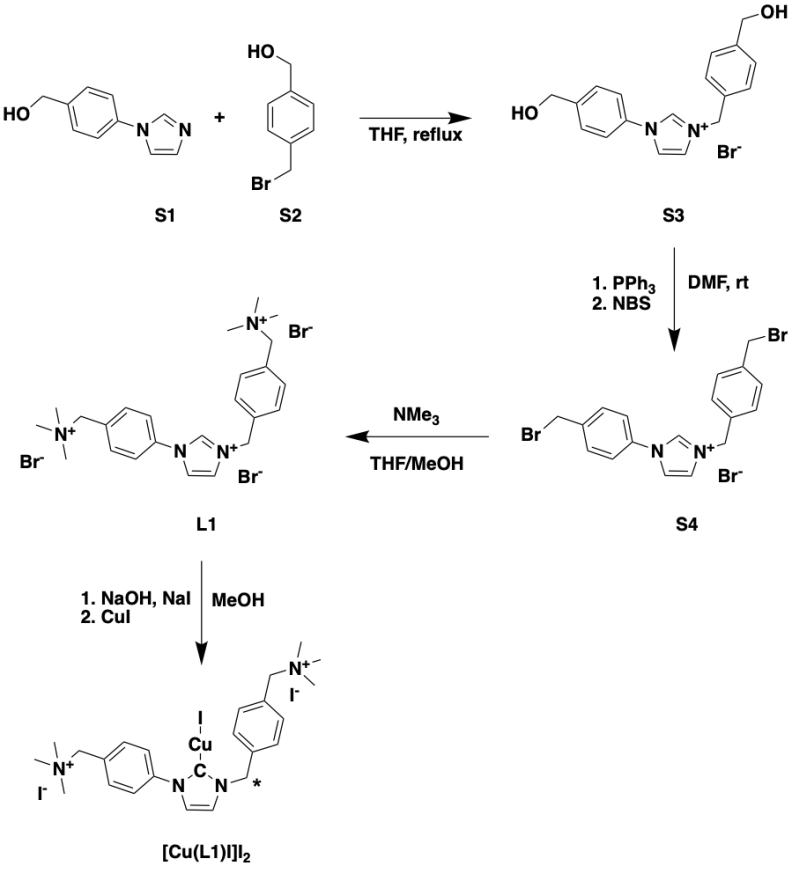

Scheme S1. *Synthesis of [Cu(**L1**)I]I_2 starting with the nucleophilic substitution of imidazole **S1** to bromide **S2**, followed by the double bromination of imidazolium salt **S3** using N-bromosuccinimide (NBS) and triphenylphosphine (PPh_3). Subsequently, Imidazolium salt **S4** is treated with trimethylamine (NMe_3) to yield **L1**. Finally, **L1** and CuI are reacted in the presence of NaOH to yield Cu(I)-NHC [Cu(**L1**)I]I_2.*

3-(4-(hydroxymethyl)benzyl)-1-(4-(hydroxymethyl)phenyl)-1*H*-imidazol-3-ium bromide (S3)

Imidazole **S1** (2.0 g, 11 mmol) and bromide **S2** (2.3 g, 11 mmol) were dissolved in THF (20 ml) and stirred overnight at reflux. Overnight a white precipitate was

formed. The precipitate was filtered hot, washed with acetone (2 x 10 ml) and dried overnight in a vacuum oven (40 °C). This yielded the product as a white powder (3.67 g, 9.78 mmol, 85%). ^{1}H-NMR (400 MHz, DMSO-d_6) δ = 10.01 (s, C*H*), 8.31 (t, C*H*, J = 1.8 Hz), 8.02 (t, C*H*, J = 1.8 Hz), 7.76 (2H, d, CH_{arom}, J = 8.6 Hz), 7.58 (2H, d, CH_{arom}, J = 8.6 Hz), 7.50 (2H, d, CH_{arom}, J = 8.2 Hz), 7.38 (2H, d, CH_{arom}, J = 8.1 Hz), 5.48 (s, CH_2), 5,42 (t, O*H*, J = 5.7 Hz), 5.25 (t, O*H*, J = 5.7 Hz), 4.59 (d, CH_2, J = 5.4 Hz), 4.51 (d, CH_2, J = 5.4 Hz). ^{13}C-NMR (101 MHz, DMSO-d_6) δ = 144.5 (C_q), 143.4 (C_q), 133.2 (C_q), 132.7 (C_q), 128.4 (*C*H$_{arom}$), 127.7 (*C*H$_{arom}$), 126.9 (*C*H$_{arom}$), 123.1 (*C*H$_{imidazole}$), 121.7 (*C*H$_{imidazole}$), 121.6 (*C*H$_{arom}$), 62.4 (HO*C*H$_{2benzyl}$), 62.0 (HO*C*H$_{2benzyl}$), 52.3 (*C*H$_{2imidazole}$). m/z calc.: 295.14 $[M]^+$, found: 295.40 $[M]^+$.

3-(4-(bromomethyl)benzyl)-1-(4-(bromomethyl)phenyl)-1H-imidazol-3-ium bromide (S4)[2]

Imidazolium salt **S3** (1.55 g, 4.13 mmol) and triphenylphosphine (4.36 g, 16.6 mmol) were dissolved in DMF (60 ml) and stirred for 20 min at 0 °C (ice bath). *N*-bromosuccinimide (2.85 g, 16.0 mmol) was added and the reaction was stirred another 90 min a room temperature. H_2O was added until a white precipitate formed. The mixture was cooled to 0 °C and after 15 minutes the precipitate was removed by filtration. The filtrated was concentrated *in vacuo* and purified over silica (0% MeOH/DCM to 8% MeOH/DCM). This yielded the desired product as a brownish oil (1.39 g, 2.77 mmol, 67%). ^{1}H-NMR (400 MHz, DMSO-d_6) δ = 10.04 (t, C*H*, J = 1.6 Hz), 8.35 (t, C*H* imidazole, J = 1.8 Hz), 8.06 (t, C*H* imidazole, J = 1.7 Hz), 7.81 (2H, d, CH_{arom}, J = 8.6 Hz), 7.74 (2H, d, CH_{arom}, J = 8.6 Hz), 7.51 (4H, s, CH_{arom}), 5.51 (s, C$H_{2imidazole}$), 4.81 (s, C$H_{2benzyl}$), 4.72 (s, C$H_{2benzyl}$). ^{13}C-NMR (101 MHz, DMSO-d_6) δ = 139.9 (C_q), 138.4 (C_q), 135.7 (C_q), 134.5 (C_q), 130.9 (*C*H$_{arom}$), 129.9 (*C*H$_{arom}$), 128.8 (*C*H$_{arom}$), 123.3 (*C*H$_{imidazole}$), 122.3 (*C*H$_{arom}$), 121.7 (*C*H$_{imidazole}$), 52.0 (*C*H$_{2imidazole}$), 33.8 (Br*C*H$_{2benzyl}$), 32.9 (Br*C*H$_{2imidazole}$). m/z calc.: 420.97 $[M]^+$, found: 420.60 $[M]^+$

3-(4-((trimethylamine)methyl)benzyl)-1-(4-((trimethyl)methyl)phenyl)-1H-imidazol-3-ium tris bromide (L1)

Imidazolium salt **S4** (1.39 g, 2.77 mmol) was dissolved in a mixture of THF and MeOH (1:1 20 ml). NMe_3 (4.63 ml (4.2 M in EtOH), 19.5 mmol) was added and the reaction mixture was stirred overnight at room temperature. An off-white powder was obtained which was filtered and washed with acetone (2 x 10 ml). The powder was recrystallized from MeOH/diethyl ether at 4 °C, which yielded the title compound as white needles (1.21 g, 1.95 mmol, 70%). ^{1}H-NMR (400 MHz, DMSO-d_6) δ = 10.33 (t, C*H*, J = 1.6 Hz), 8.46 (t, C*H* imidazole, J = 1.8 Hz), 8.13 (t, C*H* imidazole, J = 1.7 Hz), 8.03 (2H, d, CH_{arom}, J = 8.5 Hz), 7.89 (2H, d, CH_{arom}, J = 8.5 Hz), 7.72 (2H, d, CH_{arom}, J = 8.1 Hz), 7.66 (2H, d, CH_{arom}, J = 8.1 Hz), 5.65 (s, C$H_{2imidazole}$), 4.75 (s, C$H_{2benzyl}$), 4.64 (s, C$H_{2benzyl}$), 3.11 (s, 3x CH_3), 3.06 (s, 3x CH_3). ^{13}C-NMR (101 MHz, DMSO-d_6) δ = 136.3 (C_q), 136.0 (C_q), 135.9 ($C_{carbene}$), 134.6 (*C*H$_{arom}$), 133.4 (*C*H$_{arom}$), 135.95 (C_q), 129.1 (*C*H$_{arom}$), 129.0 (C_q), 123.5 (*C*H$_{imidazole}$), 122.0 (*C*H$_{arom}$), 121.4 (*C*H$_{imidazole}$), 66.9 (Me_3NCH_2), 66.4 (Me_3NCH_2), 51.9 ($(N(CH_3)_3)_2$), 51.8 ($CH_{2imidazole}$). Elem. Anal. calc.: C: 46.55 H: 5.70 N: 9.05 Br: 38.71. Elem. Anal. exp.: C: 45.85 H: 5.97 N: 9.26 Br: 38.19. m/z calc.: 126.43 $[M]^{3+}$, found: 126.30 $[M]^{3+}$

$[Cu(L1)I]I_2$[3]

L1 (99.9 mg, 0.161 mmol) was dissolved in MeOH (dry, Ar degassed). NaI (80.2 mg, 0.535 mmol) and NaOH (9.9 mg, 0.25 mmol) were added. The reaction mixture was heated to 66 °C and stirred for 30 minutes. Subsequently CuI (30.7 mg, 0.161 mmol) was added and the reaction mixture was degassed with Argon for 5 minutes after which it was stirred for 16 hours. The desired complex precipitated as a white powder which was filtered hot, washed with acetone (2 x 10 ml) and dried in a vacuum oven (40 °C) (57.8 mg, 0.070 mmol, 44%). ^{1}H-NMR (400 MHz, DMSO-d_6) δ = 8.06 (2H, d, CH_{arom}, J = 8.4 Hz), 7.87 (d, C$H_{imidazole}$, J = 1.8 Hz), 7.70 (2H, d, CH_{arom}, J = 8.4 Hz), 7.68 (m, C$H_{imidazole}$), 7.65 (2H, d, CH_{arom}, J = 8.1 Hz), 7.55 (2H, d, CH_{arom}, J =

8.1 Hz), 5.53 (s, C*H*$_{2imidazole}$), 4.59 (s, C*H*$_{2benzyl}$), 4.51 (s, C*H*$_{2benzyl}$), 3.05 (s, 3x C*H*$_3$), 3.02 (s, 3x C*H*$_3$). ^{13}C-NMR (101 MHz, DMSO-d$_6$) δ = 180.2 (*C*Cu), 141.0 (C$_q$), 139.0 (C$_q$), 133.8 (*C*H$_{arom}$), 133.1 (*C*H$_{arom}$), 128.8 (*C*H$_{arom}$), 128.1 (C$_q$), 127.8 (C$_q$), 123.3 (*C*H$_{arom}$), 122.7 (*C*H$_{imidazole}$), 120.7 (*C*H$_{arom}$), 67.4 (Me$_3$N*C*H$_2$), 67.0 (Me$_3$N*C*H$_2$), 53.3 (*C*H$_{2imidazole}$), 51.8 ((N(*C*H$_3$)$_3$)$_2$). Elem. Anal. calc. (C$_{24}$H$_{34}$CuI$_3$N$_4$•H$_2$O): C: 34.28, H: 4.32, N: 6.66, I: 45.28, Cu: 7.56. Elem. Anal. exp. (C$_{24}$H$_{34}$CuI$_3$N$_4$•H$_2$O): C: 34.22, H: 4.57, N: 6.71, I: 45.78, Cu: 7.66.

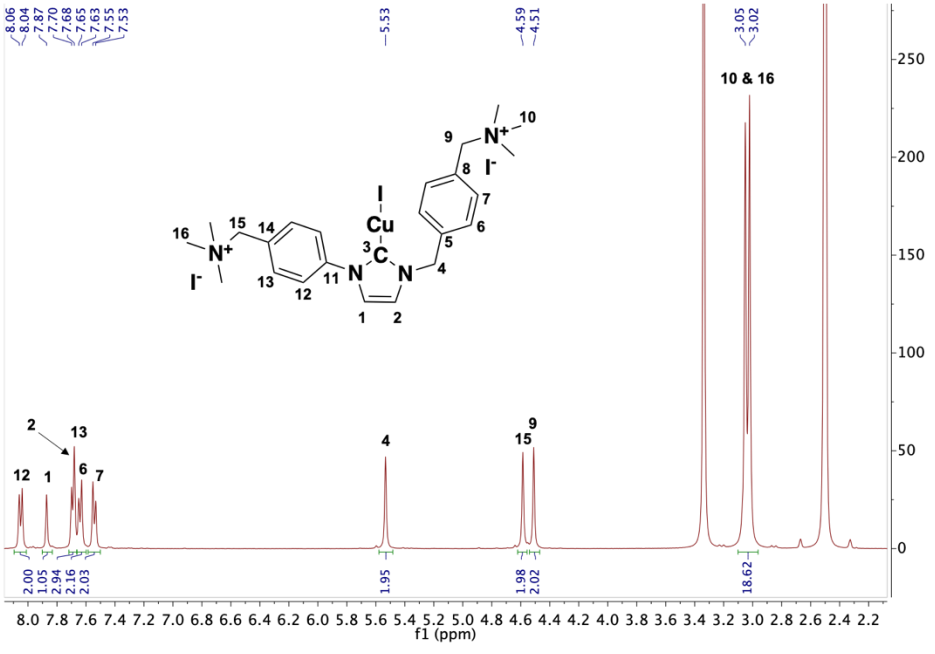

Figure S1. *^{1}H-NMR (DMSO-d6) recorded for [Cu(**L1**)I]I$_2$ with complete assignment of all proton signals.*

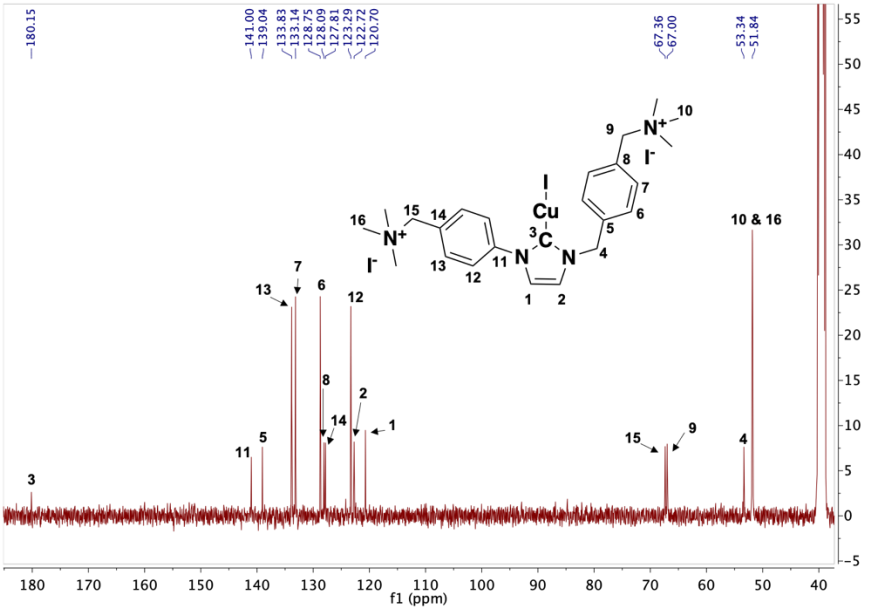

Figure S2. *^{13}C-NMR (DMSO-d6) recorded for [Cu(**L1**)I]I_2 with complete assignment of all carbon signals.*

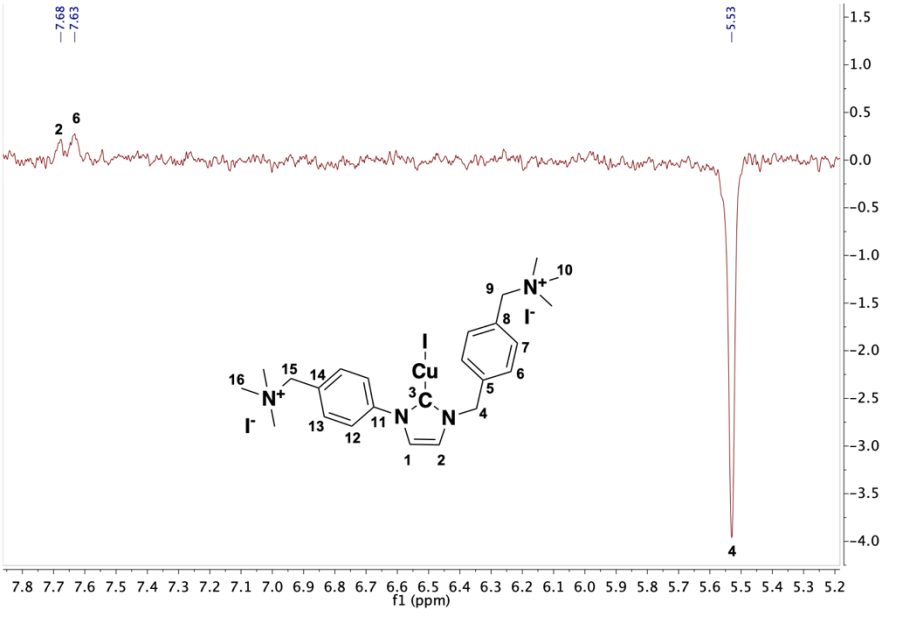

Figure S3. *^{1}H-^{1}H 1D ROESY NMR spectrum (DMSO-d_6, 400 MHz) recorded for [Cu(**L1**)I]I_2. H^4 was selectively irradiated in the region between 5.35 and 5.65 ppm using the following parameters: mixing time = 200 ms, d1 = 1.0, n = 64. Through space couplings are observed between H^4 (5.53 ppm) and H^6 (7.63 ppm) and between H^4 (5.53 ppm) and H^2 (7.68 ppm).*

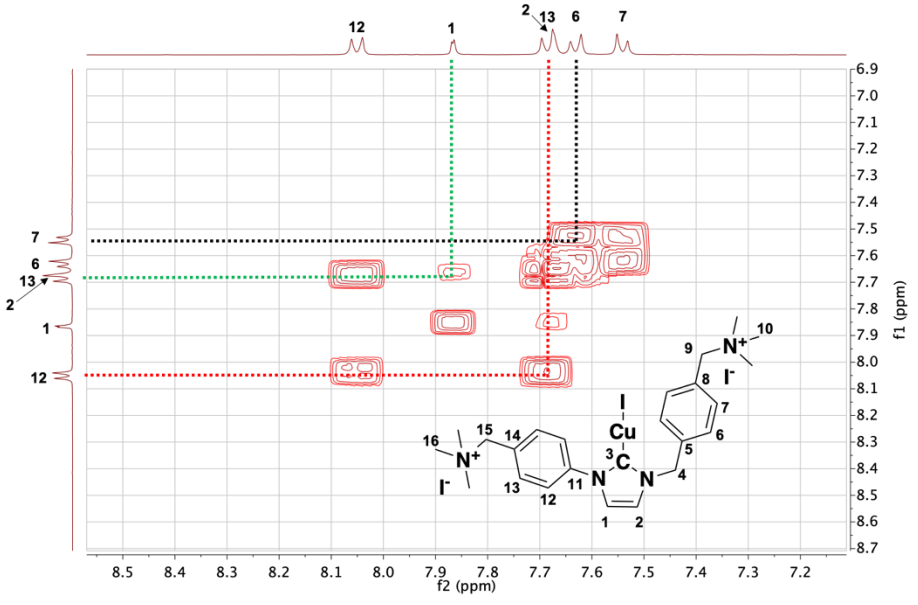

Figure S4. *^{1}H-^{1}H gCOSY NMR spectrum (DMSO-d_6) recorded for [Cu(**L1**)I]I_2. Through bond coupling is observed between: H^6 (7.63 ppm) and H^7 (7.55 ppm), H^{12} (8.06 ppm) and H^{13} (7.70 ppm) and between H^1 (7.87 ppm) and H^2 (7.68 ppm). Aromatic region is shown.*

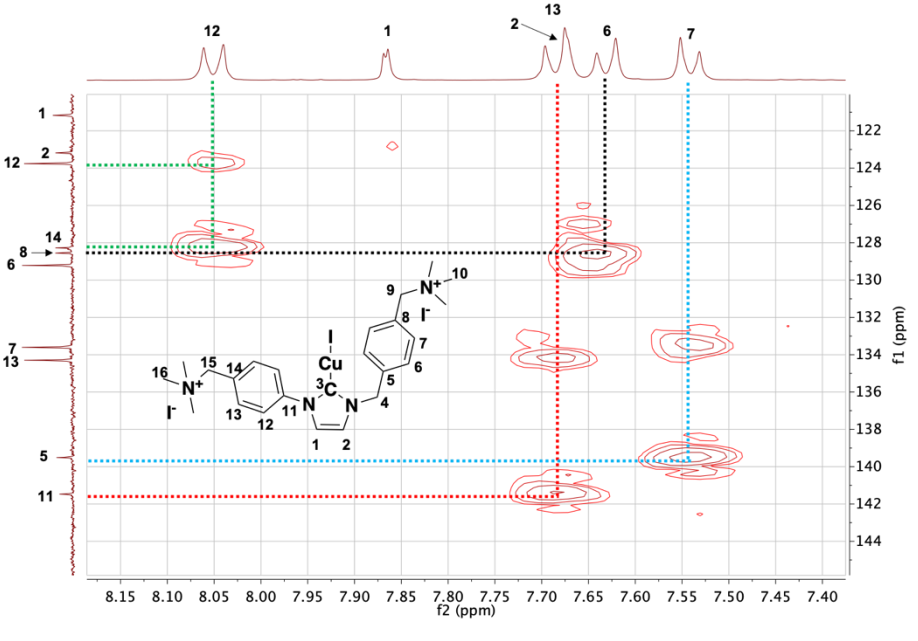

Figure S5. *^{1}H-^{13}C gHMBC NMR spectrum (DMSO-d_6, 400 MHz) recorded for [Cu(**L1**)I]I_2. Relevant long-range couplings between proton and carbon atoms are shown in the aromatic region.*

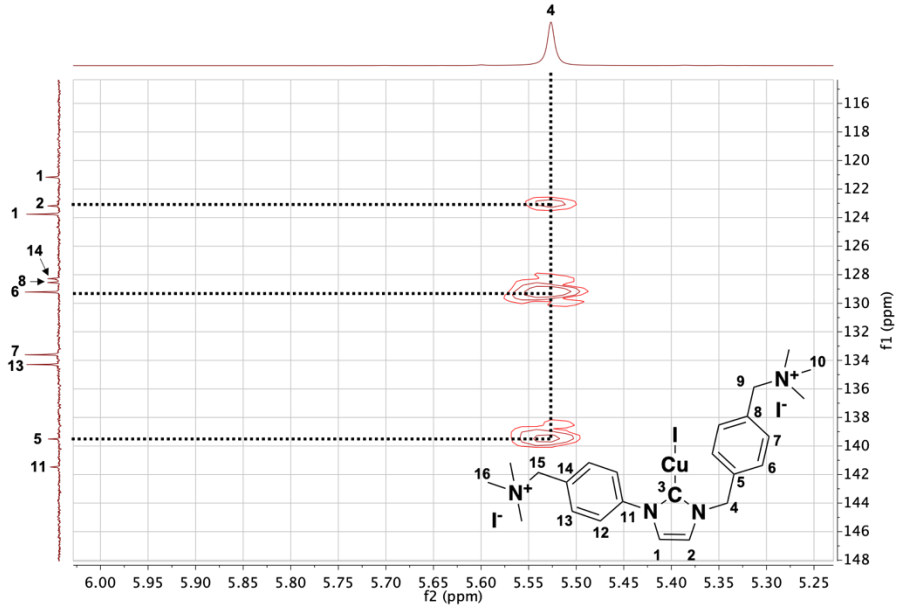

Figure S6. *^{1}H-^{13}C gHMBC NMR spectrum (DMSO-d_6, 400 MHz) recorded for [Cu(**L1**)I]I_2. Long-range cross couplings between H^4 and C^2, C^6 and C^5 are shown.*

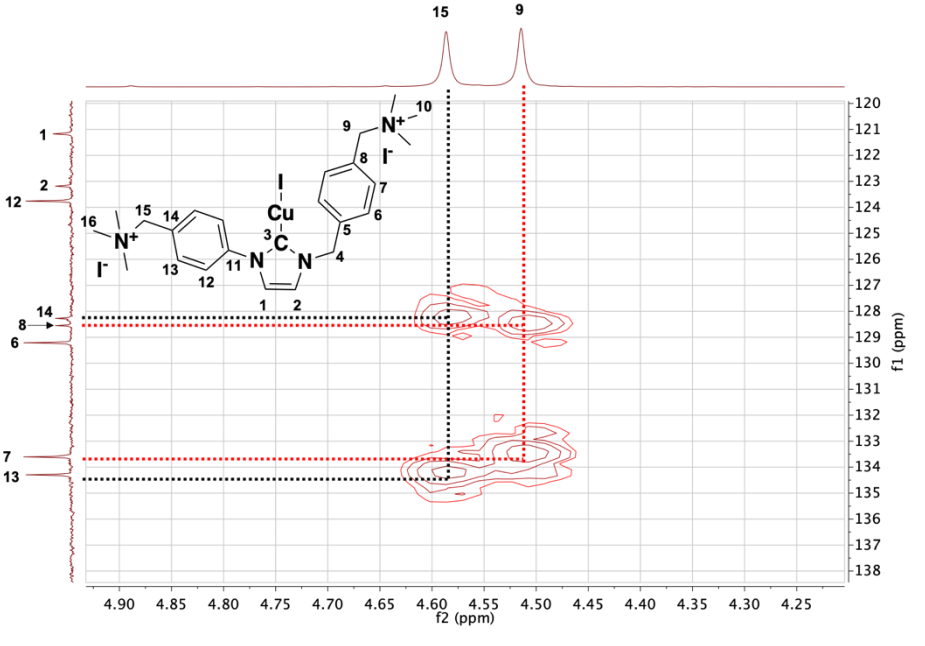

Figure S7. *^{1}H-^{13}C gHMBC NMR spectrum (DMSO-d_6, 400 MHz) recorded for [Cu(**L1**)I]I_2. Long-range couplings between H^{15} and C^{14} and C^{13} and between H^9 and C^8 and C^7 are shown.*

2.5.3 Signal molecule synthesis

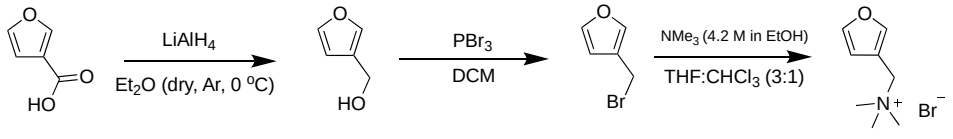

S5 S6 S7 1

***Scheme S2**. Synthetic route for the synthesis of 3-(trimethylmethanaminium)furan bromide (signal molecule **1**), starting from 3-furoic acid (**S5**) which is reduced using $LiAlH_4$ to furan-3-methanol (**S6**). Alcohol **S6** is then converted to bromide **S7** using phosphorous tribromide (PBr_3). Finally, bromide **S7** is treated with trimethylamine (NMe_3) to yield signal molecule **1**.*

Furan-3-methanol (S6)[4]

3-furoic acid (**S5)** (5.00 g, 44.6 mmol) was dissolved in dry Et_2O and cooled to 0 °C with an ice bath. $LiAlH_4$ (55 ml, 1.0 M in Et_2O) was added over the course of 5 minutes. The ice bath was removed and the reaction was stirred for 2 hours at room temperature. The reaction mixture was cooled to 0 °C using an ice bath, after which H_2O (140 ml) was added to reaction mixture. Subsequently 10% H_2SO_4 (180 ml) was added to the reaction mixture which was left to stir for 5 minutes. The aqueous layer was extracted with Et_2O (3x 150 ml). The combined organic layers were washed with brine (3 x 100 ml), dried over $MgSO_4$, concentrated *in vacuo* and purified over silica (25% EtOAc/PE). This afforded the product as a colorless oil (2.60 g, 26.5 mmol, 59%). ^{1}H-NMR (400 MHz, $CDCl_3$) δ = 7.34 (m, 2H), 6.36 (s, 1H) 4.40 (s, C*H*$_2$), 4.20 (s, O*H*). ^{13}C NMR (101 MHz, $CDCl_3$) δ = 143.1 (*C*H), 139.7 (*C*H), 125.0 (C_q), 109.8 (*C*H), 55.8 (*C*H_2). Reported values match literature values.

3-(bromomethyl)furan (S7)[5]

Furan-3-methanol (**S6**) (2.60 g, 26.5 mmol) was dissolved in anhydrous THF (26 ml) and cooled to 0 °C, using an ice bath. Phosphorous tribromide (10 ml, 1.0 M in DCM) was added slowly and the reaction was stirred for 2 hours at 0 °C, after which TLC (20% EtOAc/PE) showed a single product spot (R_f = 0.8). The reaction mixture was

concentrated *in vacuo* and purified over silica (5% EtOAc/PE), which afforded the product as a brown oil (2.40 g, 14.9 mmol, 56%). ^{1}H-NMR (400 MHz, $CDCl_3$) δ = 7.48 (m, 1H), 7.40 (s, 1H) 6.45 (s, 1H), 4.38 (s, CH_2). Reported values match reported literature values.

3-(trimethylmethanaminium)furan bromide (1)

3-(bromomethyl)furan (**S7**) (2.40 g, 14.9 mmol) was dissolved in THF/DCM (3:1) and NMe_3 (10.2 ml, 4.2 M in EtOH) was added. The reaction mixture was stirred for 4 hours at room temperature after which TLC confirmed that no starting material was left. Solvents were removed *in vacuo* and the brown precipitate was washed with hexane (3 x hexane 20 ml). This afforded the title compound (3.1 g, 14.1 mmol, 94%). ^{1}H-NMR (400 MHz, CD_3OD) δ = 7.91 (s, 1H), 7.69 (t, J = 4 Hz, 1H), 6.69 (d, J = 4 Hz, 1H), 4.48 (s, CH_2), 3.13 (s, N(CH_3)$_3$). ^{13}C-NMR (101 MHz, CD_3OD) δ = 147.6 (*C*H), 146.0 (*C*H), 114.3 (C_q), 113.3 (*C*H), 61.6 (*C*H_2), 53.0 (N(*C*H_3)$_3$). m/z calc.: 140.11 $[M]^+$, found: 139.90 $[M]^+$

2.5.4 Triazole synthesis

2-(4-(hydroxymethyl)-1H-1,2,3-triazol-1-yl)pentanedioic acid (5)

Azide **3** (47.3 mg, 0.273 mmol), propargyl alcohol (**4**, 20 µl, 0.346 mmol), $CuSO_4$•$5H_2O$ (6.2 mg, 0.0248 mmol) and sodium ascorbate (31.2 mg, 0.158 mmol) were added to a mixture of H_2O and EtOH (10 ml, 1:1) and stirred overnight at 50 °C. TLC analysis confirmed that all starting azide had been consumed. The reaction was cooled down to room temperature and filtered. The reaction mixture was concentrated and purified over silica (30% MeOH in DCM to 100% MeOH). The product was collected and dried under vacuum, yielding a yellow oil (25.6 mg, 0.11 mmol). ^{1}H-NMR (400 MHz, CD_3OD) δ = 8.04 (s, C$H_{triazole}$), 5.40 (m, 1H), 4.70 (s, 2H), 2.61 (m, CH*H*), 2.43 (m, C*H*H), 2.25 (t, J = 8 Hz, CH_2OH). ^{13}C-NMR (101 MHz, CD_3OD)

δ = 175.7 ($C_{carbonyl1}$, $C_{carbonyl2}$), 143.6 (C_q), 124.3 (CH_{arom}), 56.5 (CH_2OH), 31.0 (CH_2), 28.7 (CH_2). m/z calc.: 229.07 [M], found: 228.05 $[M-1H]^-$.

2.5.5 Click chemistry monitored by ^{1}H-NMR

The rate of conversion of the model click reaction shown in Scheme **S3** was measured by ^{1}H-NMR. A typical experiment was performed as described here. Azide **3** was dissolved in 0.9 ml buffer stock solution (solution **A**). The buffer solution (MES (100 mM, pH 6.4) or HEPES buffer (100mM, pH 7.4)) contained 5.4 mM isopropyl alcohol (IPA) as internal standard to assess conversion. A 1.3 mM stock solution of [Cu(**L1**)I]I_2 was prepared in DMSO-d_6 of which 0.3 ml was added to solution **A**. To this solution propargyl alcohol (**4**) (3.3 μl, 57 mmol) was added. After mixing, 0.6 ml of this solution was directly transferred to an NMR tube. ^{1}H-NMR spectra were recorded by automation at fixed time points (T = 25 °C). At these specific time points, conversion to triazole **5** (red and black stars in figure **S8**, **S9** and **S10)** was calculated relative to the internal standard. Figure **S8** shows the formation of triazole **5** without inhibition by CB[7]. Figure **S9** shows the 'off' state of catalyst [Cu(**L1**)I]I_2 caused by the binding to two CB[7] molecules and the subsequent activation after the addition of 3-(trimethylmethanaminium)furan bromide **1**, acting here as a chemical signal. Figure **S10** shows the catalytic activity of the 1:1 CB[7]:[Cu(**L1**)I]I_2 complex. In this experiment the catalyst was mixed with 1 molar equivalent of CB[7]. This solution was sonicated (1 min.) and incubated for 2 hours, after which propargyl alcohol **4** was added and the progress of the cycloaddition was monitored by ^{1}H-NMR.

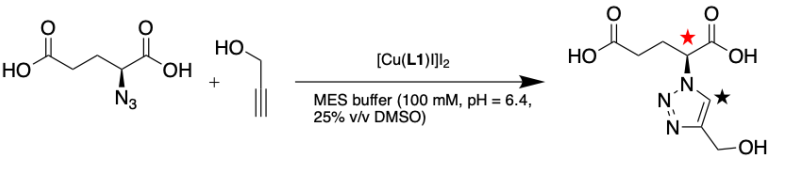

3 4 5

***Scheme S3**. Azide **3** and alkyne **4** were reacted in the presence of [Cu(**L1**)I]I_2 to yield triazole **5**. The signals of the labelled protons (red and black star in **5**) were used to monitor conversion in ^{1}H-NMR.*

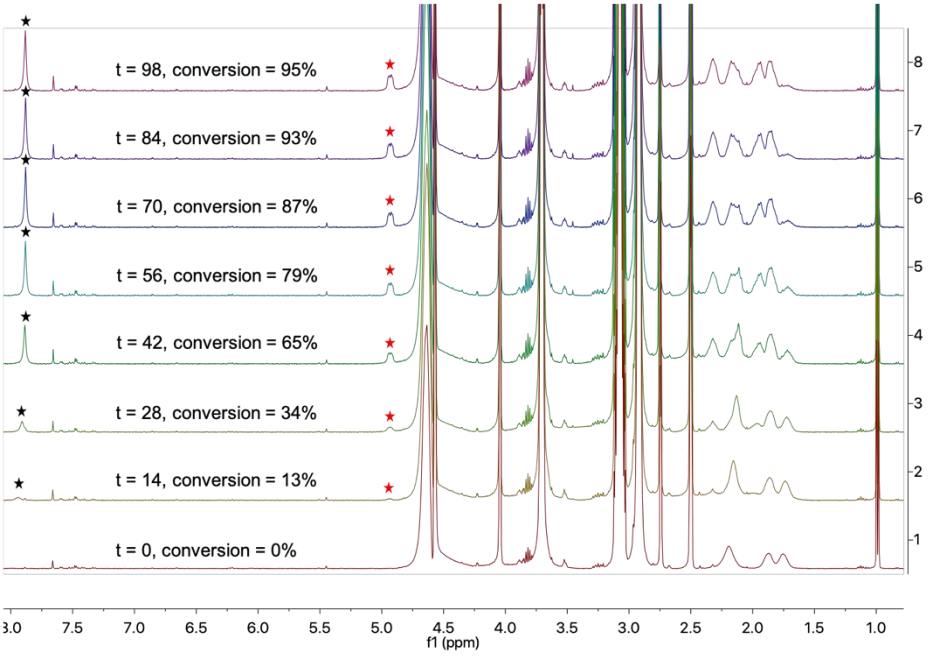

***Figure S8**. Stacked ^{1}H-NMR spectra showing formation of triazole **5** (black and red stars) (Scheme **S3**). Time (t) is in min. Conversion is relative to the theoretical maximum conversion of triazole **5**. Solvent system is MES (100 mM, pH = 6.4):DMSO-d_6 (3:1). All spectra were measured at 298 K. MES resonances are observed at 3.70 ppm, 3.07 ppm and 2.92 ppm. Propargyl alcohol (**4**) resonances are observed at 4.05 ppm (doublet) and 2.76 ppm (triplet). Isopropyl alcohol resonances are observed at 1.01 ppm (doublet).*

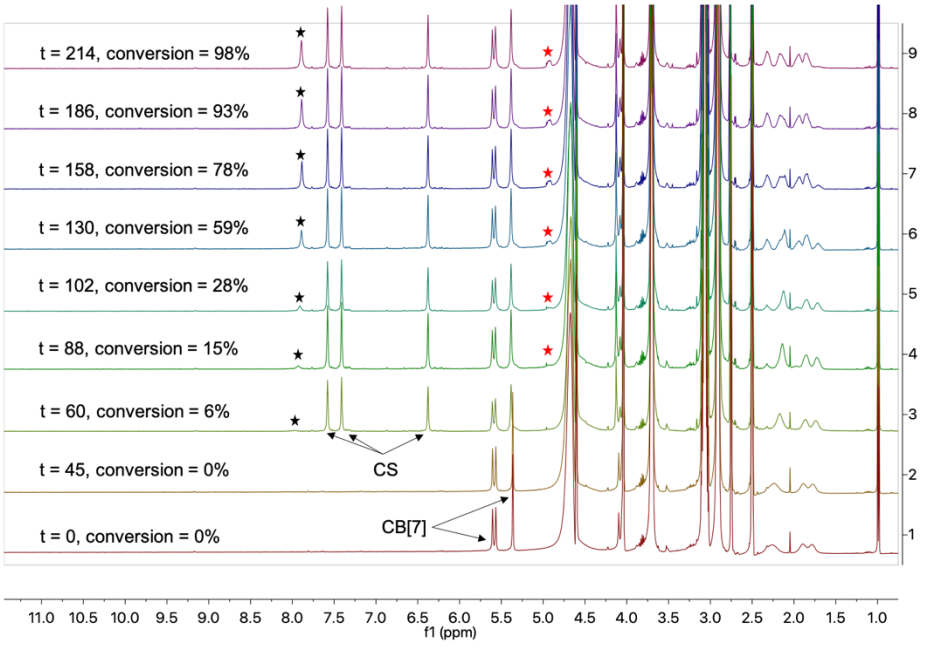

***Figure S9**. Stacked ^{1}H-NMR spectra showing the 'switched off' state of [Cu(**L1**)I]I_2 (entry 1 and 2). After 60 min chemical signal (CS) 3-(trimethylmethanaminium)furan bromide **1** is added which activates the catalyst and subsequent conversion of triazole **5** is started (black and red stars). Time (t) is in min. Conversion is relative to the theoretical maximum amount of triazole **5**. Solvent system is MES (100 mM, pH = 6.4):DMSO-d_6 (3:1). All spectra were measured at 298 K. MES resonances are observed at 3.70 ppm, 3.07 ppm and 2.92 ppm. Propargyl alcohol (**4**) resonances are observed at 4.05 ppm (doublet) and 2.76 ppm (triplet). Isopropyl alcohol resonances are observed at 1.01 ppm (doublet).*

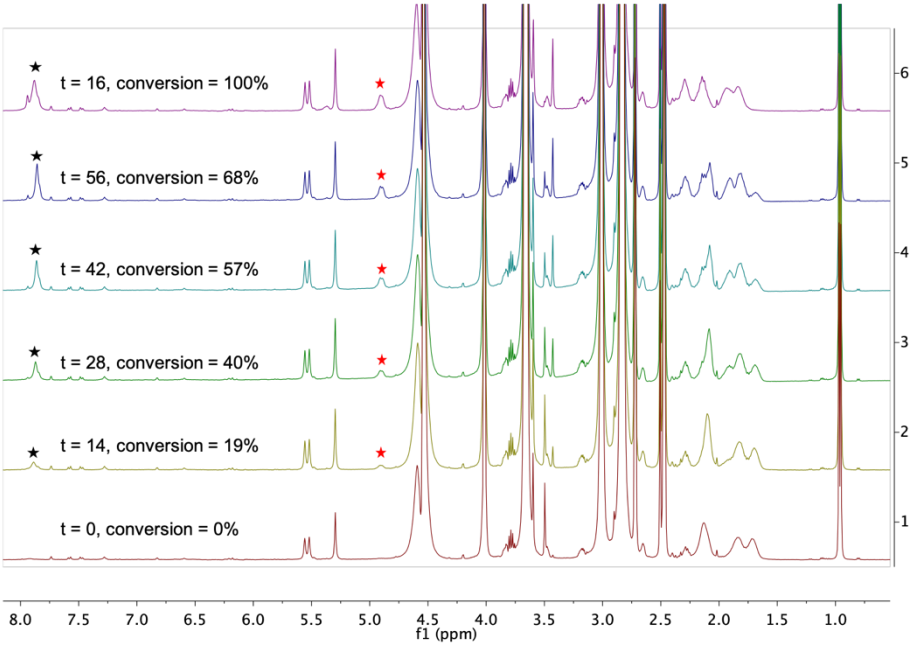

***Figure S10**. Stacked ^{1}H-NMR spectra showing the catalytic activity of the 1:1 CB[7]:[Cu(**L1**)I]I_2 complex. Conversion to triazole **5** (black and red stars) starts directly after the addition of propargyl alcohol (**4**) at t = 0. Time (t) is in min. Conversion is relative to the theoretical maximum amount of triazole **5**. Solvent system is MES (100 mM, pH = 6.4):DMSO-d_6 (3:1). All spectra were measured at 298 K. MES resonances are observed at 3.70 ppm, 3.07 ppm and 2.92 ppm. Propargyl alcohol (**4**) resonances are observed at 4.05 ppm (doublet), 2.76 ppm (triplet). Isopropyl alcohol resonances are observed at 1.01 ppm (doublet).*

2.5.6 Protein labelling experiments

Labelling experiment

In a typical labelling experiment, a DMSO:MES buffer (100 mM pH 6.4, KCl 400 mM) (1:1) stock solution of [Cu(**L1**)I]I_2 (0.3 mM) was prepared. 5 µl of this solution was mixed with 6 µl MES buffer (100 mM pH 6.4, KCl 400 mM), 1.25 µl Vinculin[6] protein stock solution (220 µM in 10 mM $NaHCO_3$ buffer, pH 8.0) and 0.25 µl of Alexa 647 fluorophore (5.23 mM in DMSO). After mixing, 12.5 µl aliquots were collected at specific time points and mixed with 10 µl EDTA solution (0.5 M in H_2O) to directly quench the catalytic activity of [Cu(**L1**)I]I_2. The degree of labelling was determined

with SDS-PAGE gel analysis as well as through gel fluorescence analysis (Typhoon, GE Healthcare). Both densitometry (for initial protein concentration) and fluorescence intensity were used as a measure for reaction completion.

Inhibition of labelling

To assess the catalyst inhibition by CB[7] an identical experiment as the labelling experiment was conducted, except for the addition of CB[7] to the catalyst stock solution. CB[7] (1.75 mM in stock solution) was added to the [Cu(**L1**)I]I_2 stock solution prepared in the labelling experiment, followed by approx. 1 min sonication.

Click on demand

The catalytic activity of [Cu(**L1**)I]I_2 was restored by the addition of hydroxymethyl-ferrocene **2**. The setup of this experiment was identical to the inhibition experiment described above, except for the addition of hydroxymethyl-ferrocene (20 times excess, relative to CB[7]) after 60 min of inhibition.

Charge density map

To better understand possible interactions of positively charged guest molecules, a charge density map of recombinant Vinculin was created, using Pymol (APBS electrostatics plugin) (Figure **S11**).

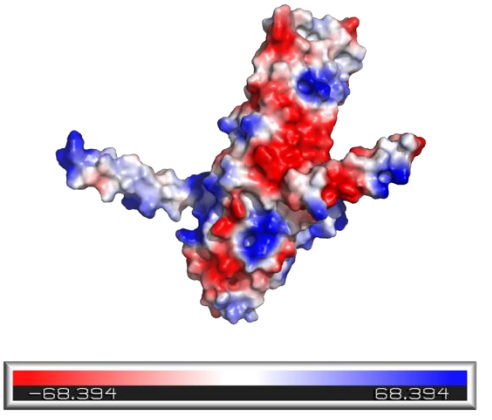

***Figure S11**. Charge density map of recombinant Vinculin.[6] Red areas are negatively charged, blue areas are positively charged and white areas are neutrally charged at pH 7.0. PBD code: 6fuy.*

2.5.7 Host-guest binding experiments

The binding between CB[7] and [Cu(**L1**)I]I_2 was characterized using the method of continuous variation (Job's plot) and by isothermal titration calorimetry (ITC).

Job's plot analysis

CB[7] (10.26 mg, 0.00602 mmol) was dissolved in MES buffer (4.5 ml, 120 mM, D_2O) to which DMSO-d_6 (1.5 ml) was added (final concentration CB[7] = 1.005 mM). [Cu(**L1**)I]I_2 (4.96 mg, 0.00603 mmol) was dissolved in DMSO-d_6 (1.5 ml) to which MES buffer (4.5 ml, 120 mM, pH 6.4, D2O) was added (final concentration [Cu(**L1**)I]I_2 = 1.006 mM). 7 solutions were prepared with varying ratios of [Cu(**L1**)I]I_2 and CB[7] (table **S1**) and were allowed to equilibrate for 2h at room temperature. ^{1}H-NMR spectra of all 7 samples were recorded and analyzed using Mestrenova (Figure **S12**). The C*H*$_2$ (proton **4**, Figure **S1**) resonance at 5.45 ppm of [Cu(**L1**)I]I_2 was monitored (black dashed line), showing a shift upfield to 4.93 ppm upon the addition of CB[7]. When the molar fraction equals a 1:1 ratio the peak shifts slightly back downfield to

5.27 ppm, indicating that the first binding site on [Cu(**L1**)I]I_2 is saturated and the second binding site starts to interact with CB[7]. Figure **S13** shows the Job's plot derived from these ^{1}H-NMR data, which shows a change above X_a = 0.35, this suggests a 2:1 binding event[7] which was subsequently confirmed in ITC experiments (Figure **S14**)

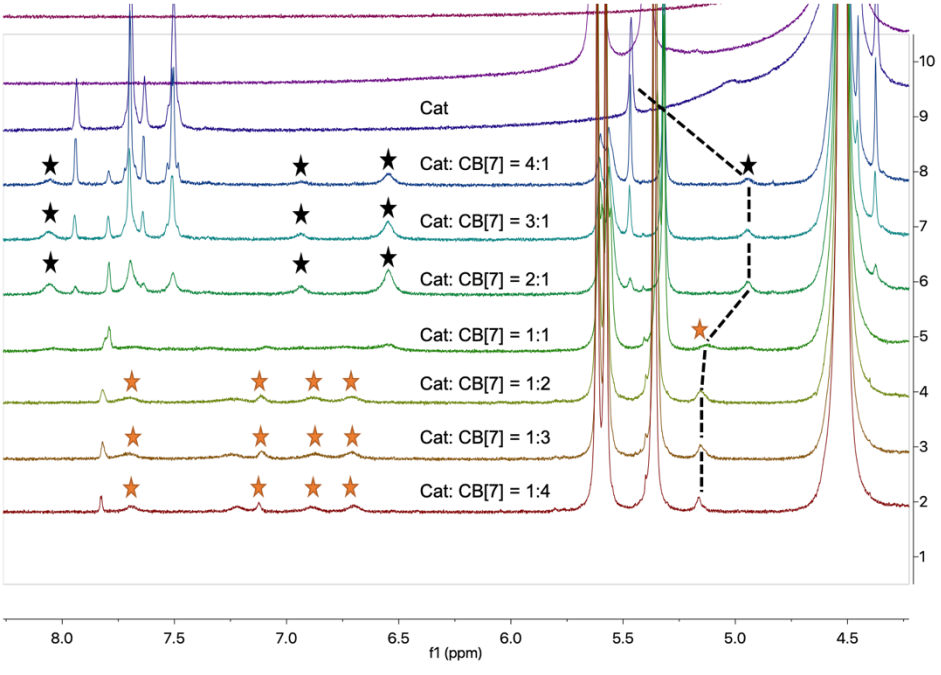

***Figure S12**. Stacked ^{1}H-NMR spectra showing the chemical shift upon the addition of CB[7]. The black dashed line indicates the CH_2 signal (proton **4** in [Cu(**L1**)I]I_2, Figure **S1**)) shifts after the addition of CB[7]. Black stars mark signals belonging to the 1:1 complex and the orange stars mark signals belonging to the 2:1 complex. Resonances at 5.3 ppm and 5.7 ppm belong to CB[7].*

Table S1. *Stock solutions of [Cu(**L1**)I]I_2* and CB[7] were mixed in the given volume ratios.
* *molar fraction of CB[7].*
** *observed chemical shift (dashed black line in Figure **S12**) of proton **4** in [Cu(**L1**)I]I_2 (Figure **S1**).*

Entry	µl [Cu(**L1**)I]I_2	µl CB[7]	X_a*	Δδ of CH_2**
1	400	100	0.20	0.52
2	375	125	0.25	0.52
3	333	167	0.34	0.52
4	250	250	0.50	0.34
5	167	333	0.67	0.31
6	125	375	0.75	0.3
7	100	400	0.80	0.3

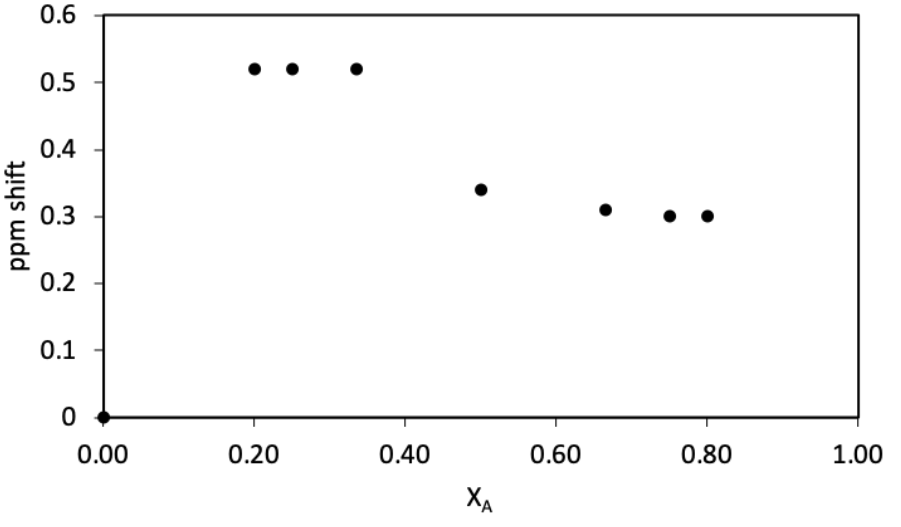

Figure S13. *Job's plot for the 1:2 binding of [Cu(**L1**)I]I_2 and CB[7] in MES buffer (100 mM, pH 6.4, D_2O) and DMSO-d_6 (3:1 v/v).*

Isothermal titration calorimetry

Isothermal titration calorimetry (ITC) experiments were conducted to obtain binding constants (K_{a1} and K_{a2}) of the 1:1 binding complex and the 2:1 binding

complex (2 CB[7] : 1 [Cu(**L1**)I]I_2). Initially the binding between **L1** and CB[7] was investigated as the ligand is the chemical motif responsible for binding to CB[7]. In this experiment a **L1** stock solution (0.690 mM in H_2O) was placed in the titration syringe and a CB[7] stock solution (0.0411 mM in H_2O) was placed in the sample cell. 36 consecutive titrations of 8 μl where titrated in the sample cell. The pattern of the binding isotherm shown in Figure **S14A** indicates a 2:1 binding event between CB[7] and **L1**. Integrated heat effects were analyzed by non-linear regression in terms of a sequential two-site binding model using the Microcal Origin software package. The parameters obtained by this method are given in table **S2** entry 1.

Binding between CB[7] and [Cu(**L1**)I]I_2 was also investigated. Due to the low solubility of [Cu(**L1**)I]I_2 in H_2O, these experiments were conducted in a DMSO/MES buffer mixture (1:1). The reference cell was loaded with the same solvent mixture to obtain accurate data. In this experiment a [Cu(**L1**)I]I_2 stock solution (0.511 mM in DMSO/MES buffer (1:1)) was placed in the titration syringe and a CB[7] stock solution (0.0455 mM in DMSO/MES buffer (1:1)) was placed in the sample cell. 36 consecutive titrations of 8 μl were titrated in the sample cell. The pattern of the binding isotherm shown in Figure **S14B** indicates a 2:1 binding event between CB[7] and [Cu(**L1**)I]I_2. The parameters obtained are given in Table **S2** entry 2.

The binding of signal molecule **1** to CB[7] was investigated in H_2O. For unknown reasons we were not able to obtain accurate data for the binding of **1** to CB[7] in the MES/DMSO (25% v/v) solvent system. Therefore, we conducted an experiment in H_2O. In this experiment a stock solution (0.34 mM in H_2O) of CB[7] was placed in the sample cell and a stock solution (1.57 mM in H_2O) of signal molecule **1** was loaded in the titration syringe. 28 consecutive injection of 10 μl where titrated in the sample cell. The pattern of the binding isotherm shown in Figure **S14C** indicates a 1:1 binding event between signal molecule **1** and CB[7]. The parameters obtained are given in Table **S2** entry 3.

Thermodynamic parameters for the binding of azide **3**, propargyl alcohol (**4**) and triazole **5** with CB[7] were determined by ITC binding experiments. The binding parameters of all three compounds were determined at 25 °C in a MES/DMSO solvent mixture (100 mM, pH 6.4, 25% (v/v) DMSO). It was found that none of the three compounds has significant affinity to CB[7] in these conditions (Figure **S15**).

***Table S2**. Thermodynamic parameters for binding of CB[7] with: ligand **L1**, catalyst [Cu(**L1**)I]I_2 and signal molecule **1** at 25 ℃ derived by fitting experimental ITC data to a two-site sequential binding model or a one site binding model.*

**solvent is H_2O.*

***solvent is DMSO/MES buffer (100 mM, pH 6.4) (1:1).*

****predetermined in the sequential two-sites binding model.*

Complex	*K_{a1} (M^{-1})*	*K_{a2} (M^{-1})*	*ΔH_1 (cal mol^{-1})*	*ΔH_2 (kcal mol^{-1})*	*N*
L1*⊂*CB[7]*	$(9.3 \pm 0.19)*10^9$	$(4.2 \pm 0.6)*10^7$	$(-3.1 \pm 0.6)*10^4$	$(-3.5 \pm 0.6)*10^3$	2^{***}
*[Cu(**L1**)I]I_2⊂CB[7]***	$(1.21 \pm 0.08)*10^9$	$(3.5 \pm 0.3)*10^6$	-42.2 ± 5.34	-459.6 ± 6.01	2^{***}
1*⊂*CB[7]*	$(1.8 \pm 0.2)*10^7$	-	$(-1.09 \pm 0.05)*10^4$	-	0.75 ± 0.002

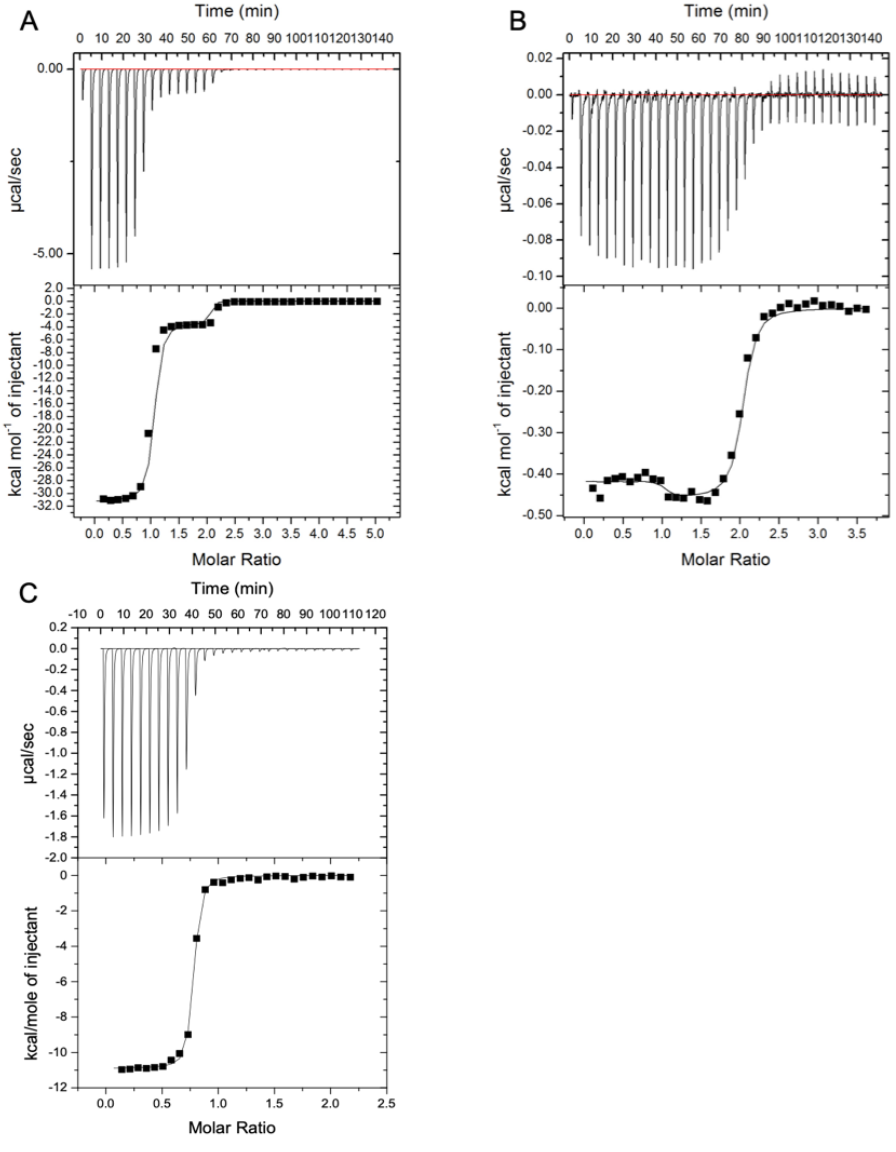

***Figure S14**. ITC data showing the characteristic biphasic binding behavior of **A) L1** and CB[7] and **B)** [Cu(**L1**)I]I$_2$ and CB[7]. **C)** ITC data showing the 1:1 binding between compound **1** and CB[7]. The differential binding curves (solid lines, lower panels) fit consistently to a sequential two-site binding model for CB[7]⊂[Cu(**L1**)I]I$_2$ and CB[7]⊂**L1**. ITC data presented in **C** were fitted to a one-site binding model. Thermodynamic parameters are given in Table **S2**.*

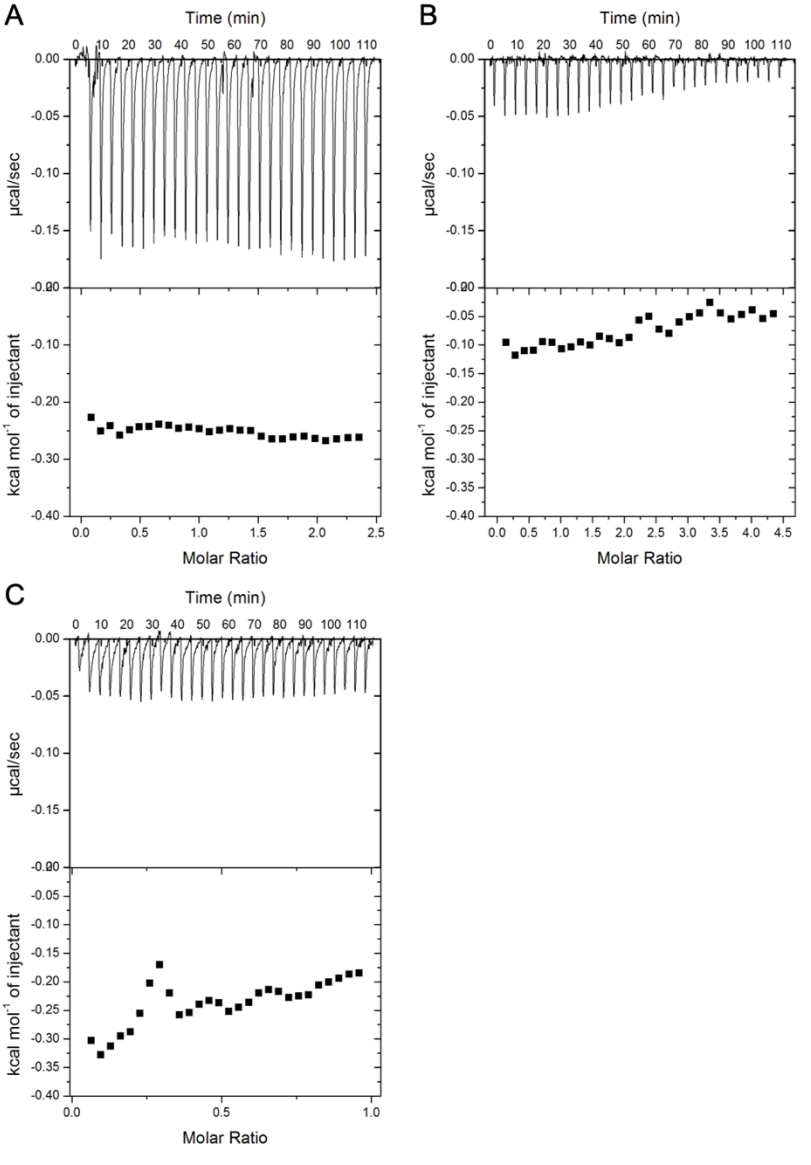

***Figure S15**. ITC data showing no affinity of azide **3** (**A**), propargyl alcohol (**4**) (**B**) and triazole **5** (**C**) to CB[7].*

2.5.8 Kinetic data

The model click reaction is assumed to be a second-order reaction (first order in both reactants). In order to obtain the kinetic rate constant, the cycloaddition reaction was performed at pseudo-first order conditions by using alkyne **4** in excess compared to azide **3**. Unless stated otherwise, concentrations used in the click reaction were 15 mM azide **3**, 451 mM propargyl alcohol (**4**) and 0.4 mM [Cu(**L1**)I]I_2.

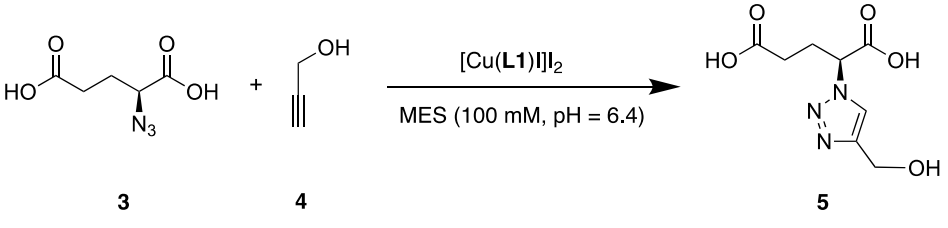

3 **4** **5**

Scheme S4*. Model click reaction. Azide **3** and alkyne **4** were reacted in the presence of [Cu(**L1**)I]I_2 to yield triazole **5**.*

Initial	t = 0	$[A]_0$	$[A]_0$	0
	t = t	$[A]_t = [A]_0 - [C]_t$	$[B]_t = [B]_0 - [C]_t$	$[C]_t$

$[A]$ is the concentration of propargyl alcohol **4**, $[B]$ the concentration of azide **3** and $[C]$ the concentration of triazole product **5**. The second order rate equation, assuming first-order in both A and B, can be expressed as:

$$rate = -k[A][B]$$

For $[A]_0 \neq [B]_0$, the second-order rate equation after integration can be expressed as:

$$ln\frac{[A]_t}{[A]_0} - ln\frac{[B]_t}{[B]_0} = k([A]_0 - [B]_0)t$$

Because propargyl alcohol **4** ($[A]$) was used in excess, it can be assumed that:

$[A]_0 \gg [B]_0$ then $\frac{[A]_t}{[A]_0} \approx 1$ and $[A]_0 - [B]_0 \approx [A]_0$

Therefore, the rate equation can be written as:

$$\frac{[B]_t}{[B]_0} = e^{-k[A]_0 t}$$

$$ln\left(\frac{[B]_t}{[B]_0}\right) = -k[A]_0 t$$

$$ln\left(1 - \frac{[C]_t}{[B]_0}\right) = -k[A]_0 t$$

where $[A]_0$ is the initial propargyl alcohol (**4**) concentration, $[B]_0$ the initial azide **3** concentration, $[C]_t$ the triazole **5** concentration at time t and k the rate constant. Hence, by following the triazole product **5** concentration over time with ^{1}H-NMR the rate constants of the pseudo-first order reactions can be determined by fitting this equation to a linear line (y = mx).

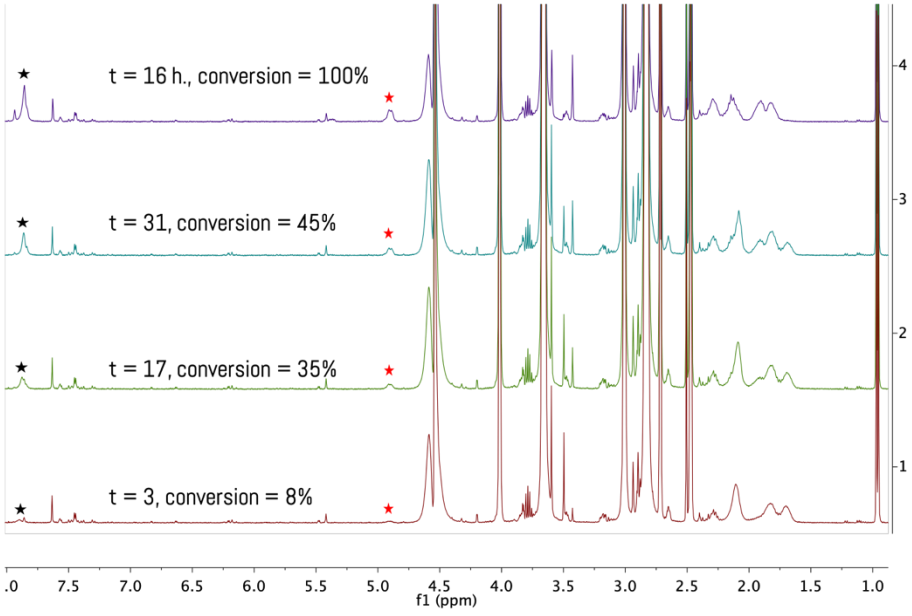

***Figure S16**. Stacked ^{1}H-NMR spectra showing formation of triazole **5** (black and red stars) (Scheme **S3**). Time (t) is in min. Conversion is relative to the theoretical maximum conversion of triazole **5**. Solvent system is MES (100 mM, pH = 6.4):DMSO-d_6 (3:1). All spectra were measured at 298 K. MES resonances are observed at 3.70 ppm, 3.07 ppm and 2.92 ppm. Propargyl alcohol **4** resonances are observed at 4.05 ppm (doublet) and 2.76 ppm (triplet). Isopropyl alcohol resonances are observed at 1.01 ppm (doublet).*

2.5.9 Equilibrium concentration of [Cu(L1)I]I_2⊂CB[7] and complex 1⊂CB[7]

The calculation here is shown for the [Cu(**L1**)I]I_2⊂CB[7] complex, but also applies for the compound **1**⊂CB[7] complex. The equilibrium concentrations can be calculated as follows:

	$[CB[7]]$	$[Cat]$	$[Cat{\subset}CB[7]]$
Initial	$[CB[7]_0] = a$	$[Cat]_0 = b$	0
Change	$-x$	$-x$	x
Equilibrium	$a - x$	$b - x$	x

$[CB[7]_0]$and $[Cat_0]$ are the CB[7] and catalyst concentrations that are added to the reaction mixture and x is the [Cu(**L1**)I]I_2⊂CB[7] complex concentration. From this, the association constant can be defined as:

$$K_a = \frac{[cat{\subset}CB[7]]}{[CB[7]][cat]} = \frac{x}{(a-x)(b-x)}$$

$$[\text{cat}{\subset}\text{CB}[7]] = \frac{a * K_a + b * K_a + 1 - \sqrt{a^2 * {K_a}^2 - 2a * b * {K_a}^2 + b^2 * {K_a}^2 + 2 * a * K_a + 2 * b * K_a + 1}}{2 * K_a}$$

$$= \frac{[\text{CB}[7]]_0 K_a + [cat]_0 K_a + 1 - \sqrt{[\text{CB}[7]]_0{}^2 K_a{}^2 - 2[\text{CB}[7]]_0 [cat]_0 K_a{}^2 + [cat]_0{}^2 K_a{}^2 + 2[\text{CB}[7]]_0 K_a + 2[cat]_0 K_a + 1}}{2K_a}$$

From this, the free CB[7] and catalyst concentrations in solution are calculated as follows:

$$[CB[7]] = [CB[7]]_0 - [Cat{\subset}CB[7]]$$

$$[Cat] = [Cat]_0 - [Cat{\subset}CB[7]]$$

$[CB[7]]$ is the uncomplexed (free) CB[7] concentration and $[Cat]$ is the uncomplexed (free) catalyst concentration.

2.5.10 Supplemental references

1. Fulmer, G. R.; Miller, A. J. M.; Sherden, N. H.; Gottlieb, H. E.; Nudelman, A.; Stoltz, B. M.; Bercaw, J. E.; Goldberg, K. I., NMR Chemical Shifts of Trace Impurities: Common Laboratory Solvents, Organics, and Gases in Deuterated Solvents Relevant to the Organometallic Chemist. *Organometallics* **2010,** *29* (9), 2176-2179.
2. Ponpipom, M. M.; Hanessian, S., A method for the selective bromination of primary alcohol groups. *Carbohydr. Res.* **1971,** *18* (2), 342-344.
3. Gaulier, C.; Hospital, A.; Legeret, B.; Delmas, A. F.; Aucagne, V.; Cisnetti, F.; Gautier, A., A water soluble CuI-NHC for CuAAC ligation of unprotected peptides under open air conditions. *Chem. Comm.* **2012,** *48* (33), 4005-4007.
4. Wang, E. S.; Choy, Y. M.; Wong, H. N. C., Synthetic studies on prehispanolone and 14,15-dihydroprehispanolone. *Tetrahedron* **1996,** *52* (37), 12137-12158.
5. Tonoi, T.; Mameda, K.; Fujishiro, M.; Yoshinaga, Y.; Shiina, I., Total synthesis of the proposed structure of astakolactin. *Beilstein J. Org. Chem.* **2014,** *10*, 2421-2427.
6. Araman, C.; Pieper-Pournara, L.; van Leeuwen, T.; Kampstra, A. S. B.; Bakkum, T.; Marqvorsen, M. H. S.; Nascimento, C. R.; Mirjam Groenewold, G. J.; van der Wulp, W.; Camps, M. G. M.; Overkleeft, H. S.; Ossendorp, F. A.; Toes, R. E. M.; van Kasteren, S. I., Bioorthogonal antigens allow the unbiased study of antigen processing and presentation. *bioRxiv* **2019**, 439323.
7. Renny, J. S.; Tomasevich, L. L.; Tallmadge, E. H.; Collum, D. B., Method of Continuous Variations: Applications of Job Plots to the Study of Molecular Associations in Organometallic Chemistry. *Angew. Chem. Int. Ed.* **2013,** *52* (46), 11998-12013.

CHAPTER

LIGHT SENSITIVE PHENACYL CROSSLINKED DEXTRAN HYDROGELS FOR CONTROLLED DELIVERY

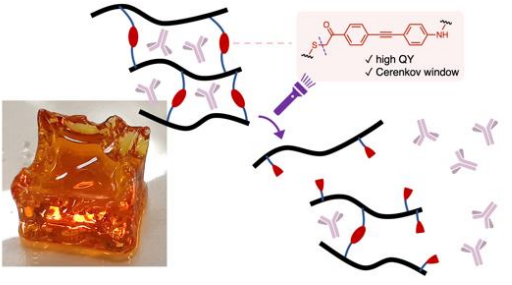

Stimuli-responsive soft materials enable controlled release of loaded drug molecules and biomolecules. Controlled release of potent chemotherapeutic or immunotherapeutic agent is crucial to reduce unwanted side effects. In an effort to develop controlled release strategies that can be triggered using Cerenkov luminescence, we have developed polymer hydrogels that can release doxorubicin, bovine serum albumin and immunoglobulin G using light (254 nm – 375 nm) as a trigger. We describe the synthesis and photochemical characterization of two light sensitive phenacyl bis-azide crosslinkers that are used to prepare transparent self-supporting hydrogel patches. One crosslinker was designed to optimize the overlap with the Cerenkov luminescence emission window, bearing an π-extended phenacyl core, resulting in a high quantum yield (14%) of photocleavage when irradiated with 375 nm light. We used the extended phenacyl crosslinker for the preparation of protein-loaded dextran hydrogel patches, which showed efficient and selective dosed release of bovine serum albumin or immunoglobulin G after irradiation with 375 nm light. Based on the high quantum yield, efficient release and large overlap with the Cerenkov window, we envision application of these photosensitive soft materials in radiation targeted drug release.

This chapter is published as:
T. G. Brevé, M. Filius, S. Weerdenburg, S. J. van der Griend, T. P. Groeneveld, A. G. Denkova, R. Eelkema, Light-sensitive phenacyl crosslinked dextran hydrogels for controlled delivery. Chem. Eur. J. ***2022****, 28, e202103523.*

3.1 INTRODUCTION

Stimuli responsive drug carrier systems have emerged as important devices in the field of biomedical applications and targeted drug delivery. General challenges for controlled release of drugs are timed or prolonged release, targeted or local release, and overcoming physicochemical barriers in the body. In order to release the cargo a phase transition or macroscopic change of the hydrogel network has to be triggered. Several triggers have been successfully applied, such as: pH, ionic strength, mechanical stress, redox potential and light. Light is of particular interest since it is spatio-temporally controlled and can be harmless when clinically applied, depending on wavelength and intensity.[1] However, human tissue limits the use of light as the penetration depth is just a few centimeters depending on the applied wavelength, which inherently limits the use of external light sources for triggered release.[2] To overcome these limitations, we were excited to investigate the potential of *in situ* generated light, known as Cerenkov luminescence (CL), and employ it as a drug release trigger. CL is generated when a charged particle, generated by the decay of radionuclides or external radiation, travels faster than the speed of light in a dielectric medium such as water or tissue. CL has a broad emission spectrum with a maximum emission around 380 nm (UV-A), and is usually generated with low intensity.[3] CL has been employed as a light source in anticancer therapies, where nanoparticles passively target solid tumors and generate reactive oxygen species (ROS).[4-10] Moreover, CL is found an effective trigger for decaging doxorubicin[11] and is employed to generate reactive singlet nitrene species, that subsequently react with extracellular proteins or lipids and 'tag' solid tumors with a drug or dye.[12] For future application with CL triggers, we aimed at developing hydrogels with light sensitive groups with an absorption maximum in the Cerenkov emission window and high quantum yield of photodegradation.

Light sensitive hydrogels have been employed in a broad variety of settings and rely on light sensitive functionalities incorporated into the hydrogel network.[13] Two

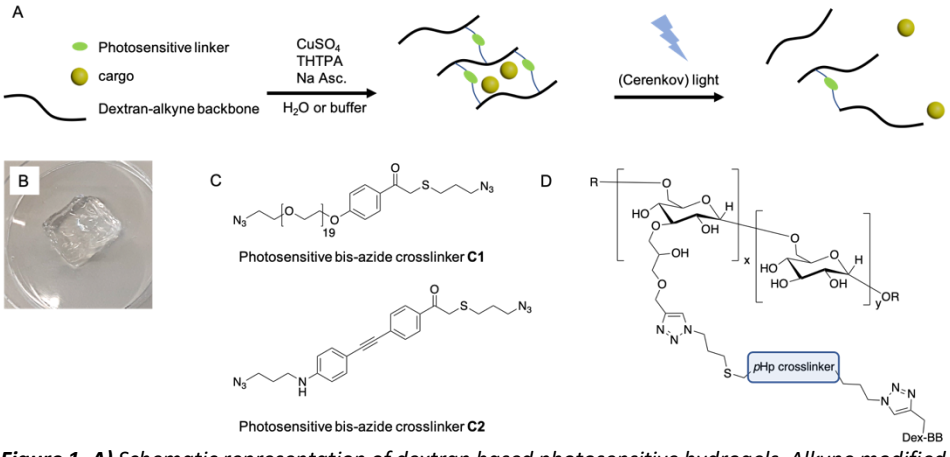

Figure 1. A) *Schematic representation of dextran based photosensitive hydrogels. Alkyne modified dextran is crosslinked with a bis-azide crosslinker using standard Cu-click conditions ($CuSO_4$, sodium ascorbate and activating ligand: Tris(3-hydroxypropyltriazolylmethyl)amine (THTPA)). UV-A light (including Cerenkov luminescence) triggers the photocleavage of the crosslinker resulting in free diffusion of the loaded cargo.* ***B)*** *Photograph of centimeter sized transparent self-supporting dextran hydrogel.* ***C)*** *Bis-azide crosslinkers* ***C1*** *and* ***C2****, synthesized and investigated in this research.* ***D)*** *Bis-azide phenacyl crosslinked dextran structure.*

well-known light sensitive moieties are the ortho-nitrobenzyl group (*o*NB) and its ortho-nitroveratryl analog.[14-18] Although ortho-nitrobenzyl and ortho-nitroveratryl groups have been employed successfully many times in a variety of studies, they have low to very low quantum yields and during photocleavage toxic nitroso adducts are formed.[19, 20] Therefore we are curious to employ phenacyl based photo cleavable hydrogel crosslinkers (Figure **1C** and **1D**), as these have a significantly higher quantum yield.[21] Photo responsive phenacyl moieties have been applied to photocage thiols,[22, 23] control the degree of swelling in polymer coatings,[24] induced light triggered folding of polymers chains[25] and to photocage a drug such as chlorambucil.[26]

Chemotherapy is one of the most important strategies to treat cancer. However, the administered dose of any particular drug is often low due to its toxicity and accompanying side effects. To mitigate these limiting factors and improve the efficacy of chemotherapeutic drugs, smart drug delivery systems are employed. Responsive hydrogel networks can be used for controlled delivery. Hydrogels are

able to covalently or non-covalently store a variety of anticancer drugs and show triggered release in the human body.[27] Alternatively, monoclonal antibodies or antibody-drug conjugates (ADC) are employed to selectively target malignant tumor cells and induce cell death.[28] Controlled antibody release can improve therapy as the total administered dose is low, on target drug concentrations are high and systemic drug exposure is low which helps to reduce side effects.[29] Release mechanisms rely on a variety of internal and external triggers, including hydrolysis,[30] temperature,[31, 32] ultrasound,[33] (UV) light[34] or enzymatic activity.[35] Also, passive release mechanisms are employed to deliver antibodies from hydrogels, where the degree of hydrogel branching and crosslink density determine the release profile of the loaded proteins.[36-38] Here, we present light cleavable dextran based hydrogels loaded with either doxorubicin, bovine serum albumin (BSA) or human Immunoglobulin G (IgG), which release their cargo when triggered by (UV-A/C) light. Photosensitivity in the Cerenkov irradiation window is introduced by crosslinking alkyne modified dextran with bis-azide phenacyl **C1** or **C2** using standard Cu-click conditions (Figure **1**).

3.2 RESULTS AND DISCUSSION

We synthesized bis-azide crosslinker **C1** starting with the protection of commercially available para-hydroxyphenacyl **1** (*p*Hp) using tert-butyldiphenyl(chloro)silane (TBDPS-Cl), affording silyl ether **2** (Scheme **1**). Next, bromination of compound **2**, using benzyltrimethylammonium tribromide ($BTMABr_3$), afforded compound **3**. In reaction step 3, using alkaline conditions, 3-chloro propane thiol was coupled to bromine **3**. The combination of prolonged reaction time and alkaline conditions also resulted in the deprotection of the slightly acid hydroxyl in bromine **3**, affording deprotected *p*Hp **4**.[39, 40] Treating *p*Hp **4** with NaN_3 afforded azide **5**, and in the final

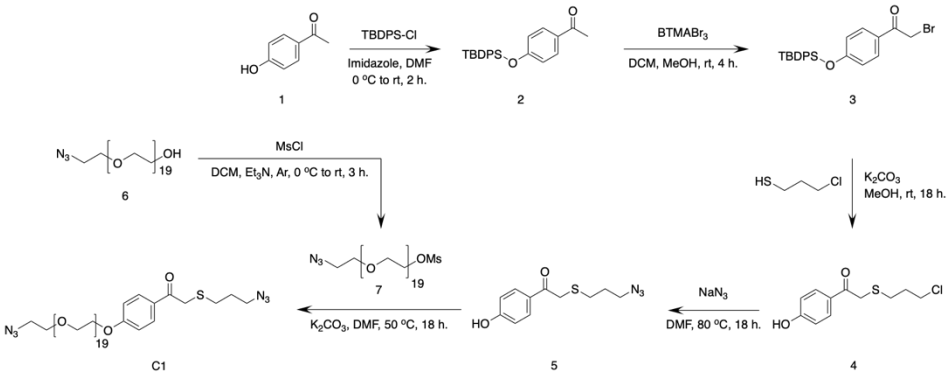

Scheme 1. *Synthetic pathway for the 6-step synthesis of bis-azide crosslinker **C1**, starting from parahydroxy phenacyl (pHp) **1**.*

reaction step azide **5** was coupled to mesylated polyethylene glycol (PEG) **7** affording bis-azide crosslinker **C1** (Figure **S1**). **C1** has an absorption maximum at 283 nm, which is not ideal for CL triggering. To gain insight in the photodegradation process of crosslinker **C1**, we performed an irradiation experiment in which one sample was irradiated with UV-C light (254 nm, 1.02 mW/cm^2) and one sample was kept in the dark as a control. We found that the absorption (283 nm) of the light irradiated sample decreases and shifts with increasing irradiation time, indicating photocleavage of **C1** (Figure **2A** and **2B** (green data)), while the non-irradiated sample remained stable over time (black data, Figure **2B**). Using standard Cu-click conditions ($CuSO_4$ (0.47 mM), sodium ascorbate (3.0 mM), activating ligand: Tris(3-hydroxypropyltriazolylmethyl)amine (THTPA) (0.24 mM)), crosslinker **C1** and alkyne modified dextran (500 kDa, DS = 36%, Figure **S3**) were reacted to prepare transparent self-supporting dextran hydrogels (Figure **2C**), having a storage modulus (G') of 4.3 x 10^2 Pa and tan δ(G''/G') of 6.7 x 10^{-3} (Figure **S11**). These hydrogels were loaded with doxorubicin (Figure **2D**) and the washed hydrogels were then placed in fresh H_2O (25 ml) and irradiated with UV-C light (254 nm, 1.02 mW/cm^2) (Figure **2F**). Aliquots were collected at selected timepoints over a period of 24 hours (Figure **S8B**) and UV/Vis analysis showed a linear increase of absorbance at 480 nm, which is doxorubicin's absorption maximum. Unfortunately, the observed increase in

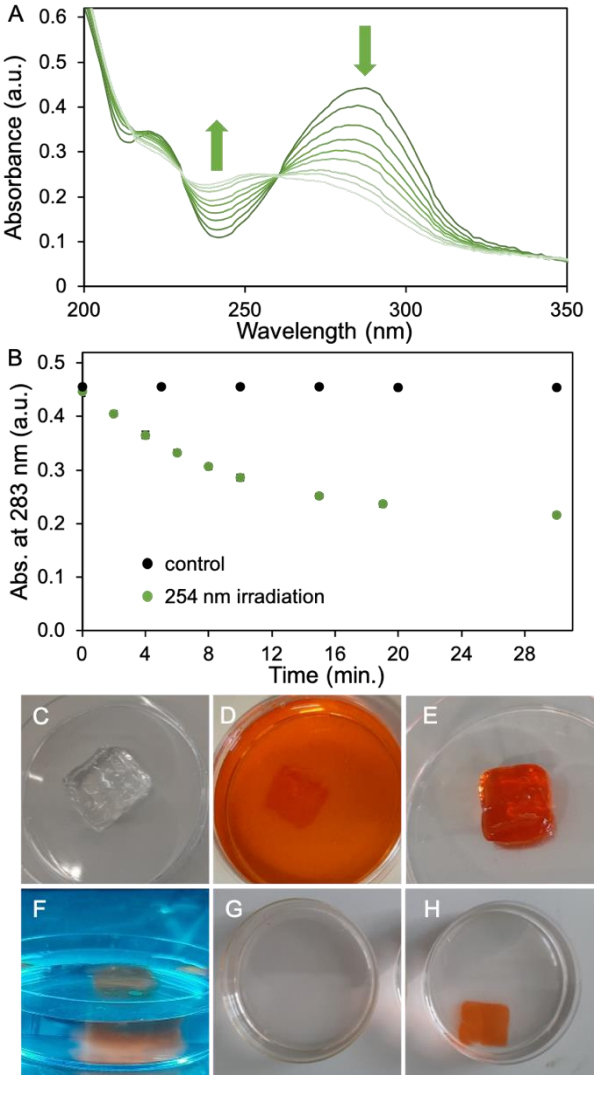

Figure 2. A) *UV/Vis data recorded during 254 nm light (1.02 mW/cm^2) irradiation experiment of crosslinker* ***C1*** *(40 μM in H_2O).* ***B)*** *Absorbance at 283 nm over time. Black data is a non-irradiated control sample, green data is irradiated sample.* ***C)-H)*** *series of photographs taken during doxorubicin load and release process.* ***C)*** *H_2O washed and swollen gel.* ***D)*** *Hydrogel submerged in doxorubicin loading solution (0.18 mM in H_2O after 148 hours incubation.* ***E)*** *Doxorubicin loaded hydrogel taken out from the doxorubicin loading solution.* ***F)*** *Doxorubicin loaded gel during 254 nm light irradiation.* ***G)*** *After irradiation, the hydrogel object has fully disintegrated.* ***H)*** *Non-irradiated control hydrogel after 24 h in H_2O.*

absorbance was very small, which is likely caused by the simultaneous photo degradation of doxorubicin. In the same experiment, a 5-fold increase in absorbance at 283 nm was observed which is contributed to degradation products of doxorubicin (Figure **S8A**). Although the photodegradation of doxorubicin is undesirable, the experiment does demonstrate that **C1** phenacyl works as a photolabile crosslinker as the hydrogels completely disintegrated upon UV-C irradiation (Figure **2G**), in contrast with the control hydrogels that remained intact and retained the loaded doxorubicin within the hydrogel matrix (Figure **2H**).

In this stage of the research we opted to develop a π-extended analogue of crosslinker **C1**, which would absorb light in the UV-A region to trigger its photocleavage. This would enable the release of proteins using our hydrogels. Since many proteins often do not absorb light above 300 nm, we expected no interference during light irradiation experiments. Also, the emission maximum of CL is centered around 380 nm light, and the increased overlap of the CL window with the absorbance spectrum of the new crosslinker would increase the efficiency of our system.[3] We synthesized crosslinker **C2** which has an extended conjugated π-system compared to crosslinker **C1** and has a maximum absorbance at 383 nm, instead of 283 nm. The synthesis of bis-azide crosslinker **C2** was started with the mesylation of 3-azido-propanol and the subsequent coupling with 4-ethynyl-aniline afforded alkyne **10** (Scheme **2**). Next, reacting 3-chloro-propane thiol with bromine **11**

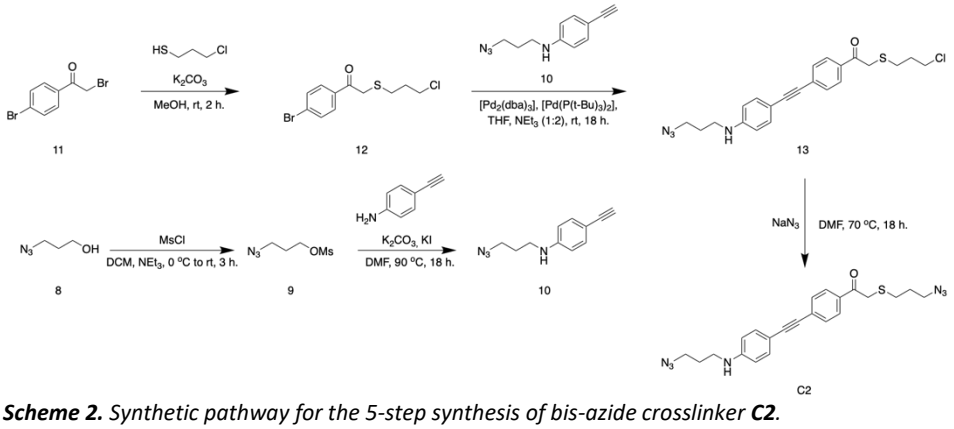

Scheme 2. *Synthetic pathway for the 5-step synthesis of bis-azide crosslinker **C2**.*

yielded bromine **12**. The Sonogashira coupling of alkyne **10** and bromine **12**, catalyzed by $[Pd_2(dba)_3]$ and $[Pd(P(t\text{-}Bu)_3)_2]$ afforded the π-extended *p*Hp **13**, which in the final reaction step was treated with NaN_3 to yield bis-azide crosslinker **C2** as a yellow powder.

To examine the photochemical properties of **C2** a solution was prepared and irradiated with 375 nm light (1240 mW, incident intensity = 2.93 ± 0.08 x 10^{15} determined by ferrioxalate actinometry[41, 42] (details in SI)). During a period of 60 minutes, aliquots were collected and analyzed using UV/Vis spectroscopy (Figure **3B**). We observed a linear decrease of absorbance (383 nm), indicating photodegradation of **C2** (Figure **3C**, blue data), while the absorbance data collected for the non-irradiated control sample remained stable over time (Figure **3C**, black data). Photodegradation was confirmed by ESI-MS analysis were we found m/z = 319.12 ($[M+H^+]$) (Figure **S4**), corresponding with the mass of the ketone photoproduct generated in the photodegradation process of **C2** (Figure **3A**).[43, 44] The photodegradation rate of **C2** was calculated (**C2** extinction coefficient = ε_{383} 27210 M^{-1} cm^{-1} (Figure **S6**)) according the collected UV/Vis (Figure **3B** and **3C**) data and equals 6.8 x 10^{-10} mol s^{-1}. Alternatively, the photodegradation process of **C2** was

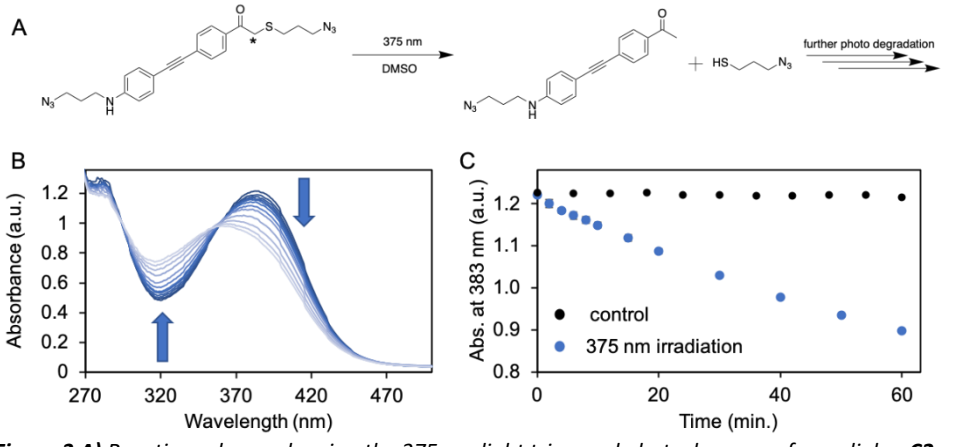

Figure 3 A) *Reaction scheme showing the 375 nm light triggered photocleavage of crosslinker* ***C2****, generating the ketone photoproduct of* ***C2*** *and 3-azido-propanethiol.* ***B)*** *UV/Vis data recorded during the 375 nm light (photon flux =* 2.93 ± 0.08 x 10^{15} * s^{-1}*) irradiation experiment of crosslinker* ***C2*** *(40 μM in DMSO).* ***C)*** *Absorbance at 383 nm over time. Black data is non-irradiated control sample, blue data is irradiated sample.*

monitored by ^{1}H-NMR analyses. Here we observed a linear decrease of the resonance at 4.03 ppm (in DMSO-d6) belonging to the α-carbon in **C2** (indicated with asterisk, Figure **3A** and **S5**), indicating the photocleavage of the thioether. Additionally, the photodegradation rate was determined according the collected ^{1}H-NMR data (Figure **S5**) and equals 6.5 x 10^{-10} mol s^{-1}, which is in line with the degradation rate determined according the UV/Vis data. The quantum yield (ϕ) of photodegradation for crosslinker **C2** equals ϕ = 0.14 calculated using UV/Vis data or ϕ = 0.13 calculated using ^{1}H-NMR data, which is in line with reported values of comparable thioether phenacyl structures,[44, 45] and is higher than typical o-nitrobenzyl or o-nitroveratryl cages.[21]

Next, we prepared hydrogel patches (4 x 4 cm, thickness ~ 2 mm) loaded with BSA as a model protein (Figure **4A**). First, a BSA stock solution (60 µl, 0.63 mg/ml, phosphate buffer (PB) (100 mM, pH 7.4)) was prepared and mixed with a dextran-alkyne solution (10 wt% in DMSO), which subsequently was mixed with a crosslinker **C2** solution (400 µl, 4.61 µM, DMSO) containing Cu-click reactants (CuI 3.2 µM, DIPEA 8.6 µM,) and transferred to a quartz cuvette (4 x 4 x 4 cm) to gel overnight. After washing the hydrogel patches (details in SI), one hydrogel was irradiated with 375 nm light in order to degrade the hydrogel matrix and release the loaded BSA (66.5 kDa). Another hydrogel was kept in the dark as a control. During irradiation, aliquots were collected and subsequently analyzed for their protein content by SDS-page gel analyses (sample mixture fluorescently labelled with NHS-Cy5, details in SI) (Figure **4B**, right lanes). Here, we observed an increasing trend in fluorescence intensity as irradiation time increases, indicating the release of BSA protein, while barely any fluorescent signal is observed in the non-irradiated control hydrogel after 24 hours (Figure **4B**, left lanes). The fluorescent protein band is located high (approximately at 500 kDa range) in the SDS-page gel, which is likely the result of resolubilized dextran polymer (500 kDa) during light irradiation, resulting in clogging of the SDS-page gel which prevents BSA to migrate freely through the SDS-page gel

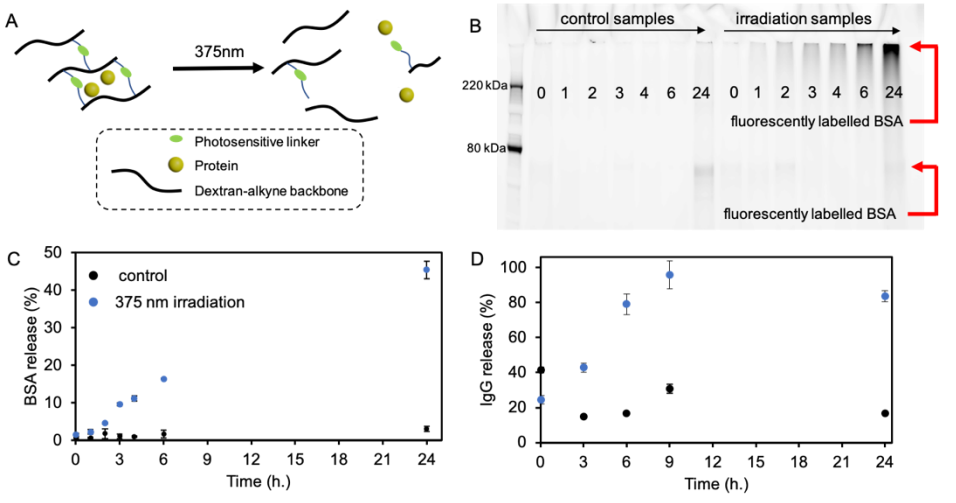

Figure 4 A) *Schematic representation of a dextran-based protein loaded hydrogel, which shows light triggered protein release.* ***B)*** *Fluorescent SDS-page gel analysis of aliquots collected during 375 nm light irradiation experiments of BSA loaded* ***C2*** *crosslinked hydrogel patches. The collected aliquots where incubated with NHS-Cy5 fluorophore prior to SDS-page gel analysis. Fluorescent intensity of the entire lane was analyzed. Control samples show no fluorescent signal except the 24-hour timepoint which shows low intensity fluorescence. An increase in fluorescence is observed over a time span of 24 hours.* ***C)*** *375 nm light triggered release of BSA from* ***C2*** *crosslinked hydrogel patches. BSA concentration was determined by UV/Vis analysis (NanoDrop). Initial BSA hydrogel loading = 1.8 μg/ml, maximal detected BSA concentration after 24 hours of light irradiation = 0.8 μg/ml (45% release efficiency). SD determined by n = 2 experiments.* ***D)*** *375 nm light triggered release of IgG from* ***C2*** *crosslinked hydrogel patches. IgG concentration was determined by a Bradford assay. Initial IgG hydrogel loading = 0.5 mg/ml, maximal detected IgG concentration after 9 hours of light irradiation = 0.48 mg/ml (96% release efficiency). SD determined by n = 2 experiments.*

material.[46] Since NHS-fluorescent labelling is specific towards protein amines, we are confident that we are observing the light triggered release of BSA protein from the dextran hydrogel matrix. This is supported by accompanying UV/Vis (NanoDrop) data we collected, which shows a linear increase of protein release reaching a 45% release efficiency after 24 hours of 375 nm light irradiation (Figure **4C**). Encouraged by these results we decided to load human IgG in our hydrogel patches. Human IgG is an interesting model protein as antibodies and antibody drug conjugates (ADC) are potent anticancer agents.[47] The molecular weight of human IgG is approximately 150 kDa which is 2.3 times heavier than BSA (66.5 kDa). Larger molecules typically

diffuse slower from a hydrogel matrix.[37] This allowed us to reduce the crosslinker **C2** loading (25% lower initial **C2** concentration) in our hydrogels while still hampering protein diffusion from the hydrogel matrix. To test antibody release, we prepared hydrogel patches as described before, and loaded human IgG (0.5 mg/ml). After gelation was complete, 375 nm light irradiation was started and the IgG release was quantified according a Bradford assay. We found a linear increase in IgG concentration with increasing irradiation time, reaching a release efficiency of 96% after 9 hours of 375 nm light irradiation (Figure **4D**).

Encouraged by our obtained results on light triggered protein release, we were curious if we could photodegrade our hydrogel using real CL, which would result in protein release. To test this, we prepared protein containing hydrogel patches of which one was placed in a ^{60}Co-source and one was kept aside as a control. The γ-radiation emitted by a ^{60}Co source (0.6 kGy/h) generates low intensity light due to the Cerenkov effect, which could potentially trigger the photocleavage of crosslinker **C2**, resulting in the triggered release of the loaded proteins. However, we did not detect a significant amount of protein in the hydrogel's supernatant aqueous solution compared to the control hydrogel, indicating that the triggered release had failed. When visually inspecting the γ-irradiated hydrogels we observed a remarkable contraction effect where the hydrogels consistently showed a macroscopic contraction of the hydrogel volume. Inspired by these results we started to investigate this contraction effect and found that the residual, unreacted alkyne moieties after initial Cu-click mediated crosslinking, form new alkyne-alkyne crosslinks. These secondary γ-irradiation induced crosslinks result in an increased hydrogel stiffness and a significantly reduced hydrogel volume.[48] Moreover, the diffusivity of the hydrogel loaded proteins is thus further restrained due to the increased crosslink density, which explains why no protein release was observed. All together, we were not able to perform proper CL triggered release experiments, due to the inference caused by the residual alkyne groups. For future hydrogel design

we will have to carefully design the polymer backbone structure and avoid residual reactive groups that potentially could interfere with γ-radiation. At present, CL-triggered release using phenacyl crosslinkers remains inconclusive.

3.3 CONCLUSION

In conclusion, we have synthesized two phenacyl bis-azide crosslinkers, which have been incorporated in dextran-based hydrogels to enable photosensitivity in the Cerenkov emission window. Crosslinker **C1** photodegrades upon 254 nm light irradiation resulting in the complete dissolution of **C1** crosslinked dextran hydrogels releasing loaded doxorubicin. However, the absorption spectrum of **C1** has a too small overlap with the CL spectrum, and UV-A irradiation leads to drug disintegration. A redesign led to extended crosslinker **C2**. **C2** crosslinked dextran hydrogels were loaded with BSA protein or human IgG antibody which was released upon 375 nm light irradiation. The release efficiency for BSA was 45% after 24 hours irradiation, and 96% for the IgG antibody after 9 hours of 375 nm light irradiation. With a quantum yield of photodegradation of 0.14 and an absorption maximum at 380 nm, crosslinker **C2** is more suited for application with CL triggers. Although we show promising photosensitivity of our protein loaded hydrogels we could not yet demonstrate protein release triggered by Cerenkov light. Development of CL triggered drug release materials is currently being pursued in our lab.

3.4 OUTLOOK

The **C2** crosslinked hydrogels discussed in this chapter show promising photo responsiveness in the Cerenkov emission window, having a relatively high quantum yield and quantitively release loaded IgG antibodies triggered by 375 nm light. However, when trying to release the loaded protein triggered by Cerenkov light we were unsuccessful. In the current polymer design, residual alkyne sidechains remain unreacted after the preparation of hydrogels, which crosslink when the hydrogel is

irradiated with γ-rays leading to hydrogel contraction and decreasing diffusivity of the loaded protein. To prevent hydrogel contraction or any other unwanted reactivity after gelation induced by γ-radiation, the ratio of alkyne sidechains and bis-azide crosslinker should be 2:1 to ensure all alkyne moieties have reacted during gelation. A small excess of bis-azide crosslinker relative to the alkyne would also be an option, although thorough washing steps after gelation are then required to remove unreacted bis-azide crosslinker.

The reported hydrogels could be further improved when considering the photosensitivity. Currently, the quantum yield of crosslinker **C2** is 0.14 which is relatively high. Since the intensity of Cerenkov luminesce is weak, the quantum yield of the used crosslinker should be as high as possible in order to achieve a rapid photo triggered release. Improving the quantum yield of crosslinker **C2** can be achieved by using other leaving groups than the current thiol. In general, the lower the pK_a of a leaving group the higher the quantum yield of dissociation is.[19] An alkyl thiol is in the range of pK_a = 10 – 11. When we select a phosphate leaving group, a significant improvement in sensitivity can be made, as the pK_a is in the range 0.5 – 1 and reported quantum yields are in the range 0.35 – 0.4. Scheme 3 shows a short-hand synthesis route to a potentially interesting crosslinker based on the π-extended phenacyl scaffold and a phosphate leaving group.[49, 50]

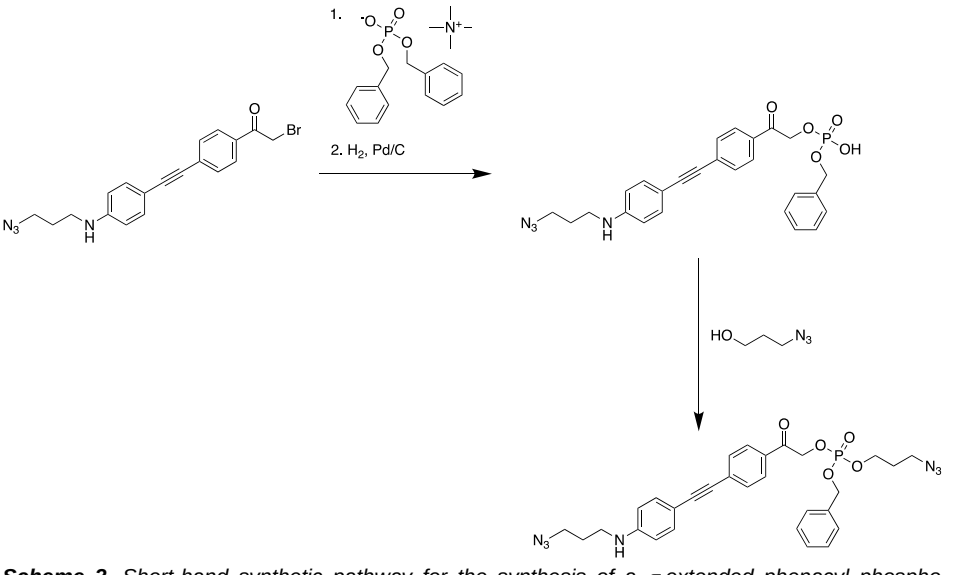

Scheme 3. *Short-hand synthetic pathway for the synthesis of a π-extended phenacyl phospho-crosslinker.*

3.5 REFERENCES

1. Fomina, N.; Sankaranarayanan, J.; Almutairi, A., Photochemical mechanisms of light-triggered release from nanocarriers. *Adv. Drug Del. Rev.* **2012,** *64* (11), 1005-1020.
2. Ash, C.; Dubec, M.; Donne, K.; Bashford, T., Effect of wavelength and beam width on penetration in light-tissue interaction using computational methods. *Lasers Med. Sci.* **2017,** *32* (8), 1909-1918.
3. Thorek, D. L.; Robertson, R.; Bacchus, W. A.; Hahn, J.; Rothberg, J.; Beattie, B. J.; Grimm, J., Cerenkov imaging - a new modality for molecular imaging. *Am. J. Nucl. Med. Mol. Imaging* **2012,** *2* (2), 163-173.
4. Duan, D.; Liu, H.; Xu, Y.; Han, Y.; Xu, M.; Zhang, Z.; Liu, Z., Activating TiO2 Nanoparticles: Gallium-68 Serves as a High-Yield Photon Emitter for Cerenkov-Induced Photodynamic Therapy. *ACS Appl. Mater. & Interfaces* **2018,** *10* (6), 5278-5286.
5. Kotagiri, N.; Cooper, M. L.; Rettig, M.; Egbulefu, C.; Prior, J.; Cui, G.; Karmakar, P.; Zhou, M.; Yang, X.; Sudlow, G.; Marsala, L.; Chanswangphuwana, C.; Lu, L.; Habimana-Griffin, L.; Shokeen, M.; Xu, X.; Weilbaecher, K.; Tomasson, M.; Lanza, G.; DiPersio, J. F.; Achilefu, S., Radionuclides transform chemotherapeutics into phototherapeutics for precise treatment of disseminated cancer. *Nat. Comm.* **2018,** *9* (1), 275.
6. Yu, B.; Ni, D.; Rosenkrans, Z. T.; Barnhart, T. E.; Wei, H.; Ferreira, C. A.; Lan, X.; Engle, J. W.; He, Q.; Yu, F.; Cai, W., A “Missile-Detonation” Strategy to Precisely Supply and Efficiently Amplify Cerenkov Radiation Energy for Cancer Theranostics. *Adv. Mater.* **2019,** *31* (52), 1904894.
7. Kamkaew, A.; Cheng, L.; Goel, S.; Valdovinos, H. F.; Barnhart, T. E.; Liu, Z.; Cai, W., Cerenkov Radiation Induced Photodynamic Therapy Using Chlorin e6-Loaded Hollow Mesoporous Silica Nanoparticles. *ACS Appl. Mater. & Interfaces* **2016,** *8* (40), 26630-26637.
8. Ni, D.; Ferreira, C. A.; Barnhart, T. E.; Quach, V.; Yu, B.; Jiang, D.; Wei, W.; Liu, H.; Engle, J. W.; Hu, P.; Cai, W., Magnetic Targeting of Nanotheranostics Enhances Cerenkov Radiation-Induced Photodynamic Therapy. *J. Am. Chem. Soc.* **2018,** *140* (44), 14971-14979.
9. Denkova, A. G.; Liu, H.; Men, Y.; Eelkema, R., Enhanced Cancer Therapy by Combining Radiation and Chemical Effects Mediated by Nanocarriers. *Adv. Ther.* **2020,** *3* (3), 1900177.
10. Liu, H.; Laan, A. C.; Plomp, J.; Parnell, S. R.; Men, Y.; Dalgliesh, R. M.; Eelkema, R.; Denkova, A. G., Ionizing Radiation-Induced Release from Poly(ε-

caprolactone-b-ethylene glycol) Micelles. *ACS Appl. Pol. Mat.* **2021,** *3* (2), 968-975.

11. Yao, C.; Li, J.; Cao, X.; Gunn, J. R.; Wu, M.; Jiang, S.; Pogue, B. W., X-ray-Induced Cherenkov Optical Triggering of Caged Doxorubicin Released to the Nucleus for Chemoradiation Activation. *ACS Appl. Mater. & Interfaces* **2020,** *12* (40), 44383-44392.
12. Das, S.; Haedicke, K.; Grimm, J., Cerenkov-Activated Sticky Tag for In Vivo Fluorescence Imaging. *J. Nucl. Med.* **2018,** *59* (1), 58.
13. Li, L.; Scheiger, J. M.; Levkin, P. A., Design and Applications of Photoresponsive Hydrogels. *Adv. Mater.* **2019,** *31* (26), 1807333.
14. Zhao, H.; Sterner, E. S.; Coughlin, E. B.; Theato, P., o-Nitrobenzyl Alcohol Derivatives: Opportunities in Polymer and Materials Science. *Macromol.* **2012,** *45* (4), 1723-1736.
15. Men, Y.; Brevé, T. G.; Liu, H.; Denkova, A. G.; Eelkema, R., Photo cleavable thioacetal block copolymers for controlled release. *Polym. Chem.* **2021**.
16. LeValley, P. J.; Neelarapu, R.; Sutherland, B. P.; Dasgupta, S.; Kloxin, C. J.; Kloxin, A. M., Photolabile Linkers: Exploiting Labile Bond Chemistry to Control Mode and Rate of Hydrogel Degradation and Protein Release. *J. Am. Chem. Soc.* **2020,** *142* (10), 4671-4679.
17. LeValley, P. J.; Sutherland, B. P.; Jaje, J.; Gibbs, S.; Jones, R. M.; Gala, R. P.; Kloxin, C. J.; Kiick, K. L.; Kloxin, A. M., On-Demand and Tunable Dual Wavelength Release of Antibodies Using Light-Responsive Hydrogels. *ACS Appl. Bio Mat.* **2020,** *3* (10), 6944-6958.
18. Kloxin, A. M.; Kasko, A. M.; Salinas, C. N.; Anseth, K. S., Photodegradable hydrogels for dynamic tuning of physical and chemical properties. *Science (New York, N.Y.)* **2009,** *324* (5923), 59-63.
19. Givens, R. S.; Rubina, M.; Wirz, J., Applications of p-hydroxyphenacyl (pHP) and coumarin-4-ylmethyl photoremovable protecting groups. *Photoch. Photobio. Sci.* **2012,** *11* (3), 472-488.
20. Du, X.; Frei, H.; Kim, S. H., Comparison of nitrophenylethyl and hydroxyphenacyl caging groups. *Biopol.* **2001,** *62* (3), 147-9.
21. Klán, P.; Šolomek, T.; Bochet, C. G.; Blanc, A.; Givens, R.; Rubina, M.; Popik, V.; Kostikov, A.; Wirz, J., Photoremovable Protecting Groups in Chemistry and Biology: Reaction Mechanisms and Efficacy. *Chem. Rev.* **2013,** *113* (1), 119-191.
22. Glassner, M.; Oehlenschlaeger, K. K.; Welle, A.; Bruns, M.; Barner-Kowollik, C., Polymer surface patterning via Diels–Alder trapping of photo-generated thioaldehydes. *Chem. Comm.* **2013,** *49* (6), 633-635.
23. Tischer, T.; Claus, T. K.; Oehlenschlaeger, K. K.; Trouillet, V.; Bruns, M.; Welle, A.; Linkert, K.; Goldmann, A. S.; Börner, H. G.; Barner-Kowollik, C., Ambient

Temperature Ligation of Diene Functional Polymer and Peptide Strands onto Cellulose via Photochemical and Thermal Protocols. *Macromol. Rapid Comm.* **2014,** *35* (12), 1121-1127.

24. Carias, V.; Wang, J.; Toomey, R., Poly(N-isopropylacrylamide) Cross-Linked Coatings with Phototunable Swelling. *Langmuir* **2014,** *30* (14), 4105-4110.
25. Claus Tanja, K.; Zhang, J.; Martin, L.; Hartlieb, M.; Mutlu, H.; Perrier, S.; Delaittre, G.; Barner-Kowollik, C., Stepwise Light-Induced Dual Compaction of Single-Chain Nanoparticles. *Macromol. Rapid Comm.* **2017,** *38* (16), 1700264.
26. Gangopadhyay, M.; Jana, A.; Rajesh, Y.; Bera, M.; Biswas, S.; Chowdhury, N.; Zhao, Y.; Mandal, M.; Singh, N. D. P., Organic Nanoparticle-Based Fluorescent Chemosensor for Selective Switching ON and OFF of Photodynamic Therapy (PDT). *Chem. Select* **2016,** *1* (20), 6523-6531.
27. Fu, X.; Hosta-Rigau, L.; Chandrawati, R.; Cui, J., Multi-Stimuli-Responsive Polymer Particles, Films, and Hydrogels for Drug Delivery. *Chem* **2018,** *4* (9), 2084-2107.
28. Diamantis, N.; Banerji, U., Antibody-drug conjugates—an emerging class of cancer treatment. *Br. J. Cancer* **2016,** *114* (4), 362-367.
29. Huynh, V.; Jesmer, A. H.; Shoaib, M. M.; D'Angelo, A. D.; Rullo, A. F.; Wylie, R. G., Improved Efficacy of Antibody Cancer Immunotherapeutics through Local and Sustained Delivery. *ChemBioChem* **2019,** *20* (6), 747-753.
30. Ashley, G. W.; Henise, J.; Reid, R.; Santi, D. V., Hydrogel drug delivery system with predictable and tunable drug release and degradation rates. *Proc. Natl. Acad. Sci. U. S. A.* **2013,** *110* (6), 2318-23.
31. Gregoritza, M.; Messmann, V.; Abstiens, K.; Brandl, F. P.; Goepferich, A. M., Controlled Antibody Release from Degradable Thermoresponsive Hydrogels Cross-Linked by Diels–Alder Chemistry. *Biomacromol.* **2017,** *18* (8), 2410-2418.
32. Chung, C. K.; Fransen, M. F.; van der Maaden, K.; Campos, Y.; García-Couce, J.; Kralisch, D.; Chan, A.; Ossendorp, F.; Cruz, L. J., Thermosensitive hydrogels as sustained drug delivery system for CTLA-4 checkpoint blocking antibodies. *J. Contr. Rel.* **2020,** *323*, 1-11.
33. Huebsch, N.; Kearney, C. J.; Zhao, X.; Kim, J.; Cezar, C. A.; Suo, Z.; Mooney, D. J., Ultrasound-triggered disruption and self-healing of reversibly cross-linked hydrogels for drug delivery and enhanced chemotherapy. *Proc. Natl. Acad. Sci. U. S. A.* **2014,** *111* (27), 9762-7.
34. Azagarsamy, M. A.; Anseth, K. S., Wavelength-controlled photocleavage for the orthogonal and sequential release of multiple proteins. *Angew Chem Int Ed Engl* **2013,** *52* (51), 13803-13807.

35. Franssen, O.; Vos, O. P.; Hennink, W. E., Delayed release of a model protein from enzymatically-degrading dextran hydrogels. *J. Contr. Rel.* **1997,** *44* (2), 237-245.
36. Kim, J.; Francis, D. M.; Thomas, S. N., In Situ Crosslinked Hydrogel Depot for Sustained Antibody Release Improves Immune Checkpoint Blockade Cancer Immunotherapy. *Nanomat. (Basel)* **2021,** *11* (2).
37. Hennink, W. E.; Talsma, H.; Borchert, J. C. H.; De Smedt, S. C.; Demeester, J., Controlled release of proteins from dextran hydrogels. *J Contr. Rel.* **1996,** *39* (1), 47-55.
38. Sun, G.; Chu, C.-C., Synthesis, characterization of biodegradable dextran–allyl isocyanate–ethylamine/polyethylene glycol–diacrylate hydrogels and their in vitro release of albumin. *Carbohydr. Polym.* **2006,** *65* (3), 273-287.
39. Wilson, N. S.; Keay, B. A., Mild base mediated desilylation of various phenolic silyl ethers. *Tetrahedron Lett.* **1997,** *38* (2), 187-190.
40. Prakash, C.; Saleh, S.; Blair, I. A., Selective removal of phenolic and alcoholic silyl ethers. *Tetrahedron Lett.* **1994,** *35* (41), 7565-7568.
41. Hatchard, C. G.; Parker, C. A.; Bowen, E. J., A new sensitive chemical actinometer - II. Potassium ferrioxalate as a standard chemical actinometer. *Proceedings of the Roy. Soc. London. Series A. Math. Phys. Sci.* **1956,** *235* (1203), 518-536.
42. Lehóczki, T.; Józsa, É.; Ősz, K., Ferrioxalate actinometry with online spectrophotometric detection. *J. Photochem. Photobiol. A: Chem.* **2013,** *251*, 63-68.
43. Sheehan, J. C.; Umezawa, K., Phenacyl photosensitive blocking groups. *J. Org. Chem.* **1973,** *38* (21), 3771-3774.
44. Specht, A.; Loudwig, S.; Peng, L.; Goeldner, M., p-Hydroxyphenacyl bromide as photoremoveable thiol label: a potential phototrigger for thiol-containing biomolecules. *Tetrahedron Lett.* **2002,** *43* (49), 8947-8950.
45. Parthiban, C.; M, P.; Reddy, L. V. K.; Sen, D.; Samuel S, M.; Singh, N. D. P., Tetraphenylethylene conjugated p-hydroxyphenacyl: fluorescent organic nanoparticles for the release of hydrogen sulfide under visible light with real-time cellular imaging. *Org. Biomol. Chem.* **2018,** *16* (42), 7903-7909.
46. Shaw, M. M.; Riederer, B. M., Sample preparation for two-dimensional gel electrophoresis. *Proteomics* **2003,** *3* (8), 1408-17.
47. Hamilton, G. S., Antibody-drug conjugates for cancer therapy: The technological and regulatory challenges of developing drug-biologic hybrids. *Biologicals* **2015,** *43* (5), 318-332.
48. Brevé, T.G.; Liu, H.; Denkova, A. G.; Eelkema, R.; *Gamma Radiation Induced Contraction of Alkyne Modified Polymer Hydrogels*. Chem*R*xiv, **2021**.

49. Gupta AK, Kumar R, Dubey DK, Kaushik MP. *p*-Toluenesulfonic Acid–Celite as a Reagent for Synthesis of Esters of Alkylphosphonic Acids under Solvent-Free Conditions. J. Chem. Res. **2007** 328-331.
50. Chan-Ho Park, Richard S. Givens, New photoactivated protecting groups. 6. p-Hydrodroxyphenacyl: A phototrigger for chemical and biochemical probes. J. Am. Chem. Soc. **1997**, *119* (10), 2453-2463

3.6 SUPPLEMENTARY INFORMATION

3.6.1 General considerations

All solvents and chemicals were purchased from Sigma Aldrich or Apollo scientific and used without further purification. ^{1}H-NMR and ^{13}C-NMR were recorded on an Agilent-400 MR DD2 (399.67 MHz for ^{1}H and 100.5 MHz for ^{13}C) at 298 K. The chemical shifts are given with respect to solvent residual signals as reported by Fulmer et al.[1] The rheological measurements were performed using a rheometer (AR G2, TA instruments) equipped with a steel plate-and-plate geometry of 40 mm in diameter and equipped with hexadecane trap. UV-Vis spectroscopic measurements were recorded on an Analytik Jena Specord 250 photo spectrometer, using quartz cuvettes (pathlength = 1 cm) at RT. Osram Puritec HNS 8W G5 OFR UV-C lamps (2 units) were used for all 254 nm light irradiation experiments. The irradiance at 254 nm was determined using a UVC-254SD meter (Lutron). All γ-irradiation experiments were conducted using a Nordion GC220 ^{60}Co source.

3.6.2 Synthesis of phenacyl photo-labile crosslinker C1

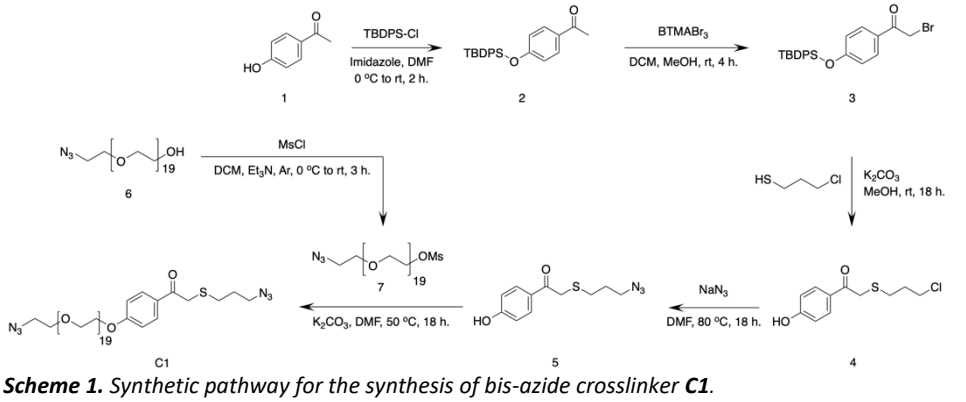

Scheme 1. *Synthetic pathway for the synthesis of bis-azide crosslinker* ***C1****.*

1-(4-((tert-butyldiphenylsilyl)oxy)phenyl)ethan-1-one (2)

4'-hydroxy-acetophenone (**1**) (6.0 g, 44 mmol) and imidazole (7.52 g, 110 mmol) were dissolved in DMF (30 ml) and cooled to 0 °C using an ice bath. Tert-butyl(chloro)diphenylsilane (17.4 ml, 66.9 mmol) was slowly added and the reaction mixture was stirred for 2 hours at RT. The reaction was quenched by the addition of H_2O (100 ml) and the product was extracted to EtOAc (3 x 100 ml). The combined organic layers were dried over $MgSO_4$, filtered, concentrated *in vacuo* and purified over silica (EtOAc/PE 5% - 25%). This afforded the product pure as a white powder (13.4 g, 35.7 mmol, 81%). ^{1}H-NMR (400 MHz, $CDCl_3$) δ = 7.75 – 7.69 (m, C*H*$_{arom}$, 6H), 7.46 – 7.36 (m, C*H*$_{arom}$, 6H), 6.80 (d, J = 8.60 Hz, C*H*$_{arom}$, 2H), 2.48 (s, C*H*$_3$, 3H), 1.11 (s, C*H*$_3$, 9H). ^{13}C-NMR (100 MHz, $CDCl_3$) δ = 197.05, 160.16, 135.53, 134.95, 132.28, 130.80, 130.46, 130.30, 129.75, 128.07, 127.84, 119.77, 26.54, 19.5. ^{1}H- and ^{13}C-NMR data match reported values.[2]

2-bromo-1-(4-((tert-butyldiphenylsilyl)oxy)phenyl)ethan-1-one (3)

Compound **2** (8.47 g, 22.6 mmol) was dissolved in MeOH/DCM (2:5, 28 ml). Benzyltrimethylammonnium tribromide ($BTMABr_3$) (9.15 g, 39.8 mmol) was slowly added and the reaction mixture was stirred 4 hours at RT. TLC analysis (EtOAc/PE, 2:8) showed a single product spot (R_f: 0.66) and subsequently H_2O (50 ml) was added to the reaction mixture. The aqueous layer was extracted with Et_2O (3 x 50 ml) and the combined organic layers were dried over $MgSO_4$, concentrated *in vacuo* and purified over silica (EtOAc/PE 5% - 25%). This afforded the product pure as a white powder (yield: 8.26 g, 18.2 mmol, 81%). ^{1}H-NMR (400 MHz, $CDCl_3$), δ = 7.78 (d, J = 8.84 Hz, C*H*$_{arom}$, 2H), 7.69 (m, C*H*$_{arom}$, 4H), 7.47 – 7.37 (m, C*H*$_{arom}$, 6H), 6.82 (d, J = 8.88 Hz, C*H*$_{arom}$, 2H), 4.33 (s, J = 8 Hz, C*H*$_2$, 2H), 1.11 (s, C*H*$_3$, 9H). ^{1}H-NMR data match reported values.[3]

2-((3-chloropropyl)thio)-1-(4-hydroxyphenyl)ethan-1-one (4)

Compound **3** (1.70 g, 3.76 mmol) and KOH (211 mg, 3.76 mmol) were dissolved in MeOH (20 mL). Then 3-chloro-1-propanethiol (403 µl, 4.14 mmol) was added and the reaction mixture was left to stir overnight at RT. Subsequently H_2O (100 ml) was added to reaction mixture and the aqueous layer was extracted with EtOAc (3 x 50 ml). The combined organic layers were washed with brine (20 ml), dried over $MgSO_4$, concentrated *in vacuo* and purified over silica (EtOAc/PE 10% to 25%). This afforded the product as a colorless oil. (427 mg, 1.75 mmol, 47%). ^{1}H-NMR (400 MHz, $CDCl_3$), δ = 7.92 (d, J = 8.76 Hz, CH_{arom}, 2H), 6.96 (d, J = 8.76 Hz, CH_{arom}, 2H), 3.79 (s, CH_2, 2H), 3.58 (t, J = 6.32, CH_2, 2H), 2.72 (t, J = 7.00, CH_2, 2H), 2.03 (q, J = 6.80, CH_2, 2H).

2-((3-azidopropyl)thio)-1-(4-hydroxyphenyl)ethan-1-one (5)

Compound **4** (20.4 g, 83.4 mmol) and NaN_3 (54.2 g, 833 mmol) were dissolved in DMF (200 ml) and stirred overnight at 80 °C. H_2O was added to the reaction mixture and extracted with EtOAc (3 x 150 ml). The combined organic layer was dried over $MgSO_4$, filtered and concentrated *in vacuo*. Residual DMF was removed using a high vacuum oil pump connected to the rotavap (40 °C). This afforded the product as a colorless oil (20.9 g, 83 mmol, quantitative). ^{1}H-NMR (400 MHz, $CDCl_3$), δ = 7.93 (d, J = 8.80 Hz, CH_{arom}, 2H), 6.93 (d, J = 8.76 Hz, CH_{arom}, 2H), 3.76 (s, CH_2, 2H), 3.37 (t, J = 6.60 Hz, CH_2, 2H), 2.65 (t, J = 7.16, CH_2, 2H), 1.85 (q, J = 6.92 Hz, CH_2, 2H). ^{13}C-NMR (100 MHz, $CDCl_3$) δ = 194.09, 161.03, 131.69, 127.99, 115.75, 50.08, 37.02, 29.46, 28.29. Mass calc.: 251.07 [M], mass found: 273.90 $[M+Na]^+$.

1-(4-((1-azido-nonadeca-ethylene glycol)phenyl)-2-((3-azidopropyl)thio)ethan-1-one (C1)

Compound **5** (175.8 mg, 0.696 mmol), mesylated PEG **7** (540 mg, 0.539 mmol) and K_2CO_3 (164.4 mg, 1.19 mmol) were dissolved in DMF (10 ml) and stirred overnight at 50 °C. TLC analysis (1% MeOH in DCM) was used to determine the progress of the reaction and revealed a single UV (254 nm) active product spot (R_f: 0.3). Water (50 ml) was added to the reaction mixture and was then extracted with EtOAc (3 x 50 ml). The combined organic layers were dried over $MgSO_4$ and concentrated *in vacuo* (residual DMF traces were removed using a high vacuum oil pump). The concentrate was then re-dissolved in DCM (2-4 ml) and purified over silica (0% MeOH to 5% MeOH in DCM) which afforded the title compound as a white paste (383 mg, 0.331 mmol, 61%). ^{1}H-NMR (400 MHz, $CDCl_3$), δ = 7.92 (d, J = 8.40 Hz, CH_{arom}, 2H), 7.92 (d, J = 8.44 Hz, CH_{arom}, 2H), 4.17 (t, J = 4.44 Hz, O-C*H2*, 2H), 3.85 (t, J = 4.60 Hz, O-C*H2*, 2H), 3.72 – 3.68 (m, 4H), 3.61 (m, -(OCH_2CH_2O)$_{19}$-, 74H), 3.37 – 3.34 (m, 4H), 2.62 (t, J = 7.26 Hz, N_3-C*H2*, 2H), 1.84 (q, J = 6.84 Hz, CH_2CH_2CH_2, 2H). ^{13}C-NMR (100 MHz, $CDCl_3$) δ = 193.16, 163.01, 131.07, 128.09, 114.45, 70.88, 70.55, 70.03, 69.47, 67.65, 50.67, 49.94, 36.79, 29.21, 28.11. Mass calc.: 1156.60 [M], mass found: 1157.42 $[M+H]^+$.

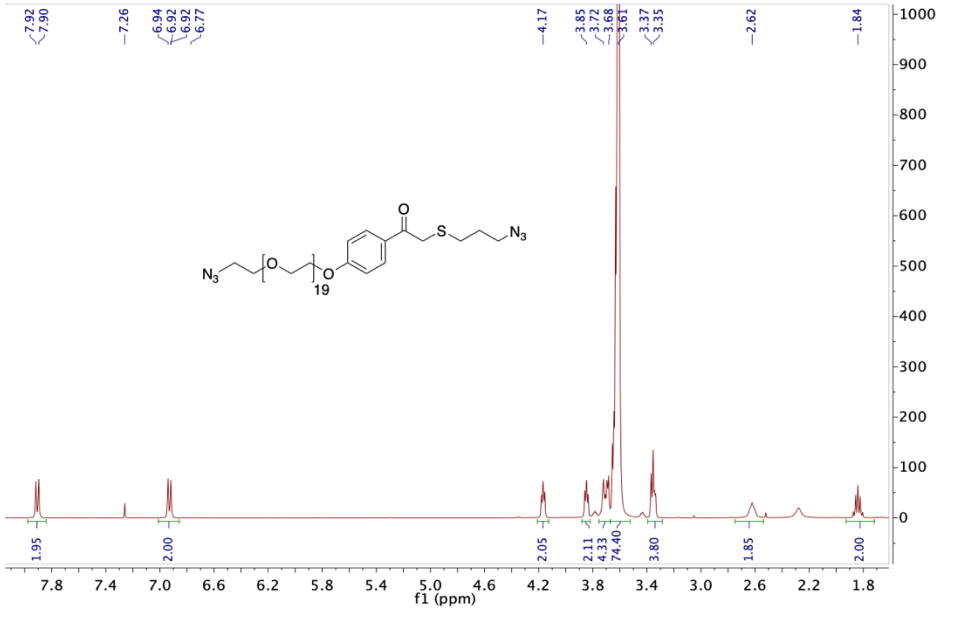

Figure S1. *^{1}H-NMR spectrum recorded for crosslinker **C1** in $CDCl_3$.*

1-azido-nonadeca-ethylene glycol methanesulfonate (7)[4]

O-(2-Azidoethyl)nonadeca-ethylene glycol (**6**) (250 mg, 0.258 mmol) and Et_3N (57 µl, 0.409 mmol) were dissolved in DCM (2 ml) and cooled using an ice bath. MsCl (23 µl, 0.295 mmol) was dissolved in DCM (2 ml) and added to the reaction mixture over the course of 1 hour using a syringe pump. The ice batch was removed and the reaction mixture was allowed to stir an additional 2 hours. Subsequently HCl (3%, 10 ml) was added to the reaction mixture and stirred for 5 minutes. The aqueous layer was extracted with DCM (3 x 25 ml). The combined organic layers were dried over $MgSO_4$ and concentrated *in vacuo*. This afforded the product as a white paste (yield: 230.2 mg, 85%). ^{1}H-NMR (400 MHz, $CDCl_3$) δ = 4.32 (t, J = 2.84 Hz, CH_2, 2H), 3.71 (t, J = 2.88 Hz, CH_2, 2H), 3.58 (m, -(OCH_2CH_2O)$_{19}$-, 76H), 3.33 (t, J = 4.28 Hz, CH_2, 2H), 3.03 (s, CH_3, 3H). ^{13}C-NMR (100 MHz, $CDCl_3$) δ = 70.53, 69.99, 69.30, 68.98, 50.64, 37.69. Mass calc.: 1001.52 [M], mass found: 1040.90 $[M+K]^+$.

3.6.3 Synthesis of π-extended phenacyl photo-labile crosslinker C2

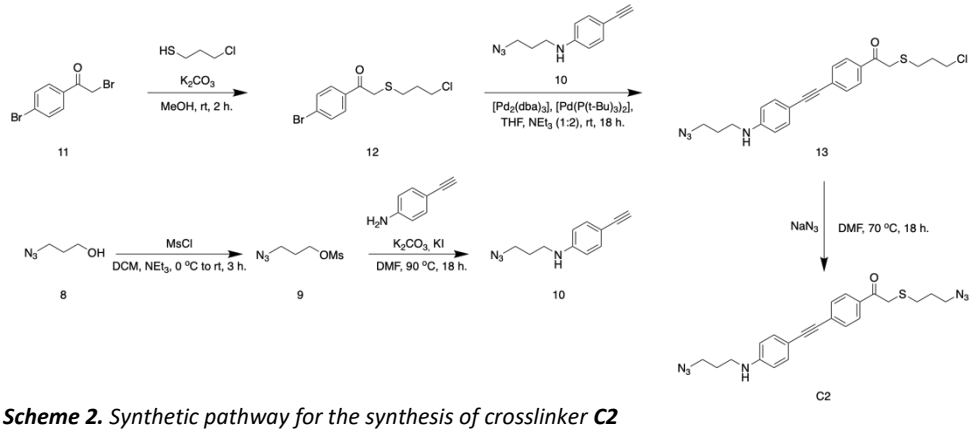

Scheme 2. *Synthetic pathway for the synthesis of crosslinker* ***C2***

3-azido-1-mesyl propane (9)

3-azido-propanol (**8**) (2.64 ml, 28.7 mmol) and Et_3N (4.8 ml, 34.4 mmol) were dissolved in DCM (5 ml) and cooled using an ice bath. MsCl (2.66 ml, 34.4 mmol) was dissolved in DCM (4 ml) and added to the reaction mixture over the course of 1 hour using a syringe pump. The ice batch was removed and the reaction mixture was allowed to stir an additional 2 hours. Subsequently, water (30 ml) was added to the reaction mixture and stirred for 5 minutes. The aqueous layer was extracted with Et_2O (3 x 50 ml). The combined organic layers were dried over $MgSO_4$ and concentrated *in vacuo*. This afforded the product as a transparent oil (yield: 5.01 g, 28.4 mmol, 99%). ^{1}H-NMR (400 MHz, $CDCl_3$) δ = 4.29 (t, J = 6.04 Hz, OC*H*$_2$, 2H), 3.46 (t, J = 6.48 Hz, N_3C*H*$_2$, 2H), 3.01 (s, C*H*$_3$, 3H), 1.98 (q, J = 6.44 Hz, CH_2C*H*$_2$$CH_2$, 2H). ^{13}C-NMR (100 MHz, $CDCl_3$) δ = 66.50, 47.22, 37.19, 28.55. ^{1}H- and ^{13}C-NMR data match reported values.[5]

N-(3-azidopropyl)-4-ethynylaniline (10)

4-ethynylaniline (3.3 g, 28 mmol), K_2CO_3 (11.8 g, 85.2 mmol) and KI (0.94 g, 5.68 mmol) were dissolved in DMF and stirred at 90 °C for 5 minutes. After all reactants

dissolved, 3-azido-1-mesyl propane (**9**) (5.01 g, 28.4 mmol) was added and the reaction mixtures was stirred overnight. The reaction progress was evaluated using TLC analysis (25% EtOAc in PE) and showed the product spot (R_f: 0.66). Subsequently, the reaction was quenched by the addition of NH_4Cl (sat.) (100 ml) and the product was extracted to EtOAc (3 x 50 ml). The combined organic layers were washed with H_2O (3 x 50 ml), dried over $MgSO_4$, concentrated *in vacuo* and purified over silica (10% EtOAc to 20% EtOAc in PE). This afforded the title compound as a red oil (yield: 1.08 g, 5.41 mmol, 19%). ^{1}H-NMR (400 MHz, $CDCl_3$) δ = 7.32 (d, J = 8.32 Hz, CH_{2arom}, 2H), 6.52 (d, J = 8.36 Hz, CH_{2arom}, 2H), 3.91 (s (broad), N*H*, 1H), 3.43 (t, J = 6.48 Hz, N_3CH_2, 2H), 3.25 (t, J = 6.4 Hz, NHCH_2, 2H), 2.96 (s, CC*H*, 1H), 1.88 (q, J = 6.6 Hz, CH_2CH_2CH_2, 2H). ^{13}C-NMR (100 MHz, $CDCl_3$) δ = 148.21 (C_{arom}), 133.49 (CH_{arom}), 112.22 (CH_{arom}), 110.17 (C_{arom}), 84.57 (C_{alkyne}), 74.79 (CH_{alkyne}), 49.23 (N_3CH_2), 40.85 ($NHCH_2$), 28.51 ($CH_2CH_2CH_2$). Mass calc.: 200.11 [M], mass found: 201.05 $[M+H]^+$.

4-bromophenacyl-3-chloropropyl-thio-1-ethanone (12)

4-bromophenacyl bromide (2.0 g, 7.2 mmol) and K_2CO_3 (1.0 g, 7.2 mmol) were dissolved in MeOH (80 ml) and stirred at room temperature for 5 minutes. Then 3-chloropropanethiol (840 µl, 863 mmol) was added and the reaction mixture stirred 2 hours at room temperature. TLC analysis (5% EtOAc in PE) showed all starting compound had reacted and revealed a single product spot (R_f = 0.3). MeOH was removed *in vacuo* and the residue was re-dissolved in EtOAc (100 mL) and washed with H_2O (3 x 100 mL). The organic layer was dried over $MgSO_4$, filtered and concentrated *in vacuo*. This afforded the title compound as a yellowish oil (yield: 2.1 g, 6.8 mmol, 95%). ^{1}H-NMR (400 MHz, $CDCl_3$) δ = 7.84 (d, J = 8.56 Hz, CH_{2arom}, 2H), 7.61 (d, J = 8.60 Hz, CH_{2arom}, 2H), 3.75 (s, CH_2, 2H), 3.60 (t, J = 6.32 Hz, CH_2, 2H), 2.69 (t, J = 7.00 Hz, CH_2, 2H), 2.05 (q, J = 6.64 Hz, CH_2, 2H). ^{13}C-NMR (100 MHz, $CDCl_3$) δ =

193.46 ($C_{carbonyl}$), 133.86 (C_{arom}), 132.18 (CH_{arom}), 130.44 (CH_{arom}), 128.85 (C_{arom}), 43.32 (CH_2), 36.98 (CH_2), 31.52 (CH_2), 29.36 (CH_2).

1-(4-((4-((3-azidopropyl)amino)phenyl)ethynyl)phenyl)-2-((3-chloropropyl)thio)ethan-1-one (13)

Compound **10** (1.0 g, 5.0 mmol), compound **12** (1.5 g, 4.9 mmol), $[Pd_2(dba)_3]$ (34.3 mg, 0.037 mmol), and $[Pd(P(t\text{-}Bu)_3)_2]$ (38.3 mg, 0.075 mmol) were charged in a round bottom flask which was evacuated and purged with Argon (3 cycles). Next, using standard Slenck techniques, triethylamine (4 ml, anhydrous) and THF (2 ml, anhydrous) were added and the reaction was stirred overnight at room temperature. TLC analysis (25% EtOAc in PE) revealed a 366 nm UV active product spot (R_f = 0.1). The reaction mixture was filtered over a Whatman (0.45 µm) filter and the residue was washed with EtOAc (3 x 5 ml). The filtrate was concentrated in vacuo and purified over silica (10% EtOAc to 30% EtOAc in PE), which afforded the product as a yellow powder (yield: 928.8 mg, 2.19 mmol, 44%). ^{1}H-NMR (400 MHz, $CDCl_3$) δ = 7.93 (d, J = 8.52 Hz, CH_{2arom}, 2H), 7.56 (d, J = 8.48 Hz, CH_{2arom}, 2H), 7.36 (d, J = 8.68 Hz, CH_{2arom}, 2H), 6.56 (d, J = 8.72 Hz, CH_{2arom}, 2H), 3.78 (s, CH_2, 2H), 3.63 (t, J = 6.32 Hz, CH_2, 2H), 3.45 (t, J = 6.44 Hz, CH_2, 2H), 3.30 (t, J = 6.76 Hz, CH_2, 2H), 2.74 (t, J = 7.00 Hz, CH_2, 2H), 2.06 (q, J = 6.76 Hz, CH_2, 2H), 1.90 (q, J = 6.60 Hz, CH_2, 2H). ^{13}C-NMR (100 MHz, $CDCl_3$) δ = 193.61 ($C_{carbonyl}$), 133.30 (CH_{arom}), 131.32 (CH_{arom}), 128.70 (CH_{arom}), 112.35 (CH_{arom}), 49.25 (CH_2), 43.22 (CH_2), 40.85 (CH_2), 36.97 (CH_2), 31.48 (CH_2), 29.28 (CH_2), 28.52 (CH_2). Mass calc.: 426.13 [M], mass found: 427.20 $[M+H]^+$.

1-(4-((4-((3-azidopropyl)amino)phenyl)ethynyl)phenyl)-2-((3-azidopropyl)thio)ethan-1-one (C2)

Compound **13** (928.8 mg, 2.19 mmol) and NaN_3 (1.5 g, 25 mmol) were dissolved in DMF (50 ml) and stirred overnight at 70 °C. Subsequently, H_2O (150 ml) was added and the product extracted to EtOAc (3 x 100 ml). The combined organic layers were dried over $MgSO_4$, filtered, concentrated *in vacuo* and purified over silica (10% EtOAc to 30% EtOAc in PE). This afforded photo cleavable crosslinker **C2** as a yellow/orange powder (yield: 777.9 mg, 1.794 mmol, 70%). ^{1}H-NMR (400 MHz, $CDCl_3$) δ = 7.93 (d, J = 8.48 Hz, CH_{2arom}, 2H), 7.56 (d, J = 8.48 Hz, CH_{2arom}, 2H), 7.39 (d, J = 8.68 Hz, CH_{2arom}, 2H), 6.59 (d, J = 8.68 Hz, CH_{2arom}, 2H), 4.22 (s_{broad}, N*H*, 1H), 3.78 (s, CH_2, 2H), 3.43 (t, J = 6.44 Hz, CH_2, 2H), 3.39 (t, J = 6.68 Hz, CH_2, 2H), 3.30 (t, J = 6.72 Hz, CH_2, 2H), 2.67 (t, J = 7.08 Hz, CH_2, 2H), 1.94 – 1.84 (m, CH_2, 4H). ^{13}C-NMR (100 MHz, $CDCl_3$) δ = 193.70 ($C_{carbonyl}$), 148.54 (C_{arom}), 133.57 (C_{arom}), 133.47 (CH_{arom}), 131.48 (CH_{arom}), 129.71 (C_{arom}), 128.86 (CH_{arom}), 112.52 (CH_{arom}), 110.77 (C_{arom}), 94.82 (C_{alkyne}), 87.11 (C_{alkyne}), 50.10 (CH_2), 49.41 (CH_2), 41.01 (CH_2), 37.11 (CH_2), 29.39 (CH_2), 28.68 (CH_2), 28.27 (CH_2). Mass calc.: 433.17 [M], mass found: 434.14 $[M+H]^+$.

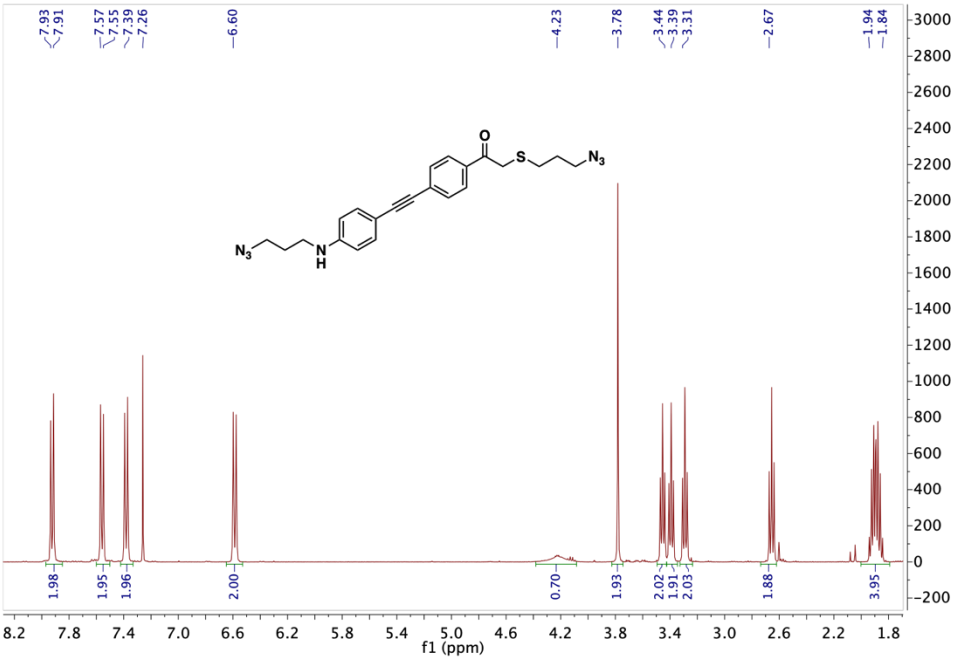

Figure S2. *^{1}H-NMR spectrum recorded for crosslinker **C2** in $CDCl_3$.*

3.6.4 Dextran-alkyne synthesis

Dextran (500 kDa, 3.4 g, 0.0068 mmol) was dissolved in a NaOH solution (30 ml, 0.1 M) and heated to 35 °C. Glycidyl propargyl ether (5 ml, 0.046 mmol) was added and the solution was stirred overnight. After cooling the reaction mixture to RT, the solution was poured in isopropyl alcohol (IPA) (500 ml) to precipitate alkyne modified dextran. The IPA was decantated and the precipitate re-dissolved in demineralized water and dialyzed (MWCO = 3.5 kDa) against demineralized water for 72 hours (4 x 2 L), after which it was freeze dried to obtain pure alkyne modified dextran as a white fluffy powder. The degree of substitution determined by ^{1}H-NMR is 36% (figure **S3**).[6] Yield: 3.1 g. ^{1}H-NMR (400 MHz, D_2O) δ = 5.36, 5.19, 5.03, 4.85 (anomeric C*H*, 1H), 4.14 (O-CH_2, HO-C*H*, 3H, s) 3.88-3.30 (9H, m), 2.82 (alkyne CC*H*, 1H, s). ^{13}C-NMR (101 MHz, D_2O) δ = 97.66, 79.50, 76.13, 73.33, 71.34, 70.70, 70.11, 69.44, 68.80, 65.45, 58.24

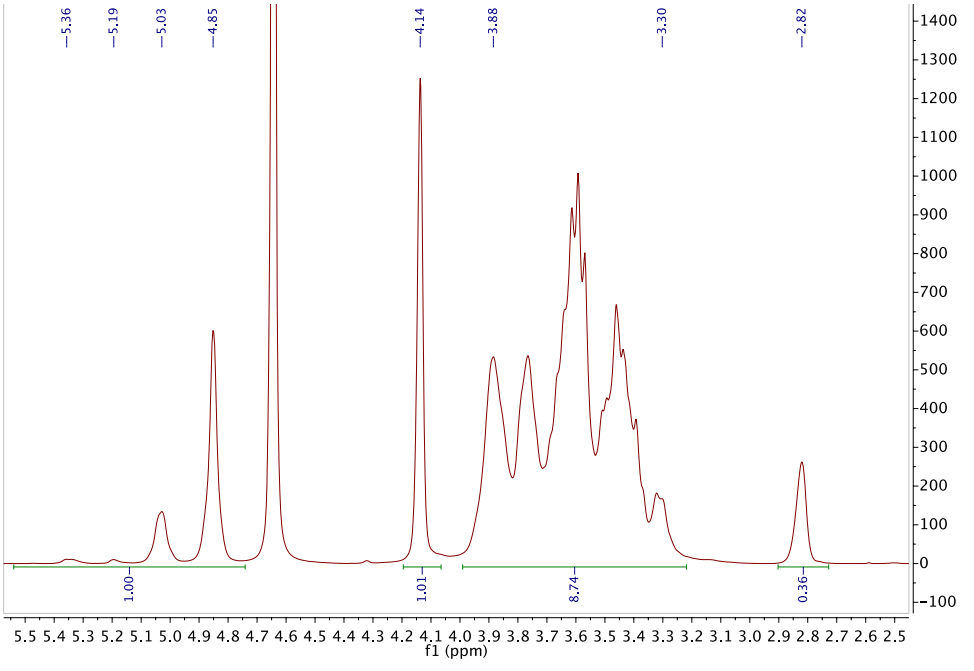

Figure S3. *^{1}H-NMR spectrum recorded for alkyne modified dextran (500 kDa) in D_2O. 5.03 ppm resonance belonging to anomeric proton of alkyne modified glucose units, 4.85 ppm resonance belonging to anomeric proton of unmodified glucose units and 2.82 ppm resonance belonging to alkyne proton. Degree of substitution (DS) = 36% (ratio between alkyne resonance (2.82 ppm) and the sum of anomeric proton resonances (5.36 to 4.85 ppm)).*

3.6.5 Dextran hydrogel preparation

Dextran hydrogel preparation using bis-azide crosslinker C1

A 10 wt% dex-alkyne solution was prepared by dissolving dex-alkyne in H_2O (300 µl), this solution was shaken for 1 hour. Crosslinker **C1** (4.0 mg, 0.004 mmol) was dissolved in a Cu-click stock solution (200 µl, ($CuSO_4$ (0.59 mM), sodium ascorbate (3.79 mM) and THTPA (0.29 mM))), which was shortly shaken to dissolve and mix all components. Next, the dex-alkyne and the crosslinker **C1** solution were mixed and shortly shaken, after which the solution was transferred in a cubic mold and left overnight to gel. After gelation was complete, the hydrogel was removed from the

mold and placed in a phosphate buffer (PB) (25 ml, 100 mM, pH 7.4) solution or demineralized water to remove Cu-click components, unreacted dex-alkyne and crosslinker **C1**. This washing step was repeated 3 times and afforded transparent self-supporting cubic hydrogels.

Dextran hydrogel preparation using bis-azide crosslinker C2

A 10 wt% dex-alkyne solution was prepared by dissolving dex-alkyne in H_2O (300 μl), this solution was shaken for 1 hour. Crosslinker **C2** was dissolved in a CuI stock solution (200 μl, 3.15 mM CuI and 8.6 μM DIPEA in DMSO), which was shortly shaken to dissolve and mix all components. Next, the dex-alkyne and crosslinker **C2** solution were mixed and shortly shaken, after which the solution was transferred in a cubic quartz cuvette (4 x 4 x 4 cm) and left overnight to gel. After gelation was complete, phosphate buffer (PB) (25 ml, 100 mM, pH 7.4) solution was carefully placed on the hydrogel patch to remove Cu-click components, unreacted dex-alkyne and crosslinker **C2**. This washing step was repeated 3 times and afforded yellow transparent self-supporting hydrogel patches.

3.6.6 Photochemical characteristics of bis-azide crosslinker C1 and C2

Photocleavage reaction of bis-azide crosslinker C1

Crosslinker **C1** was dissolved in demineralized H_2O (40 μM) and 0.5 ml was added to a quartz cuvette. The crosslinker **C1** solution was then irradiated with a UVC lamp (17 cm distance to sample) under continuous stirring and protected from other light sources. UV/Vis spectra were recorded at selected timepoints (Figure **2A**) and the absorbance at 283 nm was plotted against time (Figure **2B**).

Photocleavage reaction of bis-azide crosslinker C2 monitored by UV/Vis analysis

Crosslinker **C2** was dissolved in DMSO (40 μM) and 20 ml was added to a 4 x 4 x 4 cm quartz cuvette. The crosslinker **C2** solution was then irradiated with a 375 nm LED lamp (M375L4 (Thorlabs), 1.2 A, maximal power setting, distance to cuvette 4 cm, photon flux = 2.93 ± 0.08 x 10^{15} s^{-1}) under continuous stirring and protected from other light sources. UV/Vis spectra were recorded at selected timepoints (Figure **3B**) and the absorbance at 383 nm was plotted against time (Figure **3C**).

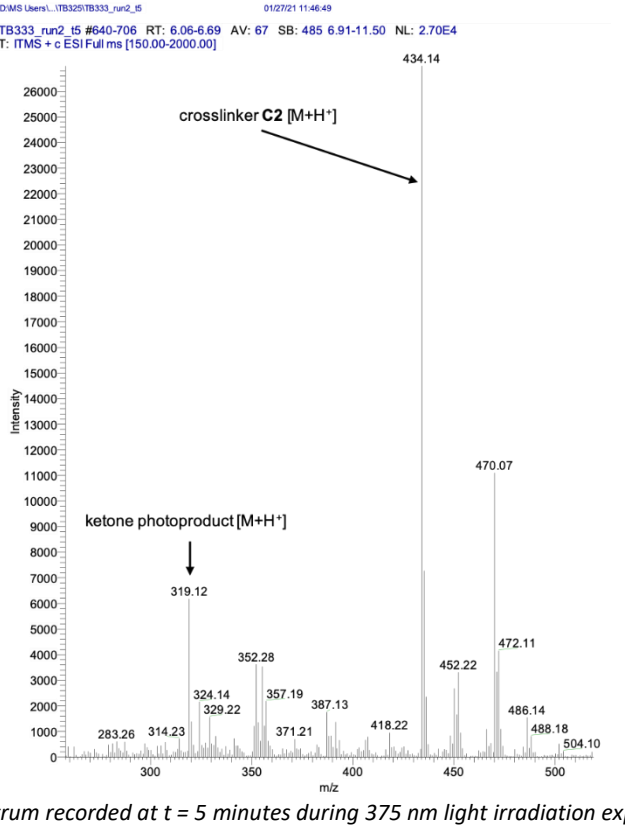

Figure S4. *ESI-MS spectrum recorded at t = 5 minutes during 375 nm light irradiation experiment. The mass of crosslinker **C2** ([M+H⁺]) and the mass of the ketone photoproduct ([M+H⁺]) is detected, indicating photocleavage of **C2**.*

Photocleavage reaction of bis-azide crosslinker C2 monitored by ^{1}H-NMR spectroscopy

Crosslinker **C2** (2.99 mg, 6.9 μmol) was placed in a quartz cuvette (4 x 4 x 4 cm) and dissolved in DMSO-d6 (6 ml). Isopropyl alcohol (IPA, 1 μl, 13 μmol) was added as internal standard. The solution was irradiated with 375 nm light (M375L4 (Thorlabs), 1.2 A, maximal power setting, distance to cuvette 4 cm, photon flux (ϕ) = 2.93 ± 0.08 x 10^{15} s^{-1}) under continuous stirring and protected from other light sources. During irradiation aliquots were collected at selected timepoints and analyzed by ^{1}H-NMR (Figure **S5**).

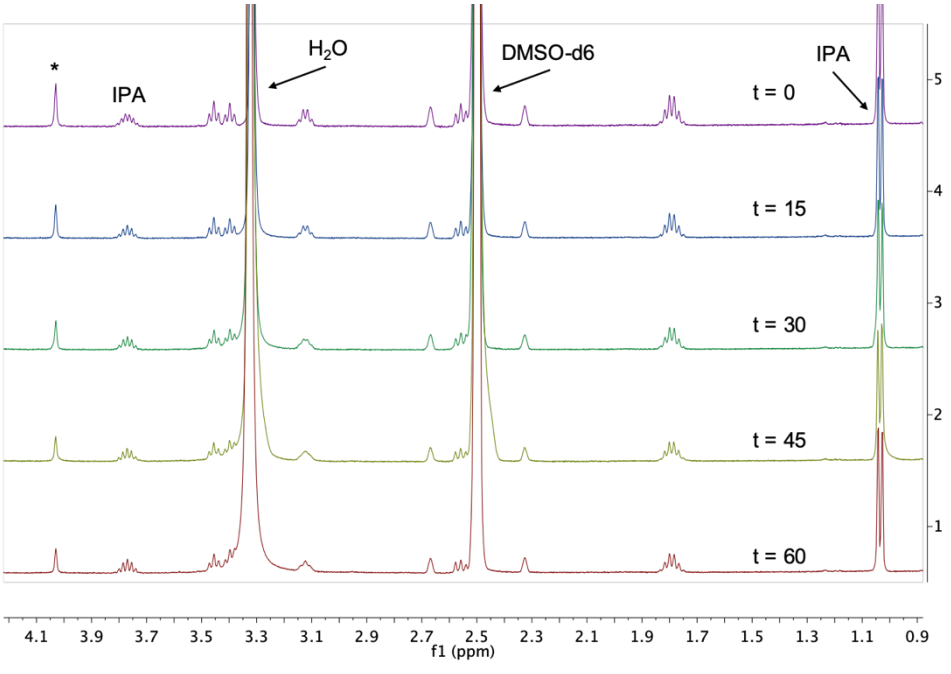

Figure S5. *Stacked ^{1}H-NMR spectra recorded during the 375 nm light irradiation of crosslinker **C2** (13.8 μM). CH_2 resonance at 4.03 ppm (indicated with asterisk) was monitored to determine the **C2** concentration over time relative to internal standard isopropyl alcohol (IPA). Spectra were recorded in DMSO-d6.*

Molar extinction coefficient determination of bis-azide crosslinker C2

A stock solution of crosslinker **C2** (6.42 mg in 50 ml DMSO) was prepared in DMSO using volumetric glassware. Subsequently a dilution series (DMSO) ranging from 21 μM to 59 μM was prepared and its absorbance was spectrophotometrically determined (Figure **S6A**). The absorbance at 383 nm was plotted against the concentration from which the molar extinction coefficient was determined (Figure **S6B**). $\varepsilon = 27210\ M^{-1}\ cm^{-1}$.

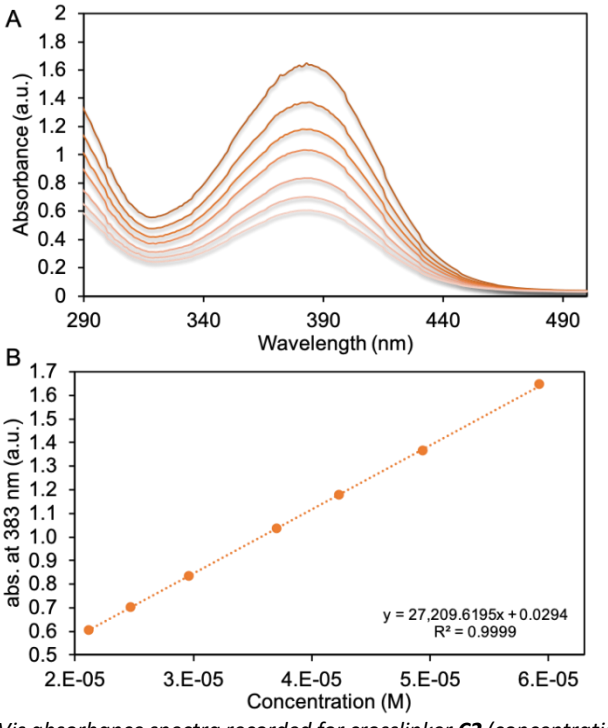

Figure S6. A) *UV/Vis absorbance spectra recorded for crosslinker* ***C2*** *(concentration range = 21 μM to 59 μM).* ***B)*** *absorbance (383 nm) plotted vs crosslinker* ***C2*** *concentration. Molar extinction coefficient (ε_{383}) = 27210 M^{-1} cm^{-1}.*

Photon flux determination of 375 nm LED using ferrioxalate actinometry

The incident photon flux (I_0) of a 375 nm LED light (Thorlabs ML375) driven by Thorlabs T-cube LED driver (1.2 A and maximum current) was determined by irradiation of the potassium ferrioxalate actinometer. In brief, the potassium

ferrioxalate solution (0.006 M in H_2SO_4 (0.05 M)) was placed in a 4 x 4 x 4 cm quartz cuvette which was irradiated with the 375 nm LED lamp (distance to cuvette 4 cm). At fixed timepoints, aliquots (100 μl) were taken and 1,10-phenanthroline (140 μl, 5 mM), acetic acid (sodium salt, 1.15 ml, 1.0 M) and sulfuric acid (750 μl, 0.5 M) were added and kept in the dark for 30 minutes. The collected aliquots were spectrophotometrically analyzed for their absorbance at 510 nm and plotted against time. The experiment was repeated three times yielding an average slope of absorbance change of $3.41 \pm 0.09 \times 10^{-3}$ s^{-1}. The incident photon flux (I_0) of the 375 nm LED lamp is: $2.93 \pm 0.08 \times 10^{15}$ s^{-1} calculated using equation **1**.[7]

$$\text{incident photon flux} = \left(\frac{dA_{510}}{dt}\right)\frac{N_A * V}{\phi_{365} * \varepsilon_{510} * l} \qquad (\mathbf{1})$$

Where,

$dA_{510} = 3.41 * 10^{-3}$ s^{-1}

$N_A = 6.02214 * 10^{23}$ mol^{-1}

$V = 0.002$ dm^3

$\varepsilon_{365} = 1.26$

$\varepsilon_{510} = 11.1 * 10^3$ mol^{-1} dm^3 cm^{-1}

$l = 1.000$ cm

Quantum yield determination of the photodegradation of crosslinker C2

The quantum yield (ϕ) of the 375 nm light driven photodegradation process of crosslinker **C2** was determined using equation **2**. The photodegradation process follows a linear trend and equals 6.2×10^{-3} s^{-1} (first 30 minutes UV/Vis data) (Figure **3B**). Number of photons absorbed is 2.93×10^{15} s^{-1}. By substituting these values in equation **2** the ϕ of photo degradation is calculated and equals: 0.14 (14%).

$$\phi = \frac{\text{number of molecules } \mathbf{C2} \text{ degraded}}{\text{number of photons absorbed}} \quad (\mathbf{2})$$

$$number\ of\ molecules\ \boldsymbol{C2}\ degraded = \frac{dA_{383} * V * N_A}{\varepsilon_{383} * l} = 4.1 * 10^{14}\ s^{-1}$$

Where,

$dA_{383} = 6.2 * 10^{-3}$

$N_A = 6.02214 * 10^{23}\ mol^{-1}$

$V = 0.003\ dm^3$

$\varepsilon_{383} = 27.2 * 10^3\ mol^{-1}\ dm^3\ cm^{-1}$

$l = 1.000\ cm$

3.6.7 Light triggered release studies

Dextran hydrogels were prepared according the protocol described in section 3.5.5, with minor modifications in order to load doxorubicin, BSA or human IgG antibody.

Light triggered doxorubicin release

A set of cubic transparent self-supporting hydrogels were prepared and washed according the protocol described in section 3.5.5 (Figure **S7A**). A doxorubicin stock solution was prepared in DMSO (100 mg/ml) which was diluted in demineralized water (30 µl doxorubicin stock in 30 ml H_2O). Then 25 ml of the diluted aqueous doxorubicin solution was added to the dextran hydrogels (Figure **S7B**) which were stored in the dark for 148 hours (Figure **S7C**). The doxorubicin loaded hydrogels were removed from the doxorubicin loading solution (Figure **S7D**) and placed in H_2O (25 ml) for 24 hours to remove excess doxorubicin (Figure **S7E**). The washed doxorubicin loaded hydrogels were then placed in fresh H_2O (25 ml) of which one was irradiated with UVC light (1.02 mW/cm^2, irradiance determined at the gel location) for 24 hours (Figure **S7F**) while the other was kept in the dark as a control.

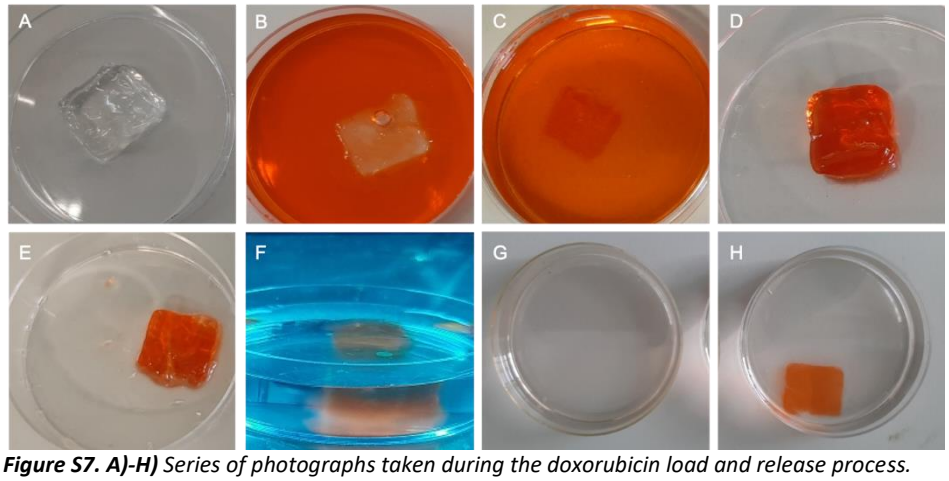

Figure S7. A)-H) *Series of photographs taken during the doxorubicin load and release process.*

The UVC irradiated hydrogel completely degraded (Figure **S7G**) in contrast to the non-irradiated hydrogels which stayed intact and retained the loaded doxorubicin inside the hydrogel matrix (Figure **S7H**). Aliquots of the surrounding solution of both samples were collected at fixed timepoints and analyzed by UV/Vis spectrophotometry. The absorbance at 283 nm and 480 nm (absorption maximum of doxorubicin) was plotted against time and shows that the absorbance at both wavelengths increased over time, in contrast to the control sample were the absorbances remain constant over time (Figure **S8A** and **S8B**). The measured absorbance characteristic for doxorubicin (480 nm) is low (0.05 to 0.07), while the absorbance at 283 nm is approximately 5-fold higher. Therefore, we conclude that the majority of the loaded and released doxorubicin is degraded as a result of the UV-C light dose. The light degradation process of doxorubicin in the hydrogels aqueous supernatant was confirmed by fluorescence analysis (excitation: 470 nm) (Figure **S9**). At t = 15 minutes (orange data) the characteristic emission spectrum of doxorubicin is detected (emission max 595 nm). However, when light irradiation is prolonged the emission spectrum significantly changes (blue and green data) and reduces in intensity, indication doxorubicin's degradation.

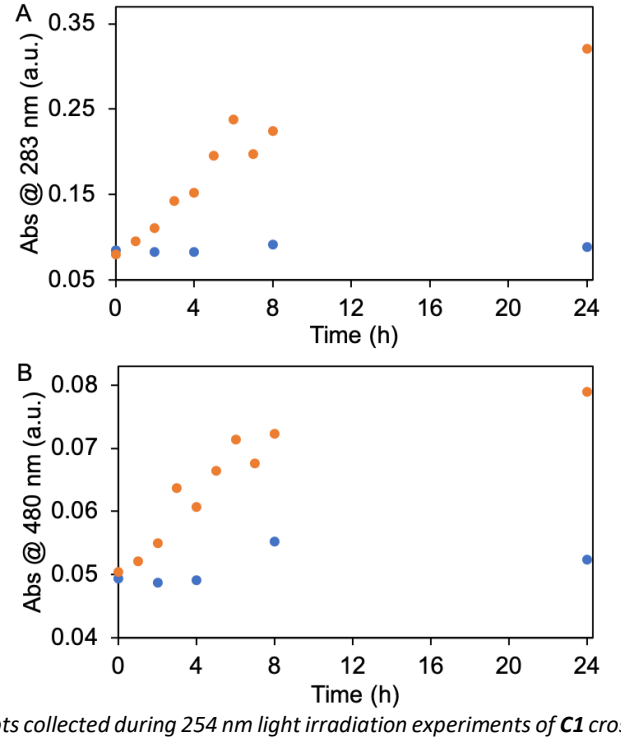

Figure S8. *Aliquots collected during 254 nm light irradiation experiments of* ***C1*** *crosslinked hydrogel cubes loaded with doxorubicin.* ***A)*** *Absorbance at 282 nm.* ***B)*** *Absorbance at 480 nm.*

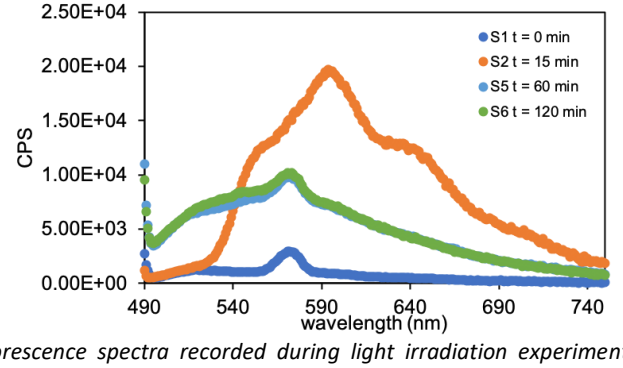

Figure S9. *Fluorescence spectra recorded during light irradiation experiments of doxorubicin loaded dextran hydrogels.*

Light triggered protein release

Hydrogel patches were prepared according the procedure described in section 3.5.5 and were loaded with bovine serum albumin (BSA) or immunoglobulin G (IgG) from

human serum. In case of BSA loading, 60 µl of a BSA stock solution (0.63 mg/ml in phosphate buffer (PB) (100 mM, pH 7.4)) was added to the liquid dextran (540 µl) phase prior to gelation. In case of IgG loading, 100 µl of an IgG stock solution (50 mg/ml in phosphate buffer (100 mM, pH 7.4)) was added to the liquid dextran (500 µl) phase prior to gelation. After gelation and washing, the protein loaded hydrogel patches were irradiated with 375 nm light and aliquots (40 µl) were collected at selected timepoints. Each of the released protein fractions was labeled with 20x excess of NHS-Cy5 in PBS at room temperature for 4 hours. The BSA protein content was determined with SDS-PAGE gel analysis and fluorescence analysis (Typhoon, GE Healthcare). The IgG protein content was determined by the Bradford assay (n = 4 experiments for irradiation samples, n = 2 experiments for non-irradiation samples).[8] A concentration plot (0 mg/ml to 1.00 mg/ml) was prepared with n = 3 experiments (Figure **S10**).

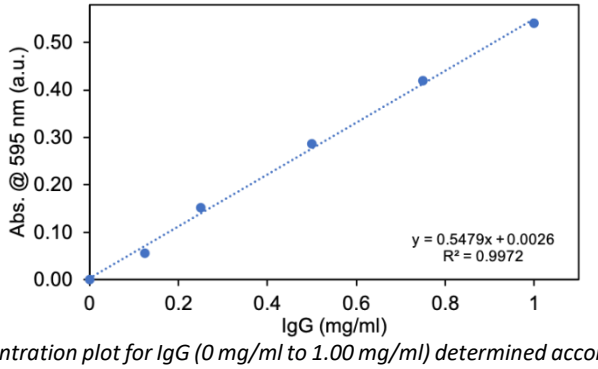

Figure S10. *Concentration plot for IgG (0 mg/ml to 1.00 mg/ml) determined according the Bradford assay.*

Cerenkov luminescence triggered protein release

Cubic hydrogels were prepared as described in section 3.5.5 with one minor modification for loading the protein solution. 30 µl of a BSA stock solution (0.63 mg/ml in phosphate buffer (PB) (100 mM, pH 7.4)) was added to the liquid dextran (270 µl) phase prior to gelation. The hydrogels were then placed in glass vials and irradiated with γ-rays (0.6 kGy/h) delivered by a ^{60}Co-source. At selected timepoints

the aliquots (30 μl) were taken and analyzed for their protein content using UV/Vis (Nanodrop) analysis and standard SDS-Page gel analysis.

3.6.8 Rheology analysis

Rheological measurements of C1 crosslinked hydrogels

Hydrogels were prepared as described in section 3.5.5. After mixing, 0.5 ml gel solution was placed on the rheometer plate (40 mm diameter steel plate-and-plate geometry, equipped with a hexadecane trap). After 90 minutes the gel point is reached, as the storage modulus surpasses the loss modulus, indicating a hydrogel has formed (Figure **S11A**). Time sweep measurements were performed at a fixed strain (γ = 1%) and frequency (ω =6.28 rad/s = 1 Hz). The frequency sweep measurements were performed from 0.1 to 100 rad/s at a fixed strain (γ = 1%), using a 40 mm steel plate-and-plate geometry (Figure **S11B**).

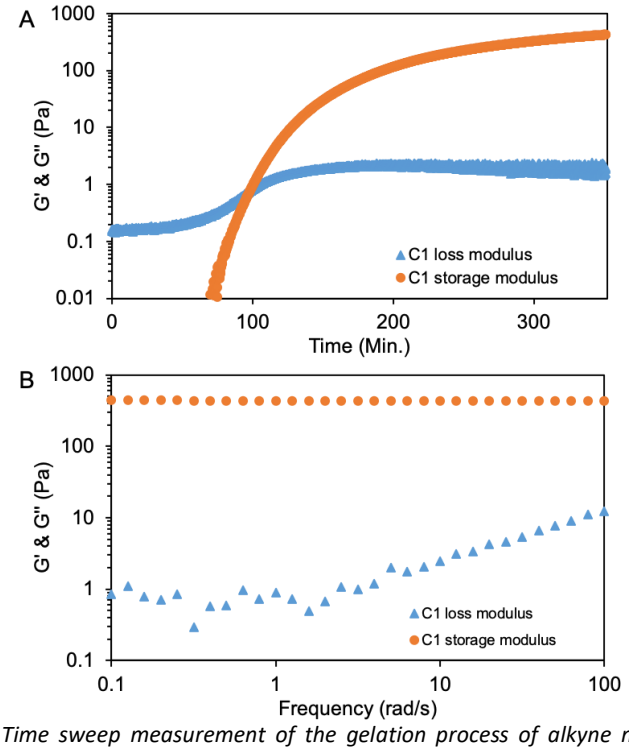

Figure S11. A) *Time sweep measurement of the gelation process of alkyne modified dextran hydrogel (10 wt%) using crosslinker* ***C1*** *(γ = 1%, ω = 1 Hz, 25 °C). The gel point is reached after approximately 90 minutes.* ***B)*** *Frequency sweep measurements of* ***C1*** *crosslinked dextran-based hydrogels.*

3.6.9 Supplemental references

1. Fulmer, G. R.; Miller, A. J. M.; Sherden, N. H.; Gottlieb, H. E.; Nudelman, A.; Stoltz, B. M.; Bercaw, J. E.; Goldberg, K. I., NMR Chemical Shifts of Trace Impurities: Common Laboratory Solvents, Organics, and Gases in Deuterated Solvents Relevant to the Organometallic Chemist. *Organometallics* **2010,** *29* (9), 2176-2179.
2. Ma, C.; Kwok, W. M.; Chan, W. S.; Zuo, P.; Wai Kan, J. T.; Toy, P. H.; Phillips, D. L., Ultrafast Time-Resolved Study of Photophysical Processes Involved in the Photodeprotection of p-Hydroxyphenacyl Caged Phototrigger Compounds. *J. Am. Chem. Soc.* **2005,** *127* (5), 1463-1472.
3. Salahi, F.; Purohit, V.; Ferraudi, G.; Stauffacher, C.; Wiest, O.; Helquist, P., pHP-Tethered N-Acyl Carbamate: A Photocage for Nicotinamide. *Org. Lett.* **2018,** *20* (9), 2547-2550.
4. Goswami, L. N.; Houston, Z. H.; Sarma, S. J.; Jalisatgi, S. S.; Hawthorne, M. F., Efficient synthesis of diverse heterodifunctionalized clickable oligo(ethylene glycol) linkers: potential applications in bioconjugation and targeted drug delivery. *Org. Biomol. Chem.* **2013,** *11* (7), 1116-1126.
5. Robinson, S. W.; Beer, P. D., Halogen bonding rotaxanes for nitrate recognition in aqueous media. *Org. Biomol. Chem.* **2017,** *15* (1), 153-159.
6. Nielsen, T. T.; Wintgens, V.; Amiel, C.; Wimmer, R.; Larsen, K. L., Facile Synthesis of β-Cyclodextrin-Dextran Polymers by "Click" Chemistry. *Biomacromol.* **2010,** *11* (7), 1710-1715.
7. Lehóczki, T.; Józsa, É.; Ősz, K., Ferrioxalate actinometry with online spectrophotometric detection. *J. Photochem. Photobiol. A: Chem.* **2013,** *251*, 63-68.
8. Bradford, M. M., A rapid and sensitive method for the quantitation of microgram quantities of protein utilizing the principle of protein-dye binding. *Anal. Biochem.* **1976,** *72* (1), 248-254.

CHAPTER

GAMMA RADIATION INDUCED CONTRACTION OF ALKYNE MODIFIED POLYMER HYDROGELS

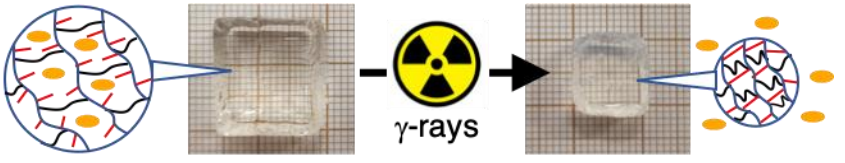

Gamma radiation triggered secondary crosslinking of dextran hydrogels leads to macroscopic hydrogel contraction. We use stable polymer hydrogels, prepared through azide-alkyne crosslinking, containing surplus alkyne groups. γ-irradiation of these gels leads to more alkyne crosslinking, enabling controlled increase of crosslink density, which in turn leads to an increase of hydrogel stiffness and macroscopic hydrogel contraction. Gel contraction scales linearly with applied radiation dose. The same mechanism is applied to achieve γ-radiation triggered release of small molecule cargo, akin to wringing out a sponge. γ-irradiation of touching hydrogel objects leads to gel fusion and the formation of a self-supporting gel connection, demonstrating the reactivity of the excess alkyne groups. We envision applications in gel gluing and the construction of complex gel architectures, as well as in responsive materials for controlled release.

This chapter is published as:
Brevé, T. G.; Liu, H.; Denkova, A. G.; Eelkema, R., Gamma Radiation Induced Contraction of Alkyne Modified Polymer Hydrogels. ***2022****. Macromol. Mater. Eng. DOI: 202100623*

4.1 INTRODUCTION

Polymer hydrogels are formed by physically or chemically crosslinking hydrophilic polymers, with the degree of crosslinking having a large impact on the mechanical and chemical properties of the hydrogel. A wide range of methods exists to make chemical crosslinks, including photo polymerization, radical induced crosslinking, and click chemistry approaches such as copper catalyzed alkyne azide coupling and Michael additions.[1] Having control over the crosslink density enables control over the release of (bio) molecules, hydrogel stiffness, cellular signaling[2-4], and eventually over the internal water volume. Crosslink density can be controlled by degradative or constructive molecular events, which depend on the desired application and can be controlled by triggers such as (UV) light, pH, enzymatic activity or reactive oxygen species (ROS). Degradative processes such as triggered crosslinker cleavage[5], are typically employed to release (bio) molecules from the hydrogel matrix. In contrast, in constructive molecular events the crosslink density is increased, through sequential or stepwise crosslink strategies such as secondary radical-mediated crosslinking[3] or by sequential photo-induced crosslinking[2-4]. Crosslink density increase is typically employed for increasing mechanical properties such as stiffness or yield stress, or to heal damage. Here, we present a γ-radiation triggered secondary crosslink strategy that enables us to have direct control over the crosslink density and eventually the macroscopic contraction of dextran hydrogels (Figure **1A**). With this finding we demonstrate that a molecular event, such as secondary crosslinking, can be translated into macroscopic motion (hydrogel contraction). Most strategies for hydrogel contraction in literature rely on physical transitions. A well-known physical strategy for hydrogel contraction is the temperature triggered phase transition of poly(N-iso-propylacrylamide) (PNIPAM) based hydrogels. When such hydrogels are heated above 32 °C, a sharp decrease in material volume is observed which is caused by the polymer switching from a hydrophilic phase to a hydrophobic phase.[6-10] Alternatively, photoredox responsive hydrogels can undergo

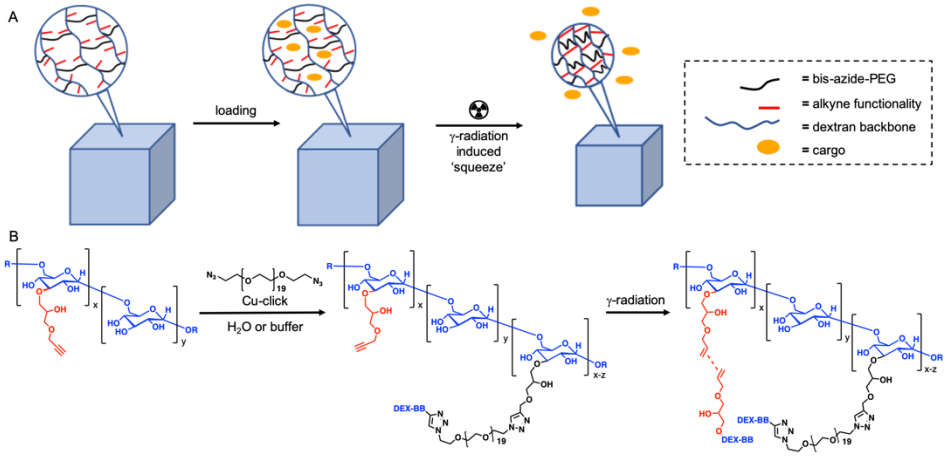

Figure 1. A) *Schematic representation of cargo-loaded dextran hydrogels, which upon γ-irradiation contract and expel cargo from the hydrogel network.* ***B)*** *Hydrogel synthesis by crosslinking the dextran backbone (DEX-BB) and bis-azide-PEG$_{19}$ using standard Cu-click conditions ($CuSO_4$, sodium ascorbate, activating ligand: tris(benzyltriazolylmethyl)amine (THTPA)). Residual alkynes are further crosslinked by γ-irradiation, resulting in contraction.*

macroscopic contraction as a result of polymer chain folding. Blue light, via an excited ruthenium photocatalyst, triggers the folding of polyviologen chains in the hydrogel network resulting in a reduction of the hydrogel volume.[11] Mechanical entanglement can also be used for material contraction using a UV light driven molecular motor to entangle a polymer network.[12, 13] Finally, enzymatic activity is employed to trigger a secondary crosslinker strategy leading to hydrogel contraction accompanied by an increased hydrogel stiffness.[14] Hydrogels find many different applications where they provide a protective environment to a loaded cargo. These loaded hydrogels enable controlled release of the cargo, through either an active or a passive release mechanism. Passive release is typically described by the standard Fickian diffusion model, where the hydrogel structure remains intact. On the contrary, active release can be controlled using external triggers such as (UV) light, temperature, pH, biological molecules or oxidative stress and changes the integrity of the hydrogel network or the hydrogel completely disintegrates. A less common trigger is ionizing radiation. A few examples exist where γ-radiation induces scissions

in dendrimer structures[15], generates reactive oxygen species (ROS) which damage the bilayer of liposomes and promote cargo release[16] or the cleavage of doxorubicin from nanoparticle drug carriers.[17] γ-radiation is a powerful tool to generate radicals on unsaturated polymer chains, leading to crosslink formation, which is widely applied.[18, 19] Crosslinking by gamma radiation is an efficient technique to form hydrogels as no monomers, initiators or catalysts are used, which are potentially harmful or toxic and are thus problematic when these hydrogels find a biological application. In general, the crosslink density can be controlled by varying the radiation dose, this enables control over the degree of swelling and material properties such as stiffness.[20, 21] When prolonged irradiation is used, the formed material continues to form crosslinks which eventually results in material contraction. This effect was observed by Angelini et al., who reported material contraction when 3% gelatin solutions were exposed to γ-irradiation dose higher than 50 kGy.[22] In our research we demonstrate contraction of stable pre-crosslinked hydrogels, where γ-irradiation leads to immediate contraction, indicating high sensitivity.

4.2 RESULTS AND DISCUSSION

Here, we present a method to contract dextran hydrogels using a covalent secondary crosslink strategy using γ-irradiation as an external stimulus. We use chemically crosslinked dextran-based hydrogels that are modified with extra alkyne functionalities on the dextran backbone. We started from dextran (MW = 500 kDa) that is randomly modified with terminal alkyne side chain groups (degree of substitution = 36%, Figure **S1**) using propargyl glycidyl ether chemistry. We then formed a hydrogel by chemically crosslinking a fraction of the alkyne moieties (theoretical maximum is 8%) via copper catalyzed azide alkyne cycloaddition with a bis-azide-PEG_{19} crosslinker (Figure **1B**). This procedure afforded transparent, self-supporting hydrogels with a storage modulus (G') of 1.6 x 10^3 Pa and tan δ(G''/G')

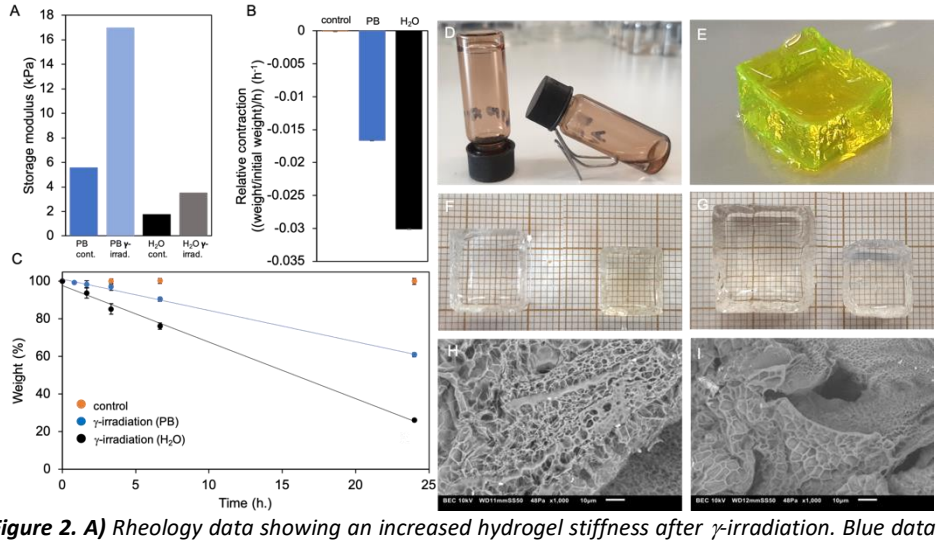

Figure 2. A) *Rheology data showing an increased hydrogel stiffness after γ-irradiation. Blue data PB swollen gels. Black data H_2O swollen gels.* ***B)*** *Relative contraction rate, control: non-irradiated samples, blue: PB swollen hydrogels, black: H_2O swollen hydrogels.* ***C)*** *Weight change of hydrogel cubes (H_2O swollen: 1.9 cm^3 and PB swollen: 0.6 cm^3 typical size) upon γ-irradiation (^{60}Co 0.6 kGy/h). Orange data: non-irradiated samples, blue data: phosphate buffer (100 mM, pH 7.4) swollen hydrogels, black data: water swollen hydrogels. Blue and black data fitted by standard linear regression model.* ***D)*** *inverted vial test. 14.4 kGy γ-irradiation resulted in gelation of alkyne modified dextran (left) but did not gel unmodified dextran (500 kDa, right).* ***E)*** *Water swollen, fluorescein colored centimeter scale dextran hydrogel.* ***F)*** *PB swollen hydrogels. Photographs taken before (left) and after 24 hours irradiation (right).* ***G)*** *H_2O swollen hydrogels. Photographs taken before (left) and after 24 hours irradiation (right).* ***H)*** *SEM image taken before irradiation.* ***I)*** *SEM image taken after 24 hours irradiation.*

of 8.0×10^{-3} (Figure **2E**). Next, we exposed centimeter-sized gel cubes to γ-irradiation from a ^{60}Co source, at doses up to 14.4 kGy. We observed that the gel cubes would shrink considerably from the start of the experiment with increasing dose, and that these contracted gels had an increased stiffness (Figure **2A** and **S3**). Control hydrogels remained virtually unchanged during the course of the 24-hour experiment, whereas the irradiated hydrogels linearly reduced in weight (Figure **2C**). The contraction rate of hydrogels swollen in PB is lower (Figure **2B**, blue data) compared to the contraction rate of hydrogels swollen in demineralized water (Figure **2B**, black data). After 24 hours irradiation (14.4 kGy) the weight reduction of the PB swollen gels and the demineralized water swollen gels is 39% and 74%,

respectively. Figure **2F** and **2G** show a set of photographs that illustrate the volume reduction. Figure **2G** shows a transparent water swollen hydrogel at the start of the γ-irradiation experiment (left) and the contracted hydrogel after 24 hours of γ-irradiation (right). During hydrogel contraction, the gels remain transparent and contract in all three dimensions equally, holding their cubic shape. A similar but less pronounced effect is observed for the PB swollen hydrogel (Figure **2F**, left the hydrogel at t = 0 and right at t = 24 hours γ-irradiation). We then conducted a frequency sweep experiment on the rheometer to determine the rheological properties of the hydrogel before and after γ-irradiation. The storage modulus (G') increased a factor 3-fold (PB swollen) or 2-fold (H2O swollen) after 24 hours of irradiation, indicating a more elastic material which is probably a result of additional crosslink formation (Figure **2B** and **S2**). Additionally, the hydrogels were analyzed by scanning electron microscopy (SEM) before and after γ-irradiation. SEM analysis revealed that the hydrogels have multiple morphologies which have different pore sizes (Figure **S3**). To demonstrate the effect of γ-irradiation on the micro-scale sized pores, a similar area in a non-irradiated hydrogel and an γ-irradiated hydrogel are shown in Figure **2H**, **I**. In the non-irradiated control hydrogel, the pore structure has a more open character compared to the γ-irradiated hydrogel. This implies that additional crosslinks are formed induced by γ-irradiation which is in agreement with the increased hydrogel stiffness (Figure **2A** and **S2**). To get more insight in the mechanism of γ-irradiation induced contraction, a control experiment was conducted in which solutions of unmodified dextran (500 kDa, 10 wt% in H_2O) and alkyne modified dextran were subjected to γ-irradiation (^{60}Co source, 0.6 kGy/h) (Figure **2D**). No changes could be observed for the unmodified dextran solution. In contrast, we found that the alkyne modified dextran solution gels overnight (14.4 kGy), which implies that the alkyne functionalities are crucial for hydrogel formation, and thus likely play a role in the observed contraction and increased stiffness. Crosslink formation may occur via the formation of reactive terminal

alkyne radicals, which could be generated directly by γ-irradiation or indirectly via the reaction products which emerge from water radiolysis. The main products of water radiolysis are hydrated electrons, HO• (hydroxyl radical), H_2, H_2O_2 and the H_2O• (hydroperoxyl radical). The HO• is the most abundant radical which can further react and create alkyne radicals.[23] Subsequently, these alkyne radicals can form crosslinks with adjacent alkyne groups resulting in the observed hydrogel contraction. Propagation can occur via an attack on the radical C1 carbon or to the cationic C2 carbon of adjacent alkyne moieties forming new C-C bonds.[24] Another possible secondary crosslink mechanism is by an attack of a radical C1 carbon on carbon C3, C4 or C5.[25] Additionally, phosphate buffer is found to act as a radical scavenger, which might explain the lower degree of hydrogel contraction we have observed in our γ-irradiation experiments (Figure **2B** and **2C**).[26] The reactivity of the residual alkyne groups suggested that it should be possible to glue[27, 28] or fuse hydrogel objects using γ-irradiation (Figure **3A**). We designed an experiment in which two hydrogel cubes were placed on top of each other inside a closed glass vial. Prior to initial gelation, a pipet tip was placed in the liquid dextran solution to provide for an easy grip handle used for lifting the hydrogels and assessing the γ-irradiation induced fusion (Figure **3B**). One set of hydrogel gel cubes was then placed in a ^{60}Co source for 24 hours and one set was kept aside as a control experiment. We found that the hydrogel cubes in the control experiment did not fuse together. When lifting the top hydrogel, the bottom hydrogel immediately detached indicating that capillary forces do not play any significant role (Figure **3B-2**). In contrast, the γ-irradiated set of hydrogels had fused together and could be lifted with the top hydrogel cube holding the weight of the bottom hydrogel cube (Figure **3B-3**). Finally, we were curious if we could release a loaded cargo from the hydrogel matrix, as a result of γ-irradiation triggered hydrogel contraction (Figure **3C**). In this experiment, we used hydrogels loaded with model compound 1,4-phthalic acid. The hydrogel cubes were isolated from the surrounding water volume by placing them

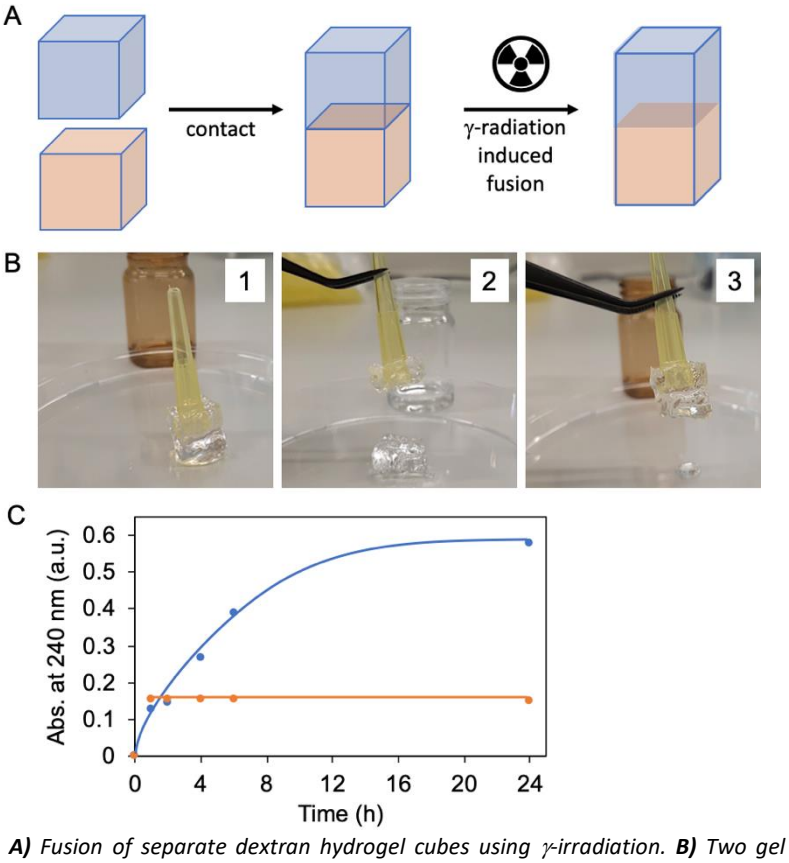

Figure 3. A) *Fusion of separate dextran hydrogel cubes using γ-irradiation.* ***B)*** *Two gel blocks pressed together (**B-1**) do not adhere in the control setting ((**B-2**), 24 hours no irradiation). When irradiated for 24 hours, the top gel can lift the bottom gel, demonstrating gel fusion (**B-3**).* ***C)*** *Cargo expulsion upon irradiation-induced contraction. UV-Vis data show expelled 1,4-phthalic acid (monitored at 240 nm) upon prolonged γ-irradiation (0.6 kGy/h). Orange data: non-irradiated control hydrogel. Blue data: irradiated hydrogel. Lines are to guide the eye. Orange data show a constant but non-zero absorbance due to an initial single leakage of cargo solution.*

on a glass plateau inside a closed glass vial (Figure **S4**). This experiment setup allowed us to limit passive diffusion of 1,4-phthalic acid from the hydrogel matrix and only observe the 'squeezing' effect by contraction. We found that the UV/Vis absorbance (240 nm) of the water volume of the γ-irradiated hydrogel increases over time, indicating the release of 1,4-phthalic acid, while the absorbance of the water volume of the control gel remained stable over time.

4.3 CONCLUSION

In conclusion, we here demonstrate a versatile γ-irradiation triggered hydrogel crosslinking strategy that enables control over hydrogel stiffness, contraction, release and fusion. We found a linear relationship between the γ-irradiation dose and the degree of hydrogel contraction, with a more pronounced effect in water than in phosphate buffer. The stiffness of the hydrogels increased 2-fold for H_2O swollen hydrogel and 3-fold for PB swollen hydrogels after γ-irradiation, which is the result of the increased crosslink density. γ-irradiation triggered crosslinking enables fusion of hydrogel objects. In addition, we show that γ-irradiation triggered hydrogel contraction can be used to squeeze out a cargo. All together our finding provides for a γ-irradiation sensitive material having potential in material science and triggered release applications.

4.4 OUTLOOK

The γ-irradiation triggered secondary crosslink strategy presented here, is efficiently employed for the macroscopic contraction of alkyne functionalized dextran hydrogels. To improve the application further and allow for clinical application such as drug delivery systems, the sensitivity towards γ-irradiation should be increased. Using the current design, hydrogel contraction is achieved immediately after γ-irradiation starts and hydrogel contraction continues linearly for 24 hours up to doses of 14.4 kGy. In order to achieve controlled drug release the rate at which the hydrogel contraction occurs should be increased, and ideally show significant hydrogel contraction using doses below 2 Gy. This would allow the application to be used in patients and would prevent degradation of the drug molecule due to γ-irradiation. Achieving such sensitivity requires a high density of reactive ionizable sidechains in order to maximize the rate of contraction per unit of γ-radiation. In the current research it was attempted to increase the density of the ionizable alkyne moieties higher than the current degree of substitution, 36%. Using ^{1}H-NMR analysis we determined the degree of substitution to be 51% of the newly synthesized dextran batch. Unfortunately, dextran (500 kDa) having a degree of substitution with an apolar alkyne moiety this high is insoluble in water and limits the use for hydrogel preparation. Therefore, more water soluble ionizable side chains should be considered.

Furthermore, potential application of our alkyne-alkyne secondary crosslink strategy could be found in γ-ray triggered self-healing and γ-ray triggered reinforcement of materials. Mostly, gamma- and x-ray triggered systems are disruptive, which for release applications such as drug delivery devices is ideal. However, here we describe a process of bond formation induced by γ-radiation. In the field of materials science, γ-radiation shielding hydrogels are of interest to space engineering and personal protective gear. Examples of these gels are abundant

although have a limitation which is γ-radiation induced bond scissions that after a certain dose limits the use of these materials.[29,30] Such materials could be improved by incorporation of a γ-irradiation triggered secondary crosslink strategy as presented in this chapter.

4.5 REFERENCES

1. Fan, B.; Zhang, K.; Liu, Q.; Eelkema, R., Self-Healing Injectable Polymer Hydrogel via Dynamic Thiol-Alkynone Double Addition Cross-Links. *ACS Macro Lett.* **2020,** *9* (6), 776-780.
2. Hörner, M.; Raute, K.; Hummel, B.; Madl, J.; Creusen, G.; Thomas, O. S.; Christen, E. H.; Hotz, N.; Gübeli, R. J.; Engesser, R.; Rebmann, B.; Lauer, J.; Rolauffs, B.; Timmer, J.; Schamel, W. W. A.; Pruszak, J.; Römer, W.; Zurbriggen, M. D.; Friedrich, C.; Walther, A.; Minguet, S.; Sawarkar, R.; Weber, W., Phytochrome-Based Extracellular Matrix with Reversibly Tunable Mechanical Properties. *Adv. Mater.* **2019,** *31* (12), 1806727.
3. Guvendiren, M.; Burdick, J. A., Stiffening hydrogels to probe short- and long-term cellular responses to dynamic mechanics. *Nat. Comm.* **2012,** *3* (1), 792.
4. Kalayci, K.; Frisch, H.; Barner-Kowollik, C.; Truong, V. X., Wavelength-Dependent Stiffening of Hydrogel Matrices via Redshifted [2+2] Photocycloadditions. *Adv. Funct. Mater.* **2020,** *30* (15), 1908171.
5. Kloxin, A. M.; Kasko, A. M.; Salinas, C. N.; Anseth, K. S., Photodegradable Hydrogels for Dynamic Tuning of Physical and Chemical Properties. *Science* **2009,** *324* (5923), 59.
6. Zadražil, A.; Tokárová, V.; Štěpánek, F., Remotely triggered release from composite hydrogel sponges. *Soft Matter* **2012,** *8* (6), 1811-1816.
7. Kim, H.; Lee, H.; Seong, K.-Y.; Lee, E.; Yang, S. Y.; Yoon, J., Visible Light-Triggered On-Demand Drug Release from Hybrid Hydrogels and its Application in Transdermal Patches. *Adv. Healthcare Mater.* **2015,** *4* (14), 2071-2077.
8. Gutowska, A.; Seok Bark, J.; Chan Kwon, I.; Han Bae, Y.; Cha, Y.; Wan Kim, S., Squeezing hydrogels for controlled oral drug delivery. *J. Contr. Rel.* **1997,** *48* (2), 141-148.
9. Satarkar, N. S.; Hilt, J. Z., Magnetic hydrogel nanocomposites for remote controlled pulsatile drug release. *J. Contr. Rel.* **2008,** *130* (3), 246-251.
10. Chung, J. E.; Yokoyama, M.; Yamato, M.; Aoyagi, T.; Sakurai, Y.; Okano, T., Thermo-responsive drug delivery from polymeric micelles constructed using block copolymers of poly(N-isopropylacrylamide) and poly(butylmethacrylate). *J. Contr. Rel.* **1999,** *62* (1), 115-127.
11. Liles, K. P.; Greene, A. F.; Danielson, M. K.; Colley, N. D.; Wellen, A.; Fisher, J. M.; Barnes, J. C., Photoredox-Based Actuation of an Artificial Molecular Muscle. *Macromol. Rapid Comm.* **2018,** *39* (17), 1700781.
12. Foy, J. T.; Li, Q.; Goujon, A.; Colard-Itté, J.-R.; Fuks, G.; Moulin, E.; Schiffmann, O.; Dattler, D.; Funeriu, D. P.; Giuseppone, N., Dual-light control of

nanomachines that integrate motor and modulator subunits. *Nat. Nanotechnol.* **2017,** *12* (6), 540-545.

13. Li, Q.; Fuks, G.; Moulin, E.; Maaloum, M.; Rawiso, M.; Kulic, I.; Foy, J. T.; Giuseppone, N., Macroscopic contraction of a gel induced by the integrated motion of light-driven molecular motors. *Nat Nanotechnol.* **2015,** *10* (2), 161-165.
14. Arkenberg, M. R.; Lin, C.-C., Orthogonal enzymatic reactions for rapid crosslinking and dynamic tuning of PEG–peptide hydrogels. *Biomater. Sci.* **2017,** *5* (11), 2231-2240.
15. Wu, S.-Y.; Chou, H.-Y.; Yuh, C.-H.; Mekuria, S. L.; Kao, Y.-C.; Tsai, H.-C., Radiation-Sensitive Dendrimer-Based Drug Delivery System. *Adv, Sci.* **2018,** *5* (2), 1700339.
16. Deng, W.; Chen, W.; Clement, S.; Guller, A.; Zhao, Z.; Engel, A.; Goldys, E. M., Controlled gene and drug release from a liposomal delivery platform triggered by X-ray radiation. *Nat. Comm.* **2018,** *9* (1), 2713.
17. Starkewolf, Z. B.; Miyachi, L.; Wong, J.; Guo, T., X-ray triggered release of doxorubicin from nanoparticle drug carriers for cancer therapy. *Chem. Comm.* **2013,** *49* (25), 2545-2547.
18. Hennink, W. E.; van Nostrum, C. F., Novel crosslinking methods to design hydrogels. *Adv. Drug Del. Rev.* **2002,** *54* (1), 13-36.
19. Szafulera, K.; Wach, R. A.; Olejnik, A. K.; Rosiak, J. M.; Ulański, P., Radiation synthesis of biocompatible hydrogels of dextran methacrylate. *Radiat. Phys. Chem.* **2018,** *142*, 115-120.
20. Fei, B.; Wach, R. A.; Mitomo, H.; Yoshii, F.; Kume, T., Hydrogel of biodegradable cellulose derivatives. I. Radiation-induced crosslinking of CMC. *J. Appl. Polym. Sci.* **2000,** *78* (2), 278-283.
21. Singh, B.; Bala, R., Development of hydrogels by radiation induced polymerization for use in slow drug delivery. *Radiat. Phys. Chem.* **2014,** *103*, 178-187.
22. Cataldo, F.; Ursini, O.; Lilla, E.; Angelini, G., Radiation-induced crosslinking of collagen gelatin into a stable hydrogel. *J. Radioanal. Nucl. Chem.* **2008,** *275* (1), 125-131.
23. Clement, S.; Campbell, J. M.; Deng, W.; Guller, A.; Nisar, S.; Liu, G.; Wilson, B. C.; Goldys, E. M., Mechanisms for Tuning Engineered Nanomaterials to Enhance Radiation Therapy of Cancer. *Adv. Sci.* **2020,** *7* (24), 2003584.
24. Bassetti, M.; Fratoddi, I.; Lilla, L.; Pasquini, C.; Vittoria Russo, M.; Ursini, O., Synthesis of polyarylacetylenes by γ-ray-induced polymerization of terminal alkynes. Nanostructures of ortho-substituted derivatives. *J. Polym. Sci., Part A: Polym. Chem.* **2012,** *50* (24), 5097-5106.

25. Liu, Z.-Q.; Sun, L.; Wang, J.-G.; Han, J.; Zhao, Y.-K.; Zhou, B., Free-Radical-Initiated Coupling Reaction of Alcohols and Alkynes: Not C−O but C−C Bond Formation. *Org. Lett.* **2009,** *11* (6), 1437-1439.
26. M. Khosravifarsani, A. S.-M., M. Pouramir, E. Zabihi Hydroxyl Radical (ºOH) Scavenger Power of Tris (hydroxymethyl) Compared to Phosphate Buffer. *J. Mol. Biol. Res.* **2016,** *6*, 52-57.
27. Lovrak, M.; Picken, S. J.; Eelkema, R.; van Esch, J. H., Supramolecular Gluing of Polymeric Hydrogels. *ChemNanoMat* **2018,** *4* (8), 772-775.
28. Yang, J.; Bai, R.; Chen, B.; Suo, Z., Hydrogel Adhesion: A Supramolecular Synergy of Chemistry, Topology, and Mechanics. *Adv. Funct. Mater.* **2020,** *30* (2), 1901693.
29. Park, J., Kim, M., Choi, S. et al. Self-healable soft shield for γ-ray radiation based on polyacrylamide hydrogel composites. *Sci Rep*. **2020** 10, 21689
30. H. Chandrappa, Rajashekhar F. Bhajantri, B.K. Mahantesha, V. Ravindrachary, Shivaprasad Chalawadi, Physico-chemical properties of PVA-Nile blue (C20H20ClN3O) polymer composite structures for γ-ray protection: A comparative γ-ray irradiation studies, *Rad. Phys. Chem*., **2021** *184,* 109481.

4.6 SUPPLEMENTARY INFORMATION

4.6.1 General considerations

All solvents and chemicals were purchased from Sigma Aldrich or Apollo scientific and used without further purification. ^{1}H-NMR and ^{13}C-NMR were recorded on an Agilent-400 MR DD2 (399.67 MHz for ^{1}H and 100.5 MHz for ^{13}C) at 298 K. The chemical shifts are given with respect to solvent residual signals as reported by Fulmer et al.[1] The rheological measurements were performed using a rheometer (AR G2, TA instruments) equipped with a steel plate-and-plate geometry of 8 mm or 40 mm in diameter and equipped with hexadecane trap. Scanning electron microscopy images were recorded on a Jeol JSM-6010-LA machine. All γ-irradiation experiments were conducted using a Nordion GC220 ^{60}Co source. The preparation of alkyne modified dextran is described in section 3.5.4.

4.6.2 General protocol for dextran hydrogel preparation

A 10 wt% dex-alkyne solution was prepared by dissolving dex-alkyne in H_2O (300 μl), this solution was shaken for 1 hour. Bis-azide-PEG_{19} solution was prepared by mixing bis-azide-PEG_{19} (4.0 mg, 0.0038 mmol) with a Cu-click stock solution (200 μl, ($CuSO_4$ (0.59 mM), sodium ascorbate (3.79 mM) and THTPA (0.29 mM))), which was shortly shaken to dissolve and mix all components. Next, the dex-alkyne and the bis-azide-PEG_{19} solution were mixed and shortly shaken, after which the solution was transferred in a cubic mold and left overnight to gel. After gelation was complete, the hydrogel was removed from the mold and placed in a phosphate buffer (PB) (25 ml, 100 mM, pH 7.4) solution or demineralized water to remove Cu-click components, unreacted dex-alkyne and bis-azide-PEG_{19}. This washing step was repeated 3 times and afforded transparent self-supporting cubic hydrogels.

4.6.3 γ-irradiation induced contraction

The weight of swollen hydrogels (prepared as described in section 4.6.2) was determined and then placed in 15 ml glass vials and submerged with PB (10 ml, 100 mM, pH 7.4) or demineralized water (10 ml). Sample vials were irradiated with γ-rays delivered by a ^{60}Co-source and at selected timepoints the weight of the irradiated hydrogels and control hydrogels was determined (Table **S1**), using an analytical balance.

Table S1. *γ-irradiation (0.6 kGy/h) induced hydrogel contraction monitored by weight (g) determination at selected timepoints.*

	Time (min.)	0	50	100	200	400	1440
Entry	γ-irradiation (kGy)	0	0.5	1	2	4	14.4
1	S1 (g) (PB)	0.639	0.635	0.634	0.628	0.581	0.399
2	S2 (g) (PB)	0.633	0.625	0.607	0.598	0.562	0.383
3	S3 (g) (PB)	0.632	0.630	0.632	0.621	0.578	0.379
4	S1 (g) (H2O)	1.845	-	1.777	1.623	1.438	0.495
5	S2 (g) (H2O)	1.946	-	1.771	1.606	1.449	0.497
6	C1 (g) (PB)	0633	-	-	0.621	0.623	0.618
7	C2 (g) (PB)	0.585	-	-	0.590	0.594	0.592
8	C3 (g) (PB)	0.624	-	-	0.630	0.628	0.630

4.6.4 Rheological measurements of hydrogels

Dex-alkyne and bis-azide-PEG$_{19}$ solutions were prepared as described in section 4.6.2. After mixing, 0.5 ml was placed on the rheometer plate (40mm diameter steel plate-and-plate geometry, equipped with a hexadecane trap). After 33 minutes the gel point is reached, as the storage modulus surpasses the loss modules, indicating a hydrogel has formed (Figure **S2**). Time sweep measurements were performed at a fixed strain (γ = 1%) and frequency (ω =6.28 rad/s = 1 Hz).

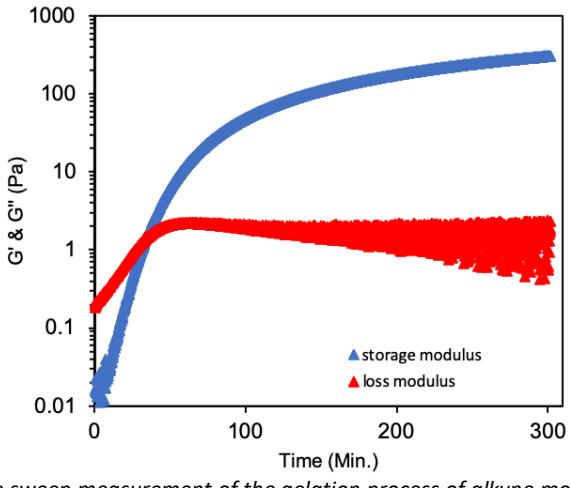

Figure S1. *Time sweep measurement of the gelation process of alkyne modified dextran hydrogel (10 wt%) using a bis-azide-PEG$_{19}$ crosslinker (γ = 1%, ω = 1 Hz, 25 ℃). The gel point is reached after approximately 33 minutes.*

The influence of γ-irradiation on the hydrogel stiffness was monitored using frequency sweep measurements and were performed at t = 0 (before γ-irradiation) and at t = 24 hours (14.4 kGy of γ-radiation). The storage modulus (G') shows a 2-fold increase after γ-irradiation for the water swollen hydrogels and 3-fold increase after γ-irradiation for the PB swollen hydrogels (Figure **S3A**), indicating more elastic behavior as a result of increased crosslink density. The loss modulus (G'') increases 1.8-fold for water swollen hydrogels and 20-fold for PB swollen hydrogels after 24 hours of γ-irradiation (14.4 kGy) (Figure **S3B**). The frequency sweep measurements were performed from 0.1 to 100 rad/s at a fixed strain (γ = 1%), using an 8 mm steel plate-and-plate geometry.

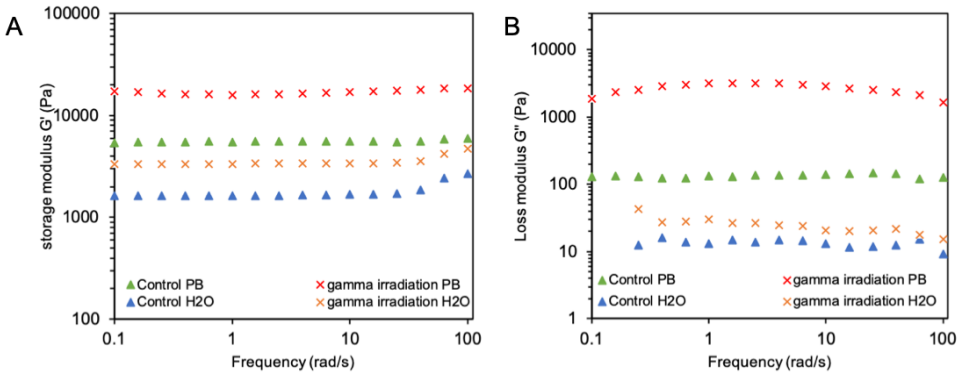

Figure S2. *Frequency sweep measurements of dextran-based hydrogels at t = 0 (before γ-irradiation) and at t = 24 hours (14.4 kGy of γ-radiation).*

4.6.5 Scanning electron microscopy analysis of hydrogels

The analyzed hydrogels were prepared following the procedure described in section 4.6.2. After hydrogel preparation the hydrogels were submerged in 5 ml H_2O inside a glass vial and placed in the ^{60}Co source or kept aside as a control. After 24 hours the gels were taken out and frozen by submerging the hydrogels in liquid nitrogen. The frozen hydrogels were then placed in a 50 ml round bottom flask and freeze-dried overnight. The freeze-dried samples were analyzed by SEM analysis.

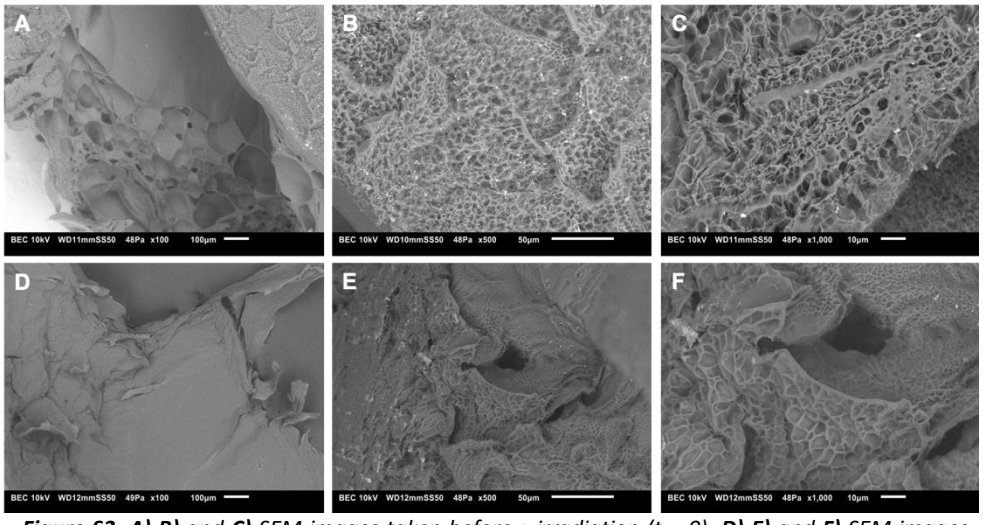

Figure S3. A) B) *and* ***C)*** *SEM images taken before γ-irradiation (t = 0).* ***D) E)*** *and* ***F)*** *SEM images taken after γ-irradiation (t = 24 hours, 14.4 kGy).*

4.6.6 γ-radiation triggered cargo release experiment

A 1,4-phthalic acid stock solution (6.02 mM, 12.2 mM $NaHCO_3$, pH 7.34 (NaOH pallet was used to adjust pH)) was prepared. Hydrogels were prepared according to the protocol described in section 4.6.2, except that dex-alkyne was dissolved in a 1,4-phthalic acid aqueous solution (300 μl) instead of demineralized water (300 μl). After gelation was complete, the hydrogels were removed from their mold and placed in 1,4-phthalic acid stock solution (25 ml) which was replaced by fresh 1,4-phthalic acid stock solution (3 x 25 ml) to wash out unreacted bis-azide crosslinker, dex-alkyne and Cu-click components. The hydrogels were then placed on a glass plateau inside a closed vial and H_2O (5 ml) was added (Figure **S4**). Subsequently, one gel was placed in the ^{60}Co source and irradiated for 24 hours and one gel was kept aside as a control. During the 24-hour period, aliquots (150 μl) were taken from the water phase below the irradiated gel and the non-irradiated control gel and analyzed by UV/Vis analyses.

Figure S4. *Example of the experimental setup used in the 1,4-phthalic acid γ-irradiation triggered release experiments.*

4.6.7 References

1. Fulmer, G. R.; Miller, A. J. M.; Sherden, N. H.; Gottlieb, H. E.; Nudelman, A.; Stoltz, B. M.; Bercaw, J. E.; Goldberg, K. I., NMR Chemical Shifts of Trace Impurities: Common Laboratory Solvents, Organics, and Gases in Deuterated Solvents Relevant to the Organometallic Chemist. *Organometallics* **2010,** *29* (9), 2176-2179.
2. Nielsen, T. T.; Wintgens, V.; Amiel, C.; Wimmer, R.; Larsen, K. L., Facile Synthesis of β-Cyclodextrin-Dextran Polymers by "Click" Chemistry. *Biomacromol.* **2010,** *11* (7), 1710-1715.

CHAPTER

MECHANICAL FORCE TRIGGERED SIGNAL MOLECULE GENERATION

Mechanical compression of flexible materials leads to cyclo-reversion reactions releasing small molecules. Here we present a force sensitive polyurethane material, releasing a signaling molecule when the material is mechanically compressed. We show synthetic procedures for the synthesis of our oxanorbornadiene mechanophore having the signal molecule incorporated. Further, a proof-of-concept is given where we detect the signal molecule after the prepared polyurethane material is compressed. Finally, we provide an outlook where we discuss the current status of the project and we introduce a new approach for mechanical force triggered signal molecule generation.

5.1 INTRODUCTION

Mechanophores are force sensitive molecules that are activated when a directional force is applied, resulting in bond cleavage or molecular rearrangements.[1, 2] Force can be applied in several ways including solution-phase ultrasonication, material compression, material stretching and through shearing. In general, polymer chains attached to the mechanophore transmit force applied to the solid polymeric material or solution in which the polymers are dissolved.[3] Most mechanophores are part of the polymeric backbone and in response to force a bond is cleaved, resulting in a color change or increase in fluorescence. Such mechanophores find purpose as reporter molecules that indicate for example microscopic material damage.[4-7] A different class of mechanophores is designed to break bonds that after breakage

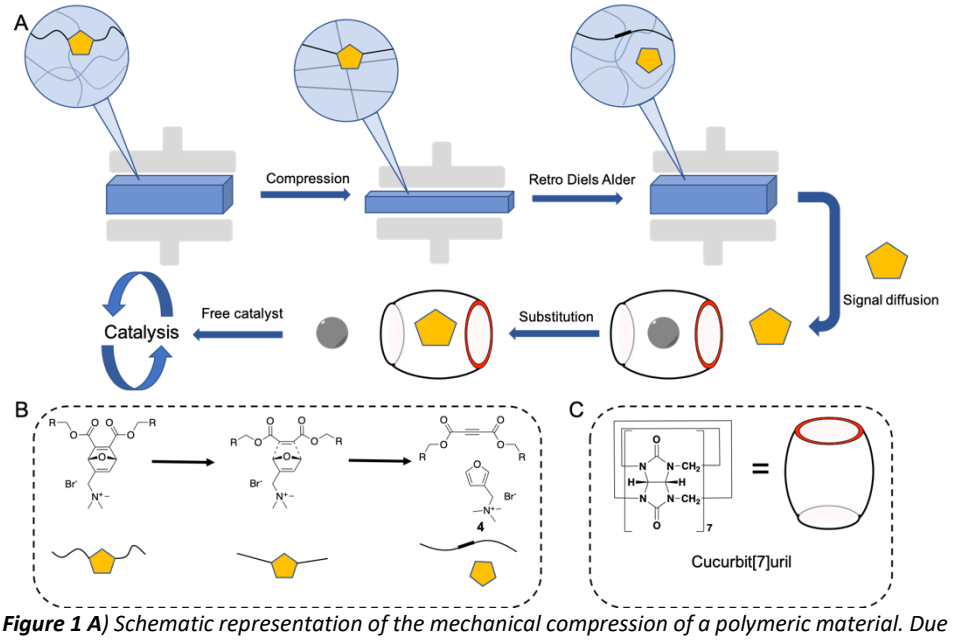

Figure 1 A*) Schematic representation of the mechanical compression of a polymeric material. Due to mechanical compression the polymeric backbone is stressed, leading to a retro Diels-Alder reaction and the release of a signal molecule. The released signal molecule can diffuse freely and bind to cucurbit[7]uril (CB[7]), substituting the inhibited catalyst.* ***B****) Mechanical force induced retro Diels-Alder reaction of the oxanorbornadiene scaffold, releasing signal molecule* ***4****.* ***C****) Molecular structure and schematic representation of cucurbit[7]uril (CB[7]).*

release a small molecule while the polymeric backbone remains intact. Such mechanophores were developed by Boydston et al., termed 'flex-activated' mechanophores and are based on the oxanorbornadiene scaffold.[8-11] Here, we aim to use the flex-activated oxanorbornadiene to incorporate a relevant signaling molecule (Figure **1B**, positively charged furan**4**) and release it in a controlled fashion using mechanical force (Figure **1A**). Flex activation of oxanorbornadienes, increases strain between the bonds of the di-ester functionality and the furan moiety and makes the oxanorbornadiene subject to force. When compressing an oxanorbornadiene containing material, the bond angle between the di-ester increases and ultimately reaches the point where the stored energy surpasses the activation energy of cyclo-reversion (Figure **1B**), resulting in the release of a small molecule. Here, the released signal molecule **4** strongly interacts with cucurbit[7]uril (CB[7]) (Figure **1C**), due to the favorable interactions between the apolar furan ring and the apolar CB[7] interior, and the positively charged quaternary amine with the hydrophilic portal region of CB[7]. The liberated signal molecule has a higher affinity for CB[7] compared to the catalyst for CB[7], resulting in the substitution of the encapsulated catalyst and subsequent onset of catalysis.[12, 13] In every compression cycle a fraction of the mechanophores is activated, allowing for stepwise generation of the signaling molecule. Using this strategy, we aim to prepare a material capable of sensing macroscopic force that is translated in a molecular event initiating a simple signaling cascade.

5.2 RESULTS AND DISCUSSION

For the synthesis of mechanophore **6**, we designed a three-step synthesis route, starting with the double esterification of acetylenedicarboxylic acid (compound **1**, Scheme **1**) with monobenzyl protected diethyleneglycol (compound **2**, Scheme **1**). In the second synthesis step we performed a [4 + 2] cycloaddition of furan **4** and alkyne **3**, however no product formation was observed. Several attempts were

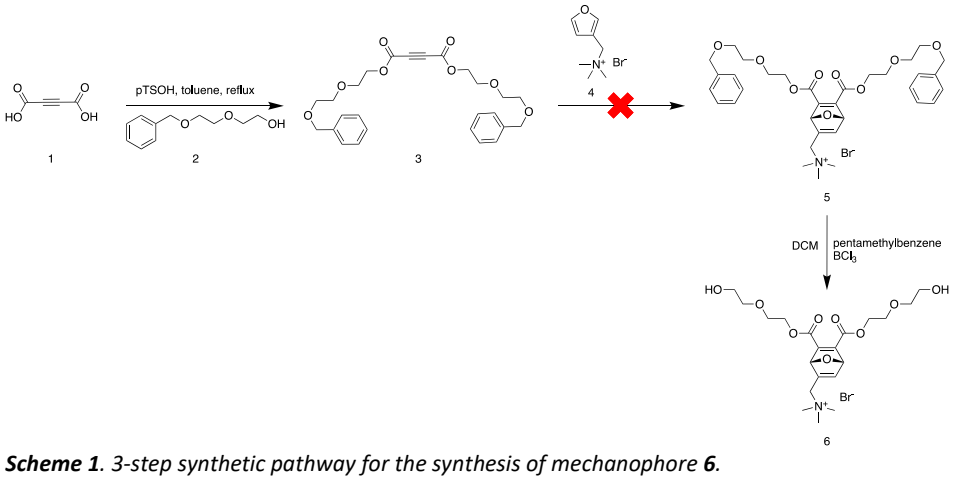

***Scheme 1**. 3-step synthetic pathway for the synthesis of mechanophore **6**.*

made to synthesize mechanophore **5** while varying the solvent, temperature and reaction pressure (table **S1**), however we did not observe the formation of mechanophore **5**. Trying to understand why the Diels-Alder reaction between alkyne **3** and furan **4** was unsuccessful, we evaluated the role of the Breslow hydrophobic effect[14] and solvent hydrogen bonding effects on the reaction progress of the Diels-Alder reaction between **3** and **4**. The Breslow hydrophobic effect and hydrogen bonding between diene, dienophile and protic solvents in the transition state of the Diels-Alder cycloaddition are the two main stabilizing effects accelerating the cycloaddition. The transition state of the Diels-Alder cycloaddition has a negative volume of activation, meaning that the volume of the separate diene and dienophile is larger than the two reactants in the transition state. Therefore, it is favorable to have solvent pressure bringing diene and dienophile in close proximity. In general, this is accounted for in the hydrophobic effect as two fairly apolar hydrocarbons in aqueous solvent systems tend to stabilize each other and approach each other closely, avoiding the unfavored interaction with water.[14] Since alkyne **3** and diene **4** are both water soluble the accelerating and stabilizing effect of the hydrophobic effect might be diminished, as both molecules are easily dissolved in polar solvents. In addition, the transition state is also stabilized by

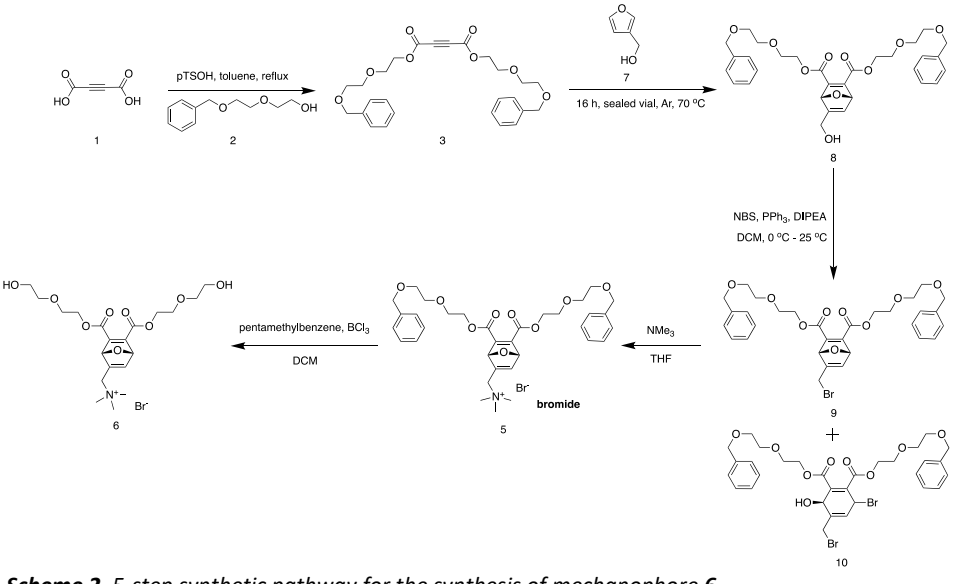

***Scheme 2**. 5-step synthetic pathway for the synthesis of mechanophore **6**.*

hydrogen bonding of solvent molecules (H_2O, MeOH, EtOH) between the carbonyls of alkyne **3** and the diene functionality of **4**. However, the positively charged quaternary amine might interfere with the stabilizing hydrogen bonding, due to a solvation shell formed around the charged amine, possibly explaining the observed failed reactions.[15, 16] To overcome this synthetic hurdle, we redesigned the synthesis route to obtain mechanophore **6** (Scheme **2**). We decided to replace the charged furan in synthesis step 2 for the non- charged 3-hydroxymethyl-furan (compound **7**, Scheme **2**) and to install the positive charge in a later stage directly on the oxanorbornadiene (Scheme **2**, step 4). Now, the Diels-Alder cycloaddition between alkyne **3** and furan **7** proceeded smoothly and afforded oxanorbornadiene **8** in moderate yield (37%). Using *N*-bromosuccinimide and triphenyl phosphine the hydroxyl moiety in **8** was reacted into a bromine, which in the next step should be bromine **10** occurred as well (confirmed by ^{1}H-NMR and LC-MS). Determined by ^{1}H-NMR, we easily converted into a quaternary amine. Although the desired oxanorbornadiene bromine **9** was formed, a ring opening of the oxanorbornadiene

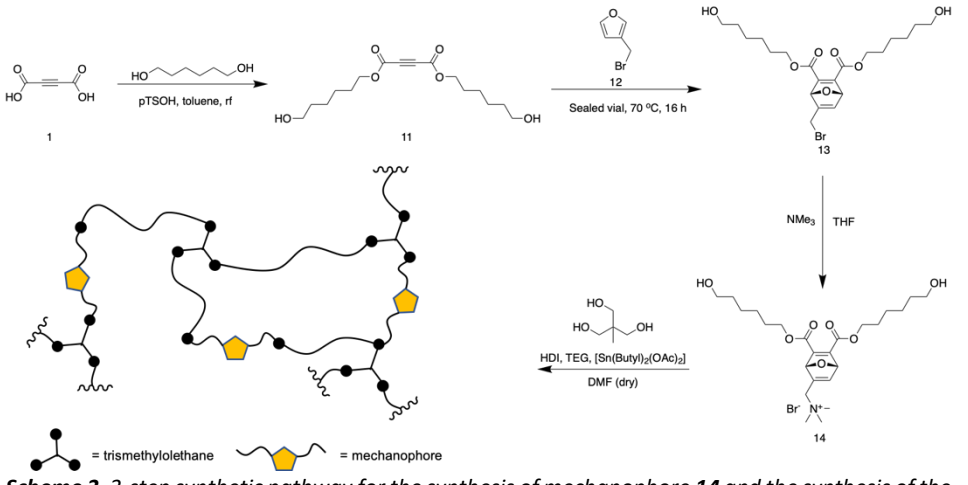

***Scheme 3**. 3-step synthetic pathway for the synthesis of mechanophore **14** and the synthesis of the polyurethane network, using triethylene glycol (TEG) and hexamethylenedi-isocyanate (HDI).*

moiety yielding found a 7:3 molar ratio between mechanophore **9** and by-product **10** (Figure **S1**). Using silica column chromatography, the purification of bromine **9** was attempted unfortunately without success, which is contributed to a too small difference in polarity between compound **9** and **10**. We again decided to redesign and simplify the synthetic route, staying close to the original design by Boydston et al. to obtain the desired mechanophore (Scheme **3**). In this approach we replaced diethylene glycol for 1,6-hexanediol, which shortens the synthetic route with 1 deprotection step and simplifies the purification of alkyne **11**. We synthesized alkyne **11** on a multigram scale, which was then further reacted to yield **13** that without purification was treated with trimethyl amine in THF to afford mechanophore **14**. Although **14** was not completely pure and was obtained in low yield, we decided to continue and as a proof of concept we prepared a polyurethane network having mechanophore **14** incorporated (Scheme **3**, details in SI). The liquid polymerization mixture was put in cylindrical molds. After curing, the solid polymer blocks were carefully removed and washed in chloroform to remove unreacted species, catalyst and solvent. After washing and drying the polyurethane material samples, we decided to test if we could mechanically activate the mechanophore

and release the signal molecule. We took two samples, of which one was compressed using a mechanical press, and one was kept aside as a control sample. After compressing the samples, we submerged the samples in CD_3OD for 60 minutes and analyzed the supernatant by LC-MS and ^{1}H-NMR. The mass of signal molecule **4** was found in the supernatant taken from the compressed sample and was not found in the supernatant taken from the control sample, indicating that mechanical force had triggered the release of our signal molecule. In addition, we recorded a ^{1}H-NMR spectrum of the supernatant collected for the compressed sample, and here we see small resonances matching signal molecule **4** (Figure **S2**). These preliminary results show the potential of the force sensitive triggering of a signaling cascade in a polymeric material that we have designed. Although the first results are promising, the system as such is not ideal and needs optimization and proper control experiments.

The current strategy for force activated signal transduction relies on mechanical activation by means of mechanical compression of polyurethane material samples releasing a signal molecule that in turn diffuses out of the material and competitively binds to a CB[7]⊂catalyst complex. One limitation here arises from the poor diffusion of small molecules in the polyurethane material samples that are dense polymeric networks. This would delay the competitive binding of the mechanically released signal molecule to the CB[7]⊂catalyst complex and the subsequent onset of catalysis. Also, the oxanorbornadiene mechanophores are synthesized in low yield and difficult to purify. To overcome these issues, a different strategy for mechanical activated signal transduction is presented in the outlook section below.

5.3 CONCLUSION

In conclusion, synthesizing mechanophore **6** designed for the mechanical force triggered signal transduction was unsuccessful following the synthesis route presented in scheme **1**, as the Diels-Alder reaction in synthesis step 2 failed. After replacing the positively charged amine substituent on furan **4** with a hydroxyl group the Diels-Alder reaction shown in scheme **2** was successful. However, in the next synthesis step, the bromination of the hydroxyl substituent, a mixture of product **9** and by-product **10** was formed which we failed to separate. In the third and final attempt the synthesis route was simplified and afforded the desired mechanophore, although in low yield and low purity. As a proof of concept, we incorporated the mechanophore in a polyurethane network and obtained a polymeric solid material. When compressing the material samples, low quantities of signal molecule **4** were detected by means of LC-MS and ^{1}H-NMR. In the outlook an alternative system is presented, providing a general concept where mechanical force triggers signal transduction to modulate catalyst activity.

5.4 OUTLOOK

Several strategies are employed to trigger mechanophores, one of them is compression of solid materials as described in the initial research approach. Alternatively, ultrasound or sonication is an efficient method to apply mechanical force on molecules. Using sonication, the mechanophore is typically in solution while being triggered, which would eliminate slow diffusion of the released signal molecule as the CB[7]⊂catalyst complex and the signal molecule are in the same phase, resulting in a quicker overall response. Only a few examples in literature exist demonstrating the release of small molecules from mechanophores triggered by sonication. The work of Herrmann et al. demonstrates the mechanically induced scission of a disulfide, leaving a reactive intermediate that further reacts via an intramolecular cyclization resulting in the release of small molecules (Scheme **4A**). The approach by Herrmann and Göstl et al. is a general concept enabling the mechanically controlled release of small molecules bearing an alcohol or amine group over periods of several hours (using a 20 kHz, Ip = 15.84 W/cm^{-2} sonication probe). An interesting feature of the reported mechanophores is the ability to release two different small molecules originating from one mechanophore after it is mechanically activated which could be of interest when two different signaling molecules are required.[17-19] Alternatively, Robb et al. published a general method, demonstrating the release of small molecules using sonication which triggers a retro Diels-Alder reaction, generating an instable furfuryl carbonate intermediate that further fragments into a small molecule and CO_2. This approach allows for the mechanically triggered release of small molecules bearing an aryl amine, alkyl amine, alcohol, phenol, carboxylic acid or sulfonic acid groups making it broadly applicable.[20] The latest research by Robb et al. included fine-tuning of their mechanophore, leading to a highly sensitive mechanophore that releases small molecules connected via a phenol group nearly instantaneously (using a 20 kHz, Ip = 8.2 W/cm^{-2} sonication probe).[21] Further, the mechanophores reported by

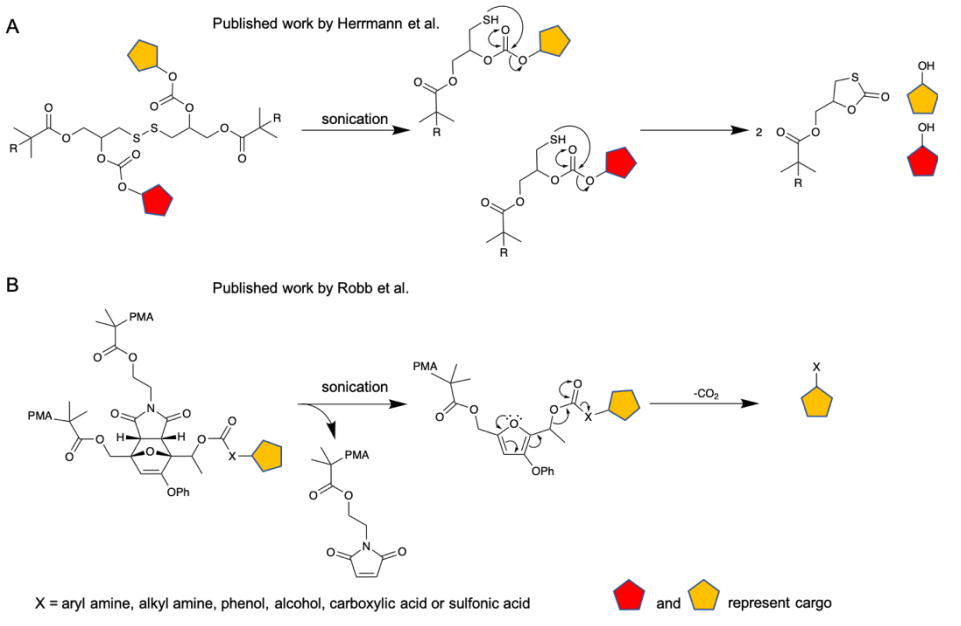

Scheme 4. A*) reaction cascade of disulfide mechanophore triggered by sonication leading to the release of two small molecules.* ***B****) Retro Diels-Alder reaction triggered by sonication, leading to an instable furfuryl intermediate releasing CO_2 and a small molecule.*

Herrmann and Göstl et al. are also triggered by reducing agents, making the concept prone to interference, compared to the mechanophores reported by Robb et al. Moreover, the sensitivity towards mechanical activation of the mechanophores reported by Robb et al. is substantially higher compared to the mechanophores reported by Herrmann and Göstl et al. Therefore, the mechanophore intended to implement in our mechanically triggered signal transduction strategy is based on the concept described by Robb et al.

The copper carbene catalyst described in chapter 2 of this thesis is efficiently inhibited and showing no catalytic activity when bound to CB[7].[12] The catalysis is switched 'on' immediately after the manual addition of a competitive guest (signal molecule), such as hydroxymethyl ferrocene or positively charged furan **4** (figure **1B**). In order to maintain such direct control over copper catalyzed click chemistry, it is important to consider that the signal molecule is not competitively binding to CB[7]⊂catalyst complex when bound to the mechanophore. In this particular

example, using an alkyl amine based signal molecule could provide the desired selectivity in binding affinity towards CB[7]. The signal molecule bound to the mechanophore is expected to have a low association constant in the range of K_a = 1.0 x 10^4 – 1.0 x 10^5 M^{-1} comparable to the affinity of aniline for CB[7].[26] The copper carbene catalyst presented in chapter 2 binds CB[7] relatively strong with association constants of K_{a1} = 1.21 x 10^9 and K_{a2} = 3.5 x 10^6.[22] Therefore, the catalyst remains inhibited when the signal molecule is bound to the mechanophore. However, when the mechanophore is triggered by sonication and releases the signal molecule, the alkyl amine in the signal molecule will be protonated in water, resulting in a much higher affinity for CB[7] compared to the mechanophore-bound signal molecule. Positively charged amines typically bind relatively strong (K_a = 1.0 x 10^5 – 1.0 x 10^7 M^{-1})[23, 24] to CB[7], resulting in the substitution of the copper carbene catalyst.[25, 26] Since the modulation of catalytic activity by CB[7] is a general concept and the release of a variety of signal molecules from mechanophores designed by Robb et al. as well, many different mechanically induced signal transduction cascades can be designed using the strategy presented in figure **2**.

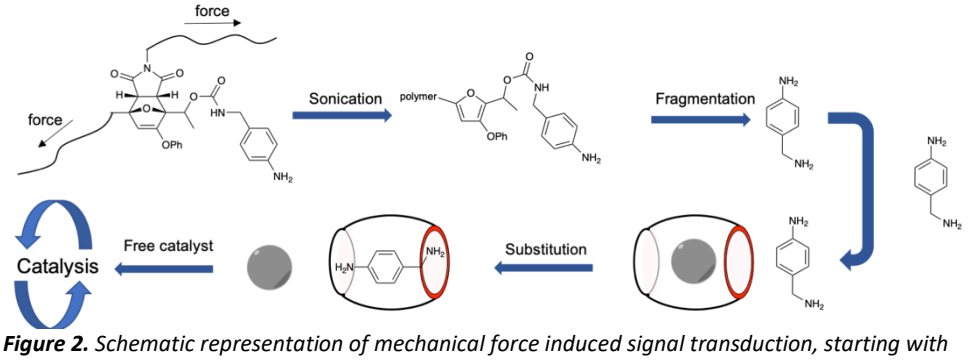

Figure 2. *Schematic representation of mechanical force induced signal transduction, starting with the activation of the mechanophore generating an instable furfuryl intermediate, that after fragmentation releases a competitive guest for CB[7]⊂catalyst complex. The competitive guest binds stronger to CB[7] substituting the inhibited catalyst resulting in the onset of catalysis.*

5.5 REFERENCES

1. Beyer, M. K.; Clausen-Schaumann, H., Mechanochemistry: the mechanical activation of covalent bonds. *Chem Rev* **2005,** *105* (8), 2921-48.
2. Brantley, J. N.; Wiggins, K. M.; Bielawski, C. W., Polymer mechanochemistry: the design and study of mechanophores. *Polym. Int.* **2013,** *62* (1), 2-12.
3. Piermattei, A.; Karthikeyan, S.; Sijbesma, R. P., Activating catalysts with mechanical force. *Nat. Chem.* **2009,** *1* (2), 133-137.
4. Weder, C., Polymers react to stress. *Nature* **2009,** *459* (7243), 45-46.
5. Li, M.; Liu, W.; Zhang, Q.; Zhu, S., Mechanical Force Sensitive Acrylic Latex Coating. *ACS Appl. Mater. & Interfaces* **2017,** *9* (17), 15156-15163.
6. Davis, D. A.; Hamilton, A.; Yang, J.; Cremar, L. D.; Van Gough, D.; Potisek, S. L.; Ong, M. T.; Braun, P. V.; Martínez, T. J.; White, S. R.; Moore, J. S.; Sottos, N. R., Force-induced activation of covalent bonds in mechanoresponsive polymeric materials. *Nature* **2009,** *459*, 68.
7. Woodcock, J. W.; Beams, R.; Davis, C. S.; Chen, N.; Stranick, S. J.; Shah, D. U.; Vollrath, F.; Gilman, J. W., Observation of Interfacial Damage in a Silk-Epoxy Composite, Using a Simple Mechanoresponsive Fluorescent Probe. *Adv. Mater. Interfaces* **2017,** *4* (10), 1601018.
8. Ghanem, M. A.; Basu, A. Behrou, R.; Boechler, N.; Boydston, A. J.; Craig, S. L.; Lin, Y.; Lynde, B. E.; Nelson, A.; Shen, H.; Storti, D. W., The role of polymer mechanochemistry in responsive materials and additive manufacturing. *Nat. Rev. Mater.* **2021,** *6* (1), 84-98.
9. Larsen, M. B.; Boydston, A. J., "Flex-Activated" Mechanophores: Using Polymer Mechanochemistry To Direct Bond Bending Activation. *J. Am. Chem. Soc.* **2013,** *135* (22), 8189-8192.
10. Larsen, M. B.; Boydston, A. J., Successive Mechanochemical Activation and Small Molecule Release in an Elastomeric Material. *J. Am. Chem. Soc.* **2014,** *136* (4), 1276-1279.
11. Shen, H.; Larsen, M. B.; Roessler, A. G.; Zimmerman, P. M.; Boydston, A. J., Mechanochemical Release of N-Heterocyclic Carbenes from Flex-Activated Mechanophores. *Angew. Chem. Int. Ed.* **2021,** *60* (24), 13559-13563.
12. Brevé, T. G.; Filius, M.; Araman, C.; van der Helm, M. P.; Hagedoorn, P.-L.; Joo, C.; van Kasteren, S. I.; Eelkema, R., Conditional Copper-Catalyzed Azide–Alkyne Cycloaddition by Catalyst Encapsulation. *Angew. Chem. Int. Ed.* **2020,** *59* (24), 9340-9344.
13. Li, G.; Trausel, F.; van der Helm, M. P.; Klemm, B.; Brevé, T. G.; van Rossum, S. A. P.; Hartono, M.; Gerlings, H. H. P. J.; Lovrak, M.; van Esch, J. H.; Eelkema, R.,

Tunable Control of Organocatalytic Activity through Host–Guest Chemistry. *Angew. Chem. Int. Ed.* **2021,** *60* (25), 14022-14029.

14. Breslow, R., Hydrophobic effects on simple organic reactions in water. *Acc. Chem. Res.* **1991,** *24* (6), 159-164.
15. Blake, J. F.; Jorgensen, W. L., Solvent effects on a Diels-Alder reaction from computer simulations. *J. Am. Chem. Soc.* **1991,** *113* (19), 7430-7432.
16. Blake, J. F.; Lim, D.; Jorgensen, W. L., Enhanced Hydrogen Bonding of Water to Diels-Alder Transition States. Ab Initio Evidence. *J. Org. Chem.* **1994,** *59* (4), 803-805.
17. Huo, S.; Zhao, P.; Shi, Z.; Zou, M.; Yang, X.; Warszawik, E.; Loznik, M.; Göstl, R.; Herrmann, A., Mechanochemical bond scission for the activation of drugs. *Nat. Chem.* **2021,** *13* (2), 131-139.
18. Shi, Z. Song, Q.; Göstl, R.; Herrmann, A., Mechanochemical activation of disulfide-based multifunctional polymers for theranostic drug release. *Chem. Sci.* **2021,** *12* (5), 1668-1674.
19. Shi, Z.; Wu, J. Song, Q.; Göstl, R.; Herrmann, A., Toward Drug Release Using Polymer Mechanochemical Disulfide Scission. *J. Am. Chem. Soc.* **2020,** *142* (34), 14725-14732.
20. Hu, X.; Zeng, T.; Husic, C. C.; Robb, M. J., Mechanically Triggered Small Molecule Release from a Masked Furfuryl Carbonate. *J. Am. Chem. Soc.* **2019,** *141* (38), 15018-15023.
21. Hu, X.; Zeng, T.; Husic, C. C.; Robb, M. J., Mechanically Triggered Release of Functionally Diverse Molecular Payloads from Masked 2-Furylcarbinol Derivatives. *ACS Cent. Sci.* **2021**.
22. Brevé, T. G.; Filius, M.; Araman, C.; van der Helm, M. P.; Hagedoorn, P.-L.; Joo, C.; van Kasteren, S. I.; Eelkema, R., Conditional Copper-Catalyzed Azide–Alkyne Cycloaddition by Catalyst Encapsulation. *Angew. Chem. Int. Ed.* **2020,** *59* (24), 9340-9344.
23. Meschke, C.; Buschmann, H. J.; Schollmeyer, E., Complexes of cucurbituril with alkyl mono- and diammonium ions in aqueous formic acid studied by calorimetric titrations. *Thermochim. Acta* **1997,** *297* (1), 43-48.
24. Hoffmann, R.; Knoche, W.; Fenn, C.; Buschmann, H.-J., Host–guest complexes of cucurbituril with the 4-methylbenzylammonium lon, alkali-metal cations and NH4+. *J. Chem. Soc., Faraday Trans.* **1994,** *90* (11), 1507-1511.
25. Assaf, K. I.; Nau, W. M., Cucurbiturils: from synthesis to high-affinity binding and catalysis. *Chem. Soc. Rev.* **2015,** *44* (2), 394-418.
26. Barrow, S. J.; Kasera, S.; Rowland, M. J.; del Barrio, J.; Scherman, O. A., Cucurbituril-Based Molecular Recognition. *Chem. Rev.* **2015,** *115* (22), 12320-12406.

27. Fulmer, G. R.; Miller, A. J. M.; Sherden, N. H.; Gottlieb, H. E.; Nudelman, A.; Stoltz, B. M.; Bercaw, J. E.; Goldberg, K. I., NMR Chemical Shifts of Trace Impurities: Common Laboratory Solvents, Organics, and Gases in Deuterated Solvents Relevant to the Organometallic Chemist. *Organometallics* **2010,** *29* (9), 2176-2179.
28. Megyesi, M.; Biczók, L.; Jablonkai, I., Highly Sensitive Fluorescence Response to Inclusion Complex Formation of Berberine Alkaloid with Cucurbit[7]uril. *J. Phys. Chem. C* **2008,** *112* (9), 3410-3416.

5.6 SUPPLEMENTARY INFORMATION

5.6.1 General considerations

All solvents and chemicals were purchased from Sigma Aldrich or Apollo scientific and used without further purification. ^{1}H-NMR and ^{13}C-NMR were recorded on an Agilent-400 MR DD2 (399.67 MHz for ^{1}H and 100.5 MHz for ^{13}C) at 298 K. The chemical shifts are given with respect to solvent residual signals as reported by Fulmer et al.[27] The synthesis of signal molecule **4** (Scheme **1**), 3-hydroxymethyl furan **7** (Scheme **2**) and 3-bromomethyl furan **12** (Scheme **3**) is described in section 2.5.3 in chapter 2 of this thesis.

5.6.2 Mechanophore synthesis

Bis(2-(2-(benzyloxy)ethoxy)ethyl) but-2-ynedioate (3)

acetylenedicarboxylic acid (2.5 g, 21.9 mmol), monobenzyl diethyleneglycol (25.8, 131.5 mmol) and *p*-toluenesulfonic acid monohydrate (0.4 g, 2.1 mmol) were dissolved in benzene (38 ml). The reaction flask was equipped with a reflux cooler and a Dean-Stark trap and heated to 80 °C and left to stir overnight. After the reaction mixture was cooled to room temperature, Et_2O was added and the organic layer was washed with $NaHCO_3$ (sat. 2 x 100 ml), H_2O (2 x 100 ml) and brine (2 x 100 ml). The organic layer was then dried over Na_2SO_4, concentrated *in vacuo* and purified over silica (EtOAc/PE 15% - 30%). This afforded the product as a yellow oil (yield: 4.4 g, 9.35 mmol, 43%). ^{1}H-NMR (400 MHz, CD_3OD) δ = 7.35 – 7.21 (m, CH_{arom}, 10H), 4.48 (s, Ph-CH_2, 4H), 4.33 – 4.30 (m, CH_2, 4H), 3.65 – 3.63 (m, CH_2, 4H), 3.59 – 3.55 (m, CH_2, 8H). ^{13}C-NMR (100 MHz, CD_3OD) δ = 152.66 ($C_{carbonyl}$), 139.49 (C_{arom}), 129.30 (CH_{arom}), 128.70 (CH_{arom}), 128.55 (CH_{arom}), 75.45 (C_{alkyne}), 73.93 (CH_2), 71.38 (CH_2), 70.44 (CH_2), 69.25 (CH_2), 66.93 (CH_2).

Bis(benzyloxy-diethyleneglycol-carbonyl)-oxabicyclo-trimethylmethanaminium (5)

Compound **3** (210 mg, 0.45 mmol) and signal molecule **4** (100 mg, 0.45 mmol) were combined in a glass vial and stirred overnight at 70 °C. Pressure was applied using a small autoclave in which the reaction vial was placed and pressurized with argon (entry 5 – 8, Table **S1**). The reaction mixture was then cooled to room temperature and analyzed by TLC and ESI-MS indicating no product had formed.

Table S1. *An overview of the reaction conditions screened for the synthesis of oxanorbornadiene **5**. The molar ratio of compound **3** and **4** is 1:1 for all attempted reactions.*

Entry	Solvent	Pressure (bar)	Temperature (°C)	Reaction time (h.)
1	MeOD	1	70	18
2	D_2O	1	70	18
3	$CDCl_3$	1	70	18
4	-	1	70	20
5	H_2O	10	50	20
6	H_2O	12	80	20
7	-	12	80	20
8	EtOH	12	80	20

Bis(benzyloxy-diethyleneglycol-carbonyl)-oxabicyclo-hydroxymethyl (8)

Compound **3** (210 mg, 0.45 mmol) and 3-hydroxymethyl furan **7** (47 mg, 0.48 mmol) were combined in a glass vial, crimped shut with a pressure seal, flushed with argon and stirred overnight at 70 °C. The reaction was then cooled to room temperature and the reaction mixture was purified over silica (EtOAc/PE 5% - 25%), affording the product as a yellowish oil (yield: 94.9 mg, 0.17 mmol, 37%). ^{1}H-NMR (400 MHz, CD_3OD) δ = 7.33 – 7.25 (m, CH_{arom}, 10H), 6.82 (m, C*H*, 1H), 5.64 (s, C*H*, 1H), 5.56 (s, C*H*, 1H), 4.51 (s, CH_2, 4H), 4.36 – 4.34 (m, CH_2, 2H), 4.32 - 4.30 (m, CH_2, 4H), 3.71 (t, J = 4.44 Hz, CH_2, 4H), 3.64 – 3.59 (m, CH_2, 8H). ^{13}C-NMR (100 MHz, CD_3OD) δ =164.33

($C_{carbonyl}$), 164.29 ($C_{carbonyl}$), 160.73 (C_{oxa}), 154.85 (C_{oxa}), 154.00 (C_{oxa}), 139.59 (C_{arom}), 139.56 (C_{arom}), 135.76 (CH_{oxa}), 129.37 (C_{arom}), 128.89 (C_{arom}), 128.86 (C_{arom}), 128.67 (C_{arom}), 128.66 (C_{arom}), 86.75 (CH_{oxa}), 86.68 (CH_{oxa}), 74.09 (CH_2-benzyl), 74.08 (CH_2-benzyl), 71.52 (CH_2), 71.46 (CH_2), 70.59 (CH_2), 69.82 (CH_2), 65.59 (CH_2), 65.52 (CH_2), 59.58 (CH_2-OH).

Bis(benzyloxy-diethyleneglycol-carbonyl)-oxabicyclo-bromomethyl (9)

Compound **8** (400 mg, 0.70 mmol), triphenyl phosphine (PPh_3) (330 mg, 1.26 mmol) and DIPEA (240 µl, 1.38 mmol) were dissolved in DCM (10 ml) and using an ice bath cooled to 0 °C. Under stirring, *N*-bromosuccinimide (NBS) was added and the reaction was left to stir for 1 hour, after which the ice bath was removed and the reaction stirred another 18 hours at room temperature. TLC analysis of the reaction mixture (60% EtOAc in PE) showed one new spot (R_f = 0.4, 254 nm and 366 nm light active), indicating formation of a new compound. H_2O (40 ml) was added to the reaction mixture and extracted with DCM (3 x 40 ml). The organic layer was then dried over Na_2SO_4, concentrated *in vacuo* and purified over silica (EtOAc/PE 15% - 50%). This afforded a mixture (ratio 7:3, Figure **S1**) of oxanorbornadiene **9** and by-product **10** as a yellow oil. Mass calc. compound **9**: 630.15 [M], mass found: 630.40 $[M+H]^+$, mass calc. compound **10**: 712.07 [M], mass found: 712.57 $[M+Na]^+$.

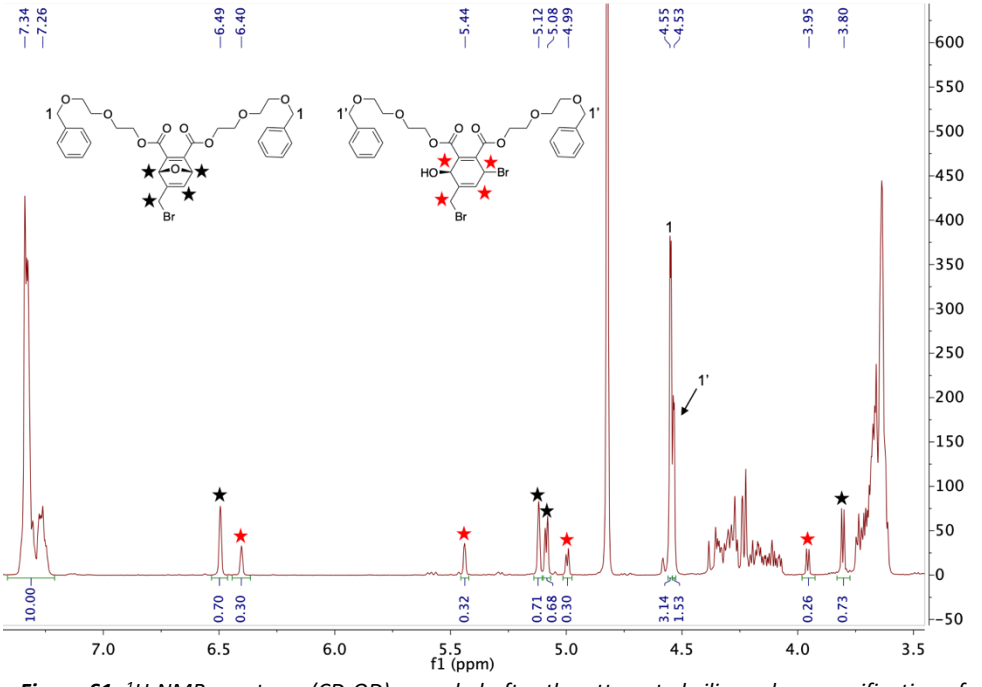

Figure S1. *^{1}H-NMR spectrum (CD_3OD) recorded after the attempted silica column purification of the product containing fraction.*

Bis(6-hydroxyhexyl) but-2-ynedioate (11)

Acetylenedicarboxylic acid (5.0 g, 43.8 mmol) and 1,6-hexanediol (52 g, 438 mmol) were dissolved in benzene (70 ml). *p*-Toluene sulfonic acid monohydrate (0.833 g, 4.38 mmol) was added and the solution was stirred and refluxed in a Dean-Stark apparatus for 6 hours. After cooling, Et_2O (50 ml) was added and the precipitate formed upon cooling was filtered off. Subsequently, the organic phase was washed with $NaHCO_3$ (sat., 2 x 50 ml), H_2O (4 x 50 ml) and brine (2 x 50 ml). The organic layer was dried over $MgSO_4$ and concentrated *in vacuo*, which afforded the product as a yellow oil (10.95 g, 34.8 mmol, 79%). ^{1}H-NMR (400 MHz, $CDCl_3$) δ = 4.23 (t, J = 6.60 Hz, C*H*$_2$, 4H), 3.64 (t, J = 6.52 Hz, C*H*$_2$, 4H), 1.68 (q, J = 6.80 Hz, C*H*$_2$, 4H), 1.57 (q, J = 6.68 Hz, C*H*$_2$, 4H), 1.42 – 1.38 (m, C*H*$_2$, 8H). ^{1}H-NMR data match reported values.[9]

5,6-bis(((6-hydroxyhexyl)oxy)carbonyl)-7-oxabicyclo-hepta-2,5-dien-2-yl)-N,N,N-trimethylmethanaminium bromide (14)

Compound **11** (1.13 g, 3.6 mmol) was combined with 3-bromomethylfuran (0.90 g, 4.05 mmol) in a glass vial. The vial was crimped shut with a pressure seal, flushed with argon and heated to 70 °C to stir overnight. Next, trimethyl amine (0.86 mL 4.2 M in EtOH) was added to the crude reaction mixture and stirred at room temperature for three days. The mixture was then partitioned between DCM (20 ml) and water (20 ml) and the water phase was washed with DCM (2x20 ml). The water phase was lyophilized to yield 600 mg of a pale yellow amorphous solid (1.12 mmol, 31%). ^{1}H-NMR (400 MHz, MeOD) δ = 6.71 (s, C*H*, 1H), 5.87 (s, C*H*, 1H), 5.83 (s, C*H*, 1H), 4.49 (s, CH_2, 2H), 4.32 – 4.22 (m, 2H), 4.17 – 4.06 (m, 2H), 3.58 (t, J = 6.48 Hz, CH_2, 4H), 3.34 (s, CH_2, 4H), 3.24 (s, CH_3, 9H), 1.85 – 1.70 (m, 4H), 1.59 – 1.55 (m, 4H), 1.46 – 1.41 (m, 4H). Mass calc.: 454.280 $[M]^+$, mass found: 454.35 $[M]^+$.

5

5.6.3 Network synthesis

Triethyleneglycol (124.7 mg, 0.83 mmol), 1,1,1-tris(hydroxymethyl)ethane (9.61 mg, 0.08 mmol) and mechanophore **14** (26.73 mg, 0.05 mmol) were dissolved in anhydrous (DMF 105 μl). Hexamethylene diisocyanate (168.2 mg, 1.0 mmol) and one drop of dibutyl tin diacetate were added. The solution was taken up into a syringe, sealed in a glass vial under argon and cured overnight at 60 °C. After curing, the material was removed from the syringe and the resulting material was washed with chloroform twice.

5.6.4 Compression experiments

Material samples were prepared as described in section 5.6.3 The material samples were placed in a mechanical press and a force of 10 MPa was applied for 1 minute.

The compressed samples were taken out and submerged in CD_3OD for 60 minutes. The supernatant was then analyzed by ESI-MS and ^{1}H-NMR (Figure **S2**) for traces of signal molecule **4**.

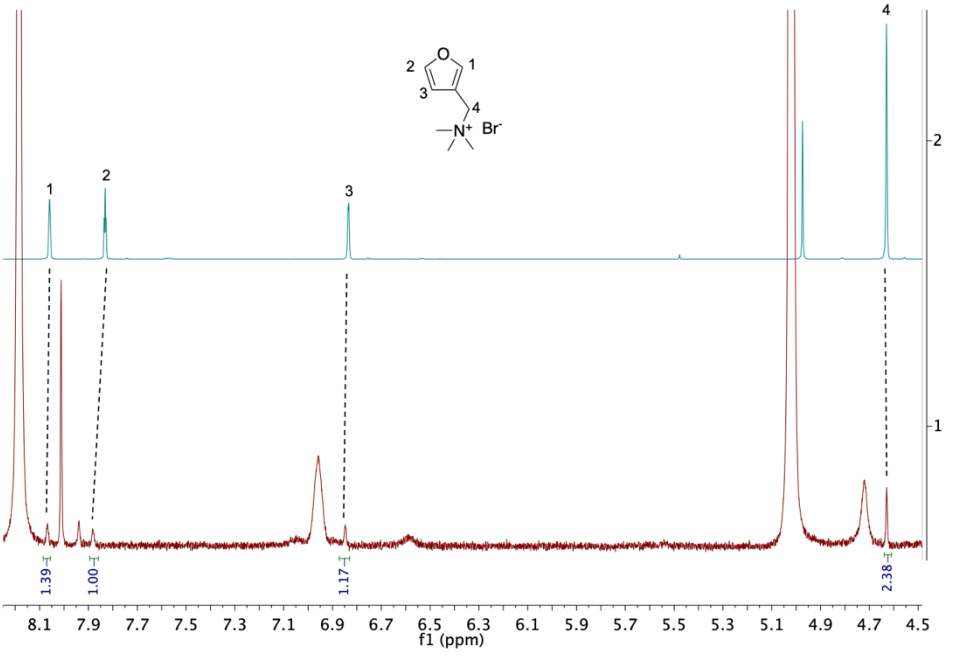

Figure S2. *Stacked ^{1}H-NMR spectra (CD_3OD) recorded for signal molecule **4** (top spectrum) and the supernatant taken after material compression (bottom).*

5.6.5 Fluorescent reporter complex

For the detection of released competitive guests, such as signal molecule **4**, a fluorescent CB[7]⊂berberine reporter complex was prepared. Berberine was selected as reporter molecule for the large (500-fold) increase in fluorescence when binding to CB[7] and the insensitivity to pH changes.[28] A CB[7] stock solution (10.4 μM) in MilliQ water was prepared, which was further diluted using MilliQ water to 5.20 μM, 2.08 μM, 1.04 μM and 0.10 μM. A stock solution (1.2 μM) of berberine was prepared in MilliQ water. Next, the berberine stock solution (150 μl) was mixed

with each of the 5 CB[7] stock solutions directly in fluorescence cuvettes and after a 5 minute equilibration period their fluorescent intensity was measured (Figure **S3**).

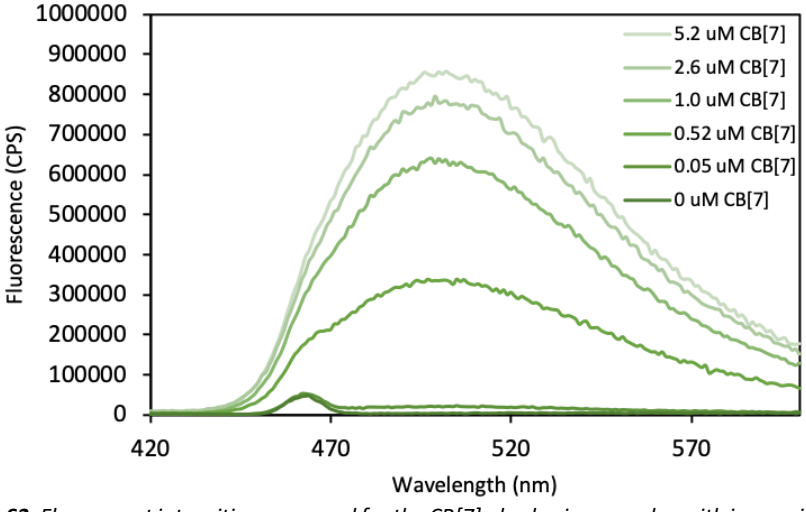

Figure S3. *Fluorescent intensities measured for the CB[7]⊂berberine complex with increasing CB[7] concentration (0 μM to 5.2 μM), having a emission maximum at 502 nm. Fluorescent intensity in counts per second (CPS). Excitation wavelength = 400 nm. Berberine concentration = 0.60 μM.*

To observe the change in fluorescent intensity of the CB[7]⊂berberine complex towards **4**, aliquots (0.3 μl, 968 μM) of **4** were consecutively added to a CB[7]⊂berberine mixture (300 μl MilliQ H_2O, 5.20 μM CB[7], 0.60 μM berberine) and after each addition the fluorescent intensity was measured. As the concentration of **4** increases, the fluorescent intensity is decreasing, indicating that berberine is substituted by **4** (Figure **S4**).

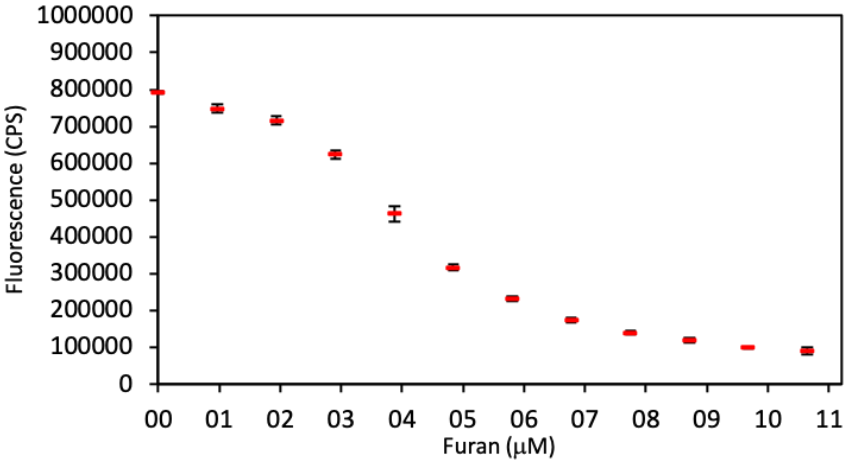

Figure S4. *Fluorescent response of the CB[7]⊂berberine complex upon 12 consecutive 0.3 μl additions of signal molecule* ***4*** *(MilliQ H_2O, 968 μM).Fluorescent intensity in counts per second (CPS). Excitation wavelength = 400 nm. Fluorescent intensities taken at emission wavelength = 500 nm.*

SUMMARY

Signal transduction is one of the primary communication mechanisms in living cells, enabling cells to respond to a changing environment. On the basis of this communication mechanism is enzyme activity that is regulated by the covalent or non-covalent binding of specific substrates. Substrate binding can initiate a signaling cascade that modulates the cellular response. Such molecular dynamics can be applied to design smart responsive materials having specific functions, such as self-healing, controlled release of cargo or controlled morphological changes. Here, we describe a strategy where host-guest chemistry is applied to mimic natural signal transduction and control catalytic activity. Furthermore, we discuss the design and synthesis of responsive hydrogels and show advanced functionality.

In Chapter 2 we describe the host-guest chemistry between a copper click catalyst and cucurbit[7]uril (CB[7]). The catalyst is designed to strongly bind CB[7], resulting in a 2:1 host-guest complex that efficiently switches catalytic activity off. We then demonstrate immediate activation of copper catalyzed click chemistry by adding a competitive binding signal molecule. Ultimately, we show on demand fluorescent labeling of a protein, demonstrating the versatility and biocompatibility of our catalyst⊂CB[7] host-guest complex.

In Chapter 3 we describe light sensitive dextran-based hydrogels that are designed to retain a cargo inside the hydrogel matrix and release upon light irradiation. We here introduce two novel light cleavable crosslinkers that are based on the *para*-hydroxyphenacyl (*p*Hp) scaffold and efficiently cleave upon UV-A and UV-C light irradiation. Using these crosslinkers, transparent self-supporting dextran hydrogels are prepared and upon light irradiation completely disintegrate. Doxorubicin and an antibody were loaded as cargo and controlled release by light irradiation is demonstrated. Finally, the use of Cerenkov luminescence as a release stimulus is investigated.

In Chapter 4 we present a curious finding where dextran-based hydrogels macroscopically contract upon γ-irradiation. We here modified dextran (500 kDa) with alkyne functionality, which first is employed to chemically crosslink the polysaccharide and form transparent self-supporting hydrogels. The residual alkyne moieties are then reacted in a secondary crosslink event initiated by γ-irradiation, resulting in macroscopic contraction of the hydrogel in all three dimensions. Finally, we show that such a reactivity can be used to 'squeeze' out cargo and to fuse separate hydrogel objects together.

In Chapter 5 we discuss a mechanical force triggered strategy for the generation of a signaling molecule, that can trigger catalysis as is described in chapter 2 of this thesis. We start with the synthesis of our mechanophore and the accompanying synthetical challenges. We then prepare flexible polyurethane based materials, having the mechanophore incorporated and as a proof of concept conduct mechanical compression experiments.

SAMENVATTING

Signaaltransductie is een van de primaire communicatiemechanismen van levende cellen. Met dit communicatiemechanisme kunnen cellen veranderingen in hun omgeving detecteren en zich hieraan aanpassen. De basis van dit communicatiemechanisme ligt bij enzymactiviteit welke gereguleerd wordt door het covalent of niet-covalent binden van substraten. Substraat binding resulteert in een signaal cascade welke de cellulaire respons reguleert. Deze moleculaire dynamiek kan toegepast worden in het ontwerp van slimme responsieve materialen welke specifieke functies hebben, zoals een zelf-herstellend vermogen, gecontroleerde afgifte van (bio)moleculen of gecontroleerde morfologische veranderingen. In dit proefschrift beschrijven we een strategie waarin *host-guest* chemie wordt toegepast om natuurlijke signaaltransductie na te bootsten en katalyse activiteit te controleren. Verder beschrijven we het ontwerp en de synthese van slimme zachte materialen welke reageren op externe signalen zoals UV-licht, kleine molecule, mechanische kracht en gammastraling.

In hoofdstuk 2 beschrijven we de *host-guest* chemie tussen een koper click katalysator en cucurbit[7]uril (CB[7]). We hebben de katalysator zo ontworpen dat het sterk bind aan CB[7], wat resulteert in een 2:1 *host-guest* complex dat efficiënt de katalytische activiteit 'uitschakelt'. Vervolgens demonstreren we signaaltransductie, door een competitief signaal molecuul toe te voegen waarmee de katalyse onmiddellijk geactiveerd kan worden. Ook laten we zien dat deze *host-guest* chemie gebruikt kan worden voor de gecontroleerde fluorescente labeling van een eiwit, wat de veelzijdigheid en bio-compatibiliteit van het beschreven katalysator⊂CB[7] *host-guest* complex aantoont.

In hoofdstuk 3 beschrijven we licht gevoelige dextran hydrogelen welke ontworpen zijn om een moleculaire lading vast te houden in de hydrogel matrix en gecontroleerd af te geven na bestraling met licht. We introduceren hier twee

nieuwe licht afbreekbare crosslinkers welke gebaseerd zijn op het *para*-hydroxyphenacyl (*p*Hp) moleculaire motief en efficiënt opbreken na bestraling met UV-A en UV-C licht. Met deze crosslinkers worden transparante hydrogelen geprepareerd welke na bestraling met licht volledig uiteen vallen. Verder, laden we doxorubicin en antilichamen in de hydrogel matrix en laten zien dat met licht bestraling gecontroleerde afgifte van doxorubicin en antilichamen mogelijk is. Ook wordt onderzocht of Cerenkov luminescentie gebruikt kan worden als stimulus voor hydrogel degradatie.

In hoofdstuk 4 presenteren we een curieuze bevinding waar dextran hydrogelen macroscopische contractie ondergaan door bestraling met γ-straling. We modificeren dextran hier met alkyn groepen welke eerst gebruikt worden voor het crosslinken van de polysacharide waarmee we transparante kubische hydrogelen maken. Vervolgens reageren de overige alkyn groepen in een secundaire crosslink reactie, geïnitieerd door γ-straling wat leidt tot de macroscopische contractie in drie dimensies van de hydrogel kubus. Als laatste laten we hier zien dat deze reactiviteit gebruikt kan worden voor het 'uitknijpen' van een moleculaire lading uit de hydrogel matrix en voor het fuseren van twee aparte hydrogel objecten.

In hoofdstuk 5 bespreken we een strategie waarin mechanische compressie gebruikt wordt voor het generen van een signaal molecuul. Dit signaal molecuul wordt in hoofdstuk 2 gebruikt voor signaaltransductie wat leidt tot de directe activatie van katalyse. We starten met de synthese van het mechanophore en de bijbehorende synthetische uitdagingen. Dan prepareren we een flexibel polyurethaan materiaal waarin het mechanophore ingebouwd is en als *proof-of-concept* voeren we mechanische compressie experimenten uit.

ACKNOWLEDGEMENTS

I enjoyed my time as PhD student at the TU Delft and would like to thank everybody who has contributed to my research in some way and helped me through it in and around the lab. First, I would like to thank my promotor Rienk Eelkema for offering me a position in the Eelkema Lab. Your guidance throughout my PhD was very valuable to me and I have learned a lot from you. I am grateful it was always possible to walk by (or zoom-by) and for all your help in paper writing, presenting data, how to convert a 'failed' experiment in publishable work and the educative discussions on my research. Many thanks also to my promotor Jan van Esch for accepting me in the Advanced Soft Matter (ASM) research group. I always felt welcome in ASM and it quickly started to feel like home.

Next, I would like to thank all my colleagues, I had a wonderful time the past 4.5 years full of joy, nice conversations, Friday afternoon experiments, BBQs, lab cleaning diners, Thursday beers, Hanos shopping's, coffee breaks and all the rest! Ben, thanks for all the great moments together, it was/is nice to have you as a colleague and a friend. It was nice to brainstorm on the countless experiments we could do in the lab, how and when we could do a BBQ and to share all the frustrations from the lab, that after a few beers were almost forgotten. Irene, thank you for being such a cheerful person, with you around I always felt a little bit on vacation in Italy! Reece, thank you for all the clarifying conversations about (polymer) chemistry and all the fun moments outside the lab. Sarah, thanks for introducing all kinds of American beverages and snacks during the Thursday drinks and demonstrating to me how golf should be played. Oh, and probably for the most hilarious moment I ever witnessed of someone trying to ride a locked bike! Peggy, thank you for your scientific advice and all the nice (mono directional German) conversations. Suellen, thanks for the spontaneous brainstorm sessions on how to solve my challenges with hydrogels in the lab. Yongjun, thank you for the nice cooperation on the light cleavable project. Bowen, thank you for all your kind help in the lab, especially measuring rheology and your tips and tricks in hydrogel preparation. Guotai, I enjoyed

working with you and discussing possible scientific opportunities using cucurbiturils, thank you! Benjamin, Yongjun, Guotai and Bowen, I have good memories on our conference trip to Lecce, Italy. It was a great week on a nice conference with delicious food and wine, great views and great company! Benjamin (S), thank you for your help and synthetic insights regarding the mechanophore project, I am pretty sure we would have managed to publish a nice paper with some more lab time. Michelle, thank you for your scientific contribution to the 'click' paper, this was very helpful. Fanny, thank you for getting me started in the cucurbiturils project, due to your enthusiastic attitude it was easy to get started on the CB topic. Susan, it was nice to have you as an office back neighbor and talk about all random things in the world and to decide whether a certain synthesis would work or not. Hendrik, we did not really work together but it was nice to have you around, thanks! Huanhuan, thank you for all your help in the Reactor Institute. It was great that you always made time for me and pick me up at the entrance of the Reactor Institute and assisted me with all the gamma-irradiation experiments. Sietse, thank you for your nice company during the multiple *borrels* and BBQs and taking care of the lab, vast improvements have been made since you joined ASM! Duco, thanks a lot for all your advice and help in the lab. Your suggestions were always helpful, and your 'dry' sense of humor made me laugh out loud quite a lot! Marcel, thank you for helping me out every time some issue occurred in the lab and your company during the Thursday drinks. Veby, thanks a lot for taking care of all the administrative stuff and for the *gezelligheid* during group events and *borrels*, you have a great personality! Furthermore, I would like to thank all other AMS and ex-ASM members, it was a great pleasure being part of the group!

Mike, a big thank you for all the great work and your determination in the pursue of quality work that ended up in two of my papers. I always enjoyed the time around in your lab discussing work and non-work-related topics, it was a pleasure doing business with you! Stephen, thank you for all your help regarding NMR, whether there were machine issues, challenges with the samples or kinetic experiments you always stood by and did everything in your power to help me. I think I will miss your near perfect

imitations of Ron, haha! Georgy, thank you for your advice on how to do science in general and your help with machines, catalysts synthesis, photochemistry, lab working procedures and for sharing a lot of knowledge (also for the random facts ;)).

Lucien, I want to thank you for supervision during my MSc thesis. During my MSc research internship, you learned me how to do proper research, be creative in solving problems and to be persistent in order to meet the research objective. I think you are a great person and during my PhD, I frequently had flashbacks to the MSc research which helped to proceed and succeed, thanks!

I would like to thank all the students I have worked with. I really enjoyed your presence and help on all the research topics. An especially big thank you to: Sven Weerdenburg, Stefan van der Griend and Tim Groeneveld. You all were very determined to tackle all synthetical challenges we met in the synthesis of various light cleavable linkers. Your work helped me in the end to complete the synthesis and to obtain light cleavable hydrogel crosslinker that are now the basis of a peer reviewed and published paper, thanks!

Next, I would like to thank my close friends: Elroy & Sanne, Sonny & Pien, Rick & Anne, Roel & Martine, Tim & Eveline, Joyce & Freek, Robert and Debbie for all the good times and great moments, this was a pleasant distraction from work and certainly helped me to keep going. Son & El, it is nice to have you as friends and to enjoy live as it is, lets maintain all the good things in the future! Roy and Dinesh, I want to thank you for initiating our first move into the academic world. This was in the beginning quite intense, but together we made it work. Rob, I want to thank you as well for our friendship and all the great moments during our MSc studies together with Roy and Dinesh. Once we started the PhD life it was very refreshing to talk about the research and hear all your opinions on the matter, especially when too much scientific conversation was rewarded with a shot of alcohol!

Then, I would like to thank my fireworks ‘family’, it is always a great pleasure to be with you and have a good time. In the past years we made some amazing trips all over the world, to which I have only good memories. Our passion for fireworks unites us and I enjoy being in a world full of vibrant colors and amazing sounds. The exciting challenges we had (and hopefully will have again) in designing fireworks displays was a good way to clear my mind and be creative and challenged in a non-scientific setting. This gave me a lot of positive energy.

Finally, I would like to thank my family for their unconditional support throughout my life. Pa & Ma, bedankt voor jullie steun door de jaren heen en dat jullie er altijd voor mij zijn. Ik vind het fijn om bij jullie te zijn en we gaan nog vele leuke tijden tegemoet. Ingrid, bedankt dat je altijd voor ons klaar staat en al jouw goede zorgen en gezelligheid. Leo & Cemile, het is fijn om bij jullie te zijn en lekker te relaxen.

Robin, jij bent het beste van alles, zonder jou was ik nooit zo ver gekomen. We zijn samen sinds de middelbare school en sindsdien is onze relatie alleen maar leuker en dieper geworden. Met jou kan ik fijn over alles praten, heerlijk brainstormen en dromen over de toekomst. In moeilijke tijden (en in goede) is het fijn om een partners als jou te hebben en ik kijk uit naar onze toekomstige avonturen. Bedankt voor de verschillende keren dat jij me eraan herinnerde, waarom ik aan een PhD begonnen ben, dit gaf me weer moed en kracht wat er toe geleid heeft dat ik dit proefschrift met succes afgerond heb. Ik hou ontzettend veel van jou.

While writing this final piece, I look back at my PhD time with a lot of joy, realizing a cheerful chapter of my life now closes. Nevertheless, a new and exciting one has started, and I hope to have many more joyful moments with all of you in the future.

Thanks!

Tobias

CURRICULUM VITAE AUCTORIS

Tobias (1990) was born in Delft, The Netherlands. In 2014 he finished his BSc studies in Molecular Science & Technology at the Leiden University and Technical University Delft. He then continued with his MSc Chemistry studies at Leiden University. Here he conducted his master thesis in the Metals in Catalysis, Biomimetics & Inorganic Materials (MCBIM) research group in under the supervision of dr. Sylvestre Bonnet. The topic was about the Synthesis and Study of L-glucose Derivatives of Ruthenium Polypyridyl Complexes. A minor MSc study was conducted in Modern Drug Discovery. He also conducted an extracurricular internship at AkzoNobel where he did research on improving the hardness of waterborne coatings under the supervision of dr. Remy van Gorkum. The MSc degree was obtained in 2016 and in April 2017 he started his PhD research under the supervision of dr. Rienk Eelkema. His research topic was about Stimuli Sensitive Polymer Materials for Signal Transduction and in particular about switchable inorganic catalysts and mechano-, light-, and gamma-ray-responsive materials. As of November 2021, he joined AkzoNobel as researcher in the Aerospace R&D department.

LIST OF PUBLICATIONS

1. T. G. Brevé, M. Filius, S. Weerdenburg, S. J. van der Griend, T. P. Groeneveld, A. G. Denkova, R. Eelkema, Light-sensitive phenacyl crosslinked dextran hydrogels for controlled delivery. Chem. Eur. J. **2022**, 28, e202103523.

2. Brevé, T. G.; Liu, H.; Denkova, A. G.; Eelkema, R., Gamma Radiation Induced Contraction of Alkyne Modified Polymer Hydrogels. **2022**. Macromol. Mater. Eng. DOI: 202100623

3. Men, Y.; Brevé, T. G.; Liu, H.; Denkova, A. G.; Eelkema, R., Photo cleavable thioacetal block copolymers for controlled release. Polym. Chem. **2021**, 12, 3612-3618

4. Li, G.; Trausel, F.; van der Helm, M. P.; Klemm, B.; Brevé, T. G.; van Rossum, S. A. P.; Hartono, M.; Gerlings, H. H. P. J.; Lovrak, M.; van Esch, J. H.; Eelkema, R., Tuneable Control of Organocatalytic Activity through Host–Guest Chemistry. Angew. Chem. Int. Ed. **2021**, 60 (25), 14022-14029.

5. Brevé, T. G.; Filius, M.; Araman, C.; van der Helm, M. P.; Hagedoorn, P.-L.; Joo, C.; van Kasteren, S. I.; Eelkema, R., Conditional Copper-Catalyzed Azide–Alkyne Cycloaddition by Catalyst Encapsulation. Angew. Chem. Int. Ed. **2020**, 59 (24), 9340-9344.

6. Lameijer, L. N.; Brevé, T. G.; van Rixel, V. H. S.; Askes, S. H. C.; Siegler, M. A.; Bonnet, S., Effects of the Bidentate Ligand on the Photophysical Properties, Cellular Uptake, and (Photo)cytotoxicity of Glycoconjugates Based on the [Ru(tpy)(NN)(L)](2+) Scaffold. Chemistry **2018**, 24 (11), 2709-2717.

7. van Dijkman, T. F.; de Bruijn, H. M.; Brevé, T. G.; van Meijeren, B.; Siegler, M. A.; Bouwman, E., Extremely bulky copper(i) complexes of [HB(3,5-{1-naphthyl}2pz)3]- and [HB(3,5-{2- naphthyl}2pz)3]- and their self-assembly on graphene. Dalton Transactions **2017**, 46 (19), 6433- 6446.

8. Lameijer Lucien, N.; Hopkins Samantha, L.; Brevé Tobias, G.; Askes Sven, H. C.; Bonnet, S., d- Versus l-Glucose Conjugation: Mitochondrial Targeting of a Light-Activated Dual-Mode-of- Action Ruthenium-Based Anticancer Prodrug. Chemistry – A European Journal **2016**, 22 (51), 18484-18491.